Summer 2019

Utilizing objective measures of acute and chronic mechanical insult to determine their contributions to post-traumatic osteoarthritis risk

Kevin Nathaniel Dibbern
University of Iowa

UTILIZING OBJECTIVE MEASURES OF ACUTE AND CHRONIC MECHANICAL INSULT TO DETERMINE THEIR CONTRIBUTIONS TO POST-TRAUMATIC OSTEOARTHRITIS RISK

by

Kevin Nathaniel Dibbern

A thesis submitted in partial fulfillment
of the requirements for the Doctor of Philosophy
degree in Biomedical Engineering in the
Graduate College of
The University of Iowa

August 2019

Thesis Supervisor: Professor Donald D. Anderson

ACKNOWLEDGEMENTS

This work would not have been possible without the support from many individuals in the Department of Orthopedics and Rehabilitation and the Orthopedic Biomechanics Laboratory, as well as from our collaborators at the University of Indiana. I would like to thank Drs. J. Lawrence Marsh, Michael Willey, Lawrence Kempton, and Todd McKinley for their support and invaluable clinical expertise, Dr. Andrew Kern for his teaching and mentoring, and Holly Thomas-Aitken, as well as Drs. Karan Rao, and Tai Holland for their aid in the many hours of analysis required to complete these studies. Also, I acknowledge and would like to thank the many students who have helped in the support of this work, in particular, Megan Andrew, Dennis Cuvalo, Matt Engelken, James Hiller, Mike Ho, Erin McFadden, Jessica Mosqueda, Kara Schneider, and Janelle Lala. Finally, I would like to sincerely thank my advisor, Dr. Donald D. Anderson, for the outstanding mentoring and guidance he has provided.

ABSTRACT

Intra-articular fractures (IAFs) are challenging injuries to study and treat clinically. Following IAF, different joints and even different regions within joints have been shown to have varying degrees of tolerance to injury severity and surgical reduction accuracy. Therefore, to determine the true effects of surgical reduction accuracy on post-traumatic osteoarthritis (PTOA) development, more sensitive and objective measures of articular injury and restoration are needed. To that end, this work details the development of objective measures of injury severity and models of restoration. Two hypotheses were posed: that surgical reduction accuracy is correlated with injury severity, and that injury severity more greatly influences outcomes than the surgical reduction.

To quantify the effects of acute injury severity on PTOA development, objective measures of the energy involved in fracturing as well as the degree of damage to the articular surface were created. Differences in the area over which the damage was delivered were also accounted for as a normalization of the fracture energy to a given joint. Inclusion of this latter factor enabled more accurate study of damage to the important areas of the bone. From these measures, a combined severity score was created that could be applied to any IAF. It was demonstrated to be predictive of the degree of PTOA development in the hip, hindfoot, and ankle.

The effects of surgical reduction accuracy were measured through contact stress, a measure that detects when forces are concentrated over small areas. When these stresses are too high and persist over time, they are associated with chronic joint degeneration. Therefore, the exposure to the contact stresses during a simulated walking gait after fracture reconstruction was

computed for each patient. The over-exposures computed over this gait cycle were strongly associated with PTOA development in all 3 joints studied.

By measuring injury severity and reduction accuracy on the same patients with IAFs of the hip, hindfoot, or ankle, relative contributions to PTOA risk were determined for each joint. Significant correlations between injury severity and reduction accuracy were found supporting our first hypothesis. The second hypothesis was refuted, as reduction accuracy was also significantly associated with PTOA development in all 3 joints. An overall model combining the injury severity and reduction accuracy measure for each case was created to assess the total mechanical contributions to PTOA. This model achieved 100% accuracy in the ankle, 88% in the calcaneus, and 91% in the acetabulum.

PUBLIC ABSTRACT

Intra-articular bone fractures are challenging injuries from both the perspective of scientific study and that of clinical treatment. Following such injuries, different joints have been found to have different apparent tolerances to the severity of the initial injury and the accuracy of their restoration after surgical treatment. Therefore, to determine the true effects of this surgical accuracy on patient outcomes, more sensitive and objective measures of the severity of injury and accuracy of restoration are needed. To that end, this work details the development of objective measures of injury severity and models of restoration accuracy. Two hypotheses were posed: that the surgical restoration accuracy is correlated with the injury severity, and that the injury severity more greatly influences outcomes than the restoration accuracy.

The injury severity was objectively quantified using measures of the energy involved in creating the fracture. The differences in area over which damage was delivered and amount of energy in important regions of bone were also accounted for to better assess damage across highly varied joint anatomies. These measures were demonstrated to be predictive of patient outcomes in the hip, hindfoot, and ankle.

The effects of surgical restoration accuracy were measured through contact stress, a measure that detects when forces are concentrated over small areas. When these stresses are too high and persist over time, they are associated with chronic joint degeneration. Therefore, the exposure to the contact stresses during a simulated walking gait after fracture reconstruction was computed for each patient. The stress over-exposures computed over this gait cycle were also strongly associated with patient outcomes in all three joints studied.

By measuring injury severity and restoration accuracy on the same patients with IAFs of the hip, hindfoot or ankle, the relative contributions of each factor to patient outcomes were

determined for each joint. Significant correlations between injury severity and restoration accuracy were found, a result that supports our first hypothesis. The second hypothesis was refuted, as reduction accuracy was also significantly associated with patient outcomes. An overall model combining the injury severity and restoration accuracy measures for each case was created to best assess and predict patient outcomes. This model achieved 100% accuracy in the ankle, 88% in the calcaneus, and 91% in the acetabulum.

TABLE OF CONTENTS

LIST OF TABLES ix
LIST OF FIGURES xi
TABLE OF NOMENCLATURE xv
PREFACE xvi
CHAPTER 1 - INTRODUCTION 1
CHAPTER 2 – LITERATURE REVIEW 6
PTOA after intra-articular fractures 6
Radiographic grading of PTOA 7
PTOA in Calcaneal Fractures 9
PTOA in Tibial Plafond Fractures 10
PTOA in Acetabular Fractures 11
Objective Measures of Acute Severity 12
Objective Measures of Surgical Reduction 15
Summary 19
CHAPTER 3 - METHODS 20
Improving measures of intraarticular injury severity 20
Fracture energy computation 20
Severity Computation 24
Articular comminution and area measurement 27
Normalized fracture severity study 30
Surface area-normalized fracture energy as a patient-specific predictor of PTOA risk in individual joints 32
Discrete element analysis 34
Analysis of results and PTOA development 35
Contact stress over-exposure in the tibial plafond after IAF 36
Contact stress over-exposure in the calcaneus after IAF 39
Contact stress over-exposure in the acetabulum after IAF 43
Statistical Models of injury severity and reduction 46
CHAPTER 4 - RESULTS 47
Contact area-normalized fracture energy as a predictor of PTOA risk: 47

Articular surface area-normalized fracture energy as a predictor of patient-specific PTOA development in individual joints 52
Contact stress over-exposure in the Tibia Plafond after IAF 59
Contact stress over-exposure in the calcaneus after IAF 66
Contact stress over-exposure in the acetabulum after IAF 74
CHAPTER 5 - DISCUSSION 82
Normalized Fracture Severity 83
Surface area-normalized fracture energy as a predictor of patient-specific PTOA development in individual joints 85
PTOA development in the Tibial Plafond after IAF 88
PTOA development in the Calcaneus after IAF 90
Contact stress over-exposure in the Acetabulum after IAF 94
Limitations 96
CHAPTER 6 - CONCLUSIONS 99
REFERENCES 101

LIST OF TABLES

Table 1. PTOA rates in joints of the upper and lower extremity after IAF 6

Table 2. PTOA rates and contact areas in the upper and lower extremity..... 31

Table 3. Comparison of surface areas and average contact areas in the lower extremity. 33

Table 4. Spearman correlations between objective measures of acute mechanical damage and PTOA status across fractures of the calcaneus, tibial plafond, and acetabulum. Significant correlations in bold. Coefficients are listed first followed by their p-value of significance. 55

Table 5. Spearman correlations between objective measures of acute mechanical damage and PTOA status across fractures of the calcaneus. Significant correlations in bold. Coefficients are listed first followed by their p-value of significance. 55

Table 6. Spearman correlations between objective measures of acute mechanical damage and PTOA status across fractures of the tibial plafond. Significant correlations in bold. Coefficients are listed first followed by their p-value of significance. 56

Table 7. Spearman correlations between objective measures of acute mechanical damage and PTOA status across fractures of the acetabulum. Significant correlations in bold. Coefficients are listed first followed by their p-value of significance. 56

Table 8. Results of logistic regressions of PTOA risk as predicted by the fracture energy in the top division in each table and by surface area-normalized fracture energy in the bottom division for all cases. For each regression, their respective parameter and odds ratio (OR) estimates are reported as well as a confidence interval of the OR. 56

Table 9. Results of logistic regressions of PTOA risk as predicted by the fracture energy in the top division in each table and by surface area-normalized fracture energy in the bottom division for the calcaneus. For each regression, their respective parameter and odds ratio (OR) estimates are reported as well as a confidence interval of the OR..... 57

Table 10. Results of logistic regressions of PTOA risk as predicted by the fracture energy in the top division in each table and by surface area-normalized fracture energy in the bottom division for the tibial plafond. For each regression, their respective parameter and odds ratio (OR) estimates are reported as well as a confidence interval of the OR. 57

Table 11. Results of logistic regressions of PTOA risk as predicted by the fracture energy in the top division in each table and by surface area-normalized fracture energy in the bottom division for the acetabulum. For each regression, their respective parameter and odds ratio (OR) estimates are reported as well as a confidence interval of the OR..... 58

Table 12. Spearman's correlations of all predictors and radiographic outcomes in the tibial plafond. Significant correlations in bold. 65

Table 13. Spearman correlation coefficients for predictors of PTOA in the subtalar joint after IAF of the calcaneus..... 73

Table 14. Spearman Correlation Coefficients between mechanical predictors of PTOA and potential confounders. 81

LIST OF FIGURES

Figure 1. Kellgren-Lawrence classification grades 1-4 demonstrated in the tibial plateau (modified from original to label different grades)[57]. 8

Figure 2. Tönnis grades 1-3 from the upper right to the lower right with grade 0, a normal hip, shown in the upper left. 9

Figure 3. The surface area for the fractured (red) and intact contralateral (green) are plotted along the length of the tibia. The total inter-fragmentary surface area is graphically represented by the blue area between the intact and fractured curves. The severe disruption and fragmentation visible in the fractured metaphysis illustrate comminution[1]. 14

Figure 4. Linear regression modeled Kellgren-Lawrence (KL) arthrosis scores as a function of a combined severity score[1]. 15

Figure 5. Semi-automated identification of bone fragments from preoperative CT imaging (colors represent each individually identified fracture fragment). 21

Figure 6. 3D surface models of the fractured bone for use in delineating intact and fractured surfaces so the interfragmentary fracture-liberated area could be quantified. 22

Figure 7. 3D models of the bone fragments are classified into intact and fracture liberated surfaces. 26

Figure 8. A graph cut was implemented to define the boundary between intact and fractured bone on each fragment so the fracture energy and articular fracture edge length could be computed. 26

Figure 9. Vastly different articular geometries of articular surface that required classifier re-training. 28

Figure 10. Subchondral energy measurement process. Previously classified (as intact or fracture liberated surface) articular fragments (left) have their subchondral surfaces identified through classification (middle), and subchondral energy is measured 10mm into the surface (shown in color on the right down to a plane marking 10mm into the bone) from the inverse of the average normal plane direction (shown with the arrow and two planes in the middle) of the articulation. 29

Figure 11. Contact stress (pressure) distributions on the superior dome of the talus after IAF of the tibial plafond. From the top left to the bottom right is heel-strike through toe-off of the 13 steps the stance phase of gait was discretized into. Top is anterior and left is lateral. 39

Figure 12. Alignment models segmented from weight-bearing CT with planes defining the appropriate alignment positions. 41

Figure 13. Inferior view of contact stresses on the talus after IAF of the calcaneus. From the top left to the bottom right are the 12 discretized steps of the gait cycle analyzed. The top is anterior and left is medial. 42

Figure 14. Patient-specific 3D models of the hip were generated from post-operative CT scans of the surgically reduced acetabular fractures. 44

Figure 15. The gait cycle was discretized into 13 quasi-static time steps (shown overlaid on one another to the left) with forces and rotations obtained form the Bergman gait data (right) [2]..... 45

Figure 16. Contact stress distributions are computed at each of the 13 loaded poses to replicate the entire stance phase of gait. 46

Figure 17. The distribution of fracture energies for calcaneal, distal tibial, proximal tibial, acetabular, and distal radial fractures. 47

Figure 18. The distribution of fracture energies for calcaneal, distal tibial, proximal tibial, acetabular, and distal radial fractures scaled by the average contact area for each joint. 48

Figure 19. High energy fractures have similar characteristics across joints with many fragments, significant comminution, and disruption of the articular surface. 49

Figure 20. A 4.29 J/cm^2 fracture of the distal radius and a 4.19 J/cm^2 fracture of the distal tibia. Similar scaled fracture energy values tend to have visually similar degrees of damage. 50

Figure 21. Fracture energies do not correlate with published rates of PTOA across the joints studied..... 50

Figure 22. Area-normalized fracture energies have a highly significant correlation with rates of PTOA. 51

Figure 23. Fracture energy and grade of radiographic arthritis. The Tönnis grade was used for the acetabulum and a truncated Kellgren-Lawrence grade (where grades 3 and 4 were combined) was used for the calcaneus and tibial plafond. 53

Figure 24. Area-normalized fracture energy and grade of radiographic arthritis. The Tönnis grade was used for the acetabulum and a truncated Kellgren-Lawrence grade (where grades 3 and 4) were combined was used for the calcaneus and tibial plafond. 53

Figure 25. Contact stress distributions on the talar dome after tibial plafond IAF reconstruction. Cases that developed PTOA tended to have more focal and higher peak contact stresses than cases that did not. 59

Figure 26. Contact stress over-exposure is highly correlated with PTOA outcomes in the tibial plafond after IAF reconstruction. 60

Figure 27. Correlations between measures of injury severity and radiographic outcomes in the tibial plafond. The area-normalized fracture energy, c, and the articular comminution, b, were normalized and combined equally to create the combined measure shown in d. 61

Figure 29. ROC curves for the tibial plafond of the combined injury severity measure, contact stress over-exposure, and the combined measure of injury severity and contact stress over-exposure. The AUC for each case is displayed on each graph. 62

Figure 28. Combined model of the best objective measures of injury severity and reduction accuracy in the tibial plafond. 62

Figure 30. Normalized fracture energy is not correlated with contact stress over-exposure in fractures of the tibial plafond. High levels of contact stress over-exposure and area-normalized fracture energy are associated with higher grades of radiographic arthritis (KL 0-1 are shown as small blue bubbles and KL 2-4 are shown as larger red bubbles). 64

Figure 31. A combined metric to estimate the severity of articular injury is not correlated with contact stress over-exposure in the tibial plafond. Low levels of contact stress over-exposure and injury severity are associated with forestallment of PTOA (small blue bubbles) while high levels of both either or both were associated with PTOA development (large red bubbles). 64

Figure 32. Differences in the maximum contact stress patches shown between a case that did not develop PTOA and a case that developed severe PTOA. 66

Figure 33. Contact stress over-exposure is correlated with PTOA outcomes after IAF in the calcaneus. 67

Figure 34. Correlations between measures of injury severity and radiographic outcomes in the calcaneus after IAF. The area-normalized fracture energy, c, and the articular comminution, b, were normalized and combined equally to create the combined measure shown in d. 68

Figure 35. Combined model of the best objective measures of injury severity and reduction accuracy in reconstructed IAFs of the calcaneus. 69

Figure 36. ROC curves for the calcaneus of the combined injury severity measure, contact stress over-exposure, and the combined measure of injury severity and contact stress over-exposure. The AUC for each case is displayed on each graph. 70

Figure 37. Normalized fracture energy is not correlated with contact stress over-exposure in the calcaneus. Cases that have low contact stress over-exposures demonstrate a lesser degree of radiographic arthritis (demonstrated by the larger red bubbles). 71

Figure 38. Combined severity measure is not correlated with contact stress over-exposure in the calcaneus. Cases that have low severity and contact stress over-exposures demonstrate lesser degrees of radiographic arthritis (demonstrated by larger red bubbles). 72

Figure 39. The contact stress over-exposure distributions for the patients who had developed PTOA at two years after surgery were substantially more focal and had significantly higher peak values. 75

Figure 40. Contact stress over-exposure is correlated with PTOA outcomes after IAF of the acetabulum. 76

Figure 41. Correlations between measures of injury severity and radiographic outcomes in the acetabulum after IAF. The area-normalized fracture energy, c, and the articular comminution, b, were normalized and combined equally to create the combined measure shown in d. 77

Figure 42. Combined model of injury severity and reduction accuracy predicts PTOA development in the acetabulum. 78

Figure 43. ROC curves for predictors of PTOA development in acetabular fractures. The combined measure of injury severity, the measure of contact stress over-exposure, and the combined measures of injury severity and contact stress over-exposure were plotted from left to right. 78

Figure 44. Normalized fracture energy is not correlated with contact stress over-exposure in fractures of the acetabulum. High levels of contact stress over-exposure and area-normalized fracture energy are associated with higher grades of radiographic arthritis (KL 0-1 are shown as small blue bubbles and KL 2-4 are shown as larger red bubbles). 79

Figure 45. A combined metric to estimate the severity of articular injury is not correlated with contact stress over-exposure in the acetabulum. Low levels of contact stress over-exposure and injury severity are associated with forestallment of PTOA (small blue bubbles) while high levels of both either or both were associated with PTOA development (large red bubbles). 80

TABLE OF NOMENCLATURE

	Unit of measure	**Description**
Fracture energy	Joules	The energy involved in liberating surface area during a fracture based upon the strain energy release rate and Hounsfield Unit intensity. Used to objectively assess the severity of injury.
Contact area-normalized fracture energy	Joules/cm^2	Averaged fracture energy as scaled to literature values of contact area. Used to control for differences in the area over which energy is transmitted across the joint. Estimates damage on a per unit area basis to help control for highly varied anatomy.
Normalized fracture energy	Joules/cm^2	Articular surface area normalized fracture energy. Scaled to articular surface areas that receive primary loading from impacts as classified on segmentations from CT scans. Differentiated from the contact area-normalized fracture energy by enabling use on a patient-specific basis. Also estimates damage on a per unit area basis.
Articular comminution energy	Joules	Fracture energy dispersed within 1 cm of the joint surface. Measured by projecting a plane 1 cm from the average normal direction of the articular surface in each fragment. Used to estimate the energy dissipated across the articular surface.
Contact stress	MPa	The forces between two mated articular surfaces distributed over discrete areas.
Contact stress over-exposure	MPa*s	The magnitude of contact stress over a given damage threshold scaled by the amount of time per gait cycle that it is exposed to those stresses. Used to assess residual incongruity and predict cartilage degeneration.

PREFACE

The purpose of this work was ultimately to determine the effects of injury severity and surgical reduction accuracy on patient outcomes after intra-articular fracture. This first necessitated creating improved measures of injury severity that could be utilized across joints. Therefore, the substantial development burden described within details the progression from fracture energy providing inadequate correlations with post-traumatic osteoarthritis (PTOA) across joints, to improving predictions by controlling for damage per unit area, and, ultimately, to including a measure of articular comminution in order to create a more comprehensive combined measure of injury severity that best describes PTOA risk for comparing against measures of surgical reduction accuracy. The surgical reduction accuracy was quantified by a more proven measure, the contact stress over-exposure. Development of this measure described in this document built upon an established model in the ankle, validated preliminary work in the hip, and new model in the calcaneus. The results and discussion sections explore the data first from a context of establishing the new measures of injury severity then move toward determining the relative contributions of injury severity and reduction accuracy to patient outcomes.

CHAPTER 1 - INTRODUCTION

The management of intra-articular fractures (IAFs) represents a common but challenging task for orthopedic traumatologists, especially when bone fragments are substantially displaced from their native anatomical position. IAFs are characterized by extension into the joint that causes disruption of the smooth articular surface. Surgical management aims to provide stable fixation of fragments in an anatomically reduced position to ensure osseous union and restore the native mechanical environment of the joint. One of the basic tenets of fracture care is that the smooth articular surface must be precisely restored, although the literature suggests that the requisite degree of precision varies by joint. The task of achieving this precise restoration of anatomy is made more challenging by a number of frequently concurrent complexities of IAFs like higher energy mechanisms that create more fragments, comminution, and displacement[1, 3-5].

IAFs are associated with rates of arthritic development up to 20 times higher than extra-articular fractures as damage to the joint is followed by rapid degeneration to post-traumatic osteoarthritis (PTOA)[6]. PTOA represents the end stage organ-level failure of an injured joint [7]. It creates a tremendous burden for the patients and the economy, with disability comparable to end stage heart failure and annual healthcare costs in the U.S. estimated to exceed $12 billion[8]. Despite the prevalence, cost, and investment in new techniques and medicine over the past 50 years, the rates of PTOA following IAF have not substantially declined[7]. The reasons are multifactorial but most probably involve under-appreciated factors in PTOA pathogenesis.

Our best understanding of PTOA pathogenesis after IAFs can be described by the three primary components of its onset and progression: the acute articular injury, the surgical reduction

accuracy, and the resulting pathobiological responses to the first two factors. The acute articular injury results directly from the injurious event and is described as the degree of damage to the joint brought about by the initial impact. The surgical reduction accuracy can be thought of as ameliorating the chronic components of IAF damage. Poor reductions can adversely impact the mechanical environment of the joint after the fracture with mal-reduced fragments after fixation altering the location, magnitude, and duration of stresses from those of a normal joint [3]. These changes frequently result in the progressive degeneration of articular joints. Pathobiological contributions to PTOA development result from the inability of the joint as an organ to restore homeostasis and can lead to failure of the joint[9]. Restoration of homeostasis is impeded by things like the residual incongruity and harmful biological responses to severe acute injuries [10, 11]. Though these three constitutive components of PTOA pathogenesis are known, and the pathomechanical components are the focus of treatment, their relative contributions to PTOA risk remain largely unknown.

Acute injury severity is widely known to influence PTOA risk after IAF but is not always considered as an independent explanation of poor patient outcomes. As more severe fractures require more challenging surgical restorations, it has been proposed that PTOA may result primarily from surgical mal-reduction. Unfortunately, there are no clinically available methods to objectively assess this important factor in a way that would enable determination of its relative contribution to patient outcomes. Instead, fracture severity assessment has relied upon joint-specific categorical fracture classification systems that suffer from poor inter-observer reliability [12, 13]. The most useful clinical classification systems focus on categorizing fractures according to various features of articular fractures that can be readily identified from radiographs or CT scans. Typically, these features include: the number of fractures, their relative locations in

the bone—especially the proximity and interaction with the articular surface, and the amount of fragment displacement. Such features, however, are not amenable to reliable and objective assessment and have failed to provide contextual information on PTOA risk.

To remedy these shortcomings, novel CT-based analysis methods have been developed to aid in the objective quantification of IAF severity[1, 14-20]. The origin of these methods was the clinical axiom that "the extent of bone, cartilage, and soft tissue damage is directly related to the energy imparted to these structures"[21]. In the case of a brittle solid, this energy can be directly related to the amount of fracture-liberated surface area and the density of the material fractured. At the high rates of loading seen in fracturing events, bone behaves as a brittle solid, and the fracture-liberated surface area and bone density can both be determined from CT scans [16, 20]. Therefore, the amount of energy in a fracture can be determined from clinically available data. This approach was originally developed using laboratory models (first, a dense polyether-urethane foam surrogate material, then in bovine bone segments) and subsequently extended for use in human clinical series[15-18]. Over the past decade, these techniques were further developed to enable large scale study of fracture severity in the clinical research setting[19, 22]. This presents an opportunity to objectively study the influence of acute fracture severity on PTOA.

Chronic pathomechanical factors, often resulting from surgical mal-reduction, are the most thoroughly studied and treated causes of PTOA progression[3, 23-27]. Mechanical factors under surgical control involve everything from ligament reconstruction to joint alignment and restoration of surface congruency. For this reason, it has been thought that cases progressing to PTOA do so primarily from a failure to adequately restore normal joint mechanics. Literature has even suggested that precise fracture reductions with step-offs less than 2mm are necessary to

achieve optimal restoration and forestall PTOA[28-30]. However, it is known that different joints—and even different regions within the same joint—can respond differently to IAFs. For example, there is clinical evidence that the accuracy of reduction as measured by step-off after an acetabular or tibial plafond fracture is highly correlated with outcomes while, by comparison, incongruities of the tibial plateau are well-tolerated[3, 28, 29, 31, 32]. Because of these inconsistencies, what constitutes optimal management of IAFs is frequently debated with arguments based more on anecdotal observation and intuition rather than on rigorous scientific evidence[7].

Recently, patient-specific computational modeling methods to estimate joint contact stresses have been developed to provide objective evidence through which the chronic mechanical environment of the joint can be evaluated[25, 33, 34]. Such models can help address the questions outlined above and definitively answer what constitutes adequate or even optimal surgical management. Preliminary studies have demonstrated significant correlations between quality of surgical reduction, as measured by contact stress, and PTOA development. However, there are cases with well-reduced fractures that still develop OA. This brings us back to the central question: if surgical methods are improving, why aren't PTOA rates decreasing? The most logical conclusion is that the acute severity of injury plays a larger role in PTOA risk than has been previously appreciated.

Despite a high likelihood of interplay between the three factors, there is a paucity of published evidence examining their relative contributions in any objective manner.Pathomechanical factors, for example, cannot be considered without accounting for the acute severity and pathobiological responses. If a joint has a high amount of damage from acute fracture severity, the surgery is more challenging and thereby less likely to restore surface

congruity, leading to chronic joint pathomechanics. Conversely, poor surgical restorations also contribute to the PTOA rates seen when studying a spectrum of acute fracture severities as the more severe fractures are more likely to have poor restorations. Tying these factors together are the pathobiological responses that serve to potentiate PTOA as a disease as a direct result of these acute and chronic factors. For acute severity, in 2011, Tochigi et al. found that chondrocyte death propagates from the fracture edges[9]. Coleman followed this up with studies that outlined potential mechanisms of action for both acute and chronic factors related to chondrocyte respiratory function that cause cartilage degeneration toward PTOA[10, 11, 35]. These works have demonstrated an opportunity for intervention as we begin to understand potential methods to treat not only the chronic factors surgically, but the acute factors biologically[35].

It is in this context that the present work was performed to develop methods that enable injury severity and reduction accuracy to be well characterized in individual patients in order to study their relative contributions to PTOA risk. Method development was driven by two hypotheses. The first hypothesis is that the severity of articular injury correlates with reduction accuracy. It was posed to determine if this long held notion has an objective mechanical basis. The second hypothesis is that the injury severity more greatly influences PTOA risk than the reduction accuracy. This hypothesis is founded in the context of stagnant PTOA rates after injury despite ostensibly improved surgical care. These questions are central to the future of IAF treatment and could potentially have different answers in the context of different joints.

CHAPTER 2 – LITERATURE REVIEW

PTOA after intra-articular fractures

The clinical management of displaced IAFs focuses primarily on the surgical reduction and stabilization of articular fragments. However, even in the best of hands, an IAF still frequently leads to disabling PTOA. IAF commonly occurs in the hindfoot, ankle, knee, hip, and wrist; after IAF, PTOA occurs in 25-85% of these joints (Table 1). Across joints of the upper and lower extremities, the incidence of PTOA has remained stubbornly unchanged despite decades of improvements in technology and surgical management[7]. Marsh et al. 2002 first questioned the assumption that excellent surgical restoration will prevent PTOA, asking whether anatomic reduction improves outcomes. If it does not, then the acute severity of fracture may explain why PTOA rates have not changed.

Table 1. PTOA rates in joints of the upper and lower extremity after IAF

Site of IAF	PTOA Rate
Calcaneus[36-38]	85.7 (60.4-95.4%)
Distal Tibia[39-41]	48.1 (40.8-74.0%)
Proximal Tibia[42-45]	24.5 (11.0-36.5%)
Acetabulum[3, 29, 46]	27.9 (12.0-39.5%)
Distal radius[47-49]	43.4 (35.0-73.0%)

The idea that PTOA risk after IAF is related to the fracture type and its severity is widely held, even across different surgical treatment approaches[3, 50, 51]. Clinical assessment of IAF severity is most often completed using categorical classification systems or rank ordering for study of severity within a series. Using these techniques, some have even found that initial

severity may be the primary determinant of PTOA development[51-55]. Conversely, it has also been found that different joints and even different areas within joints have different tolerances for articular reduction, most often quantified through step-off and gap measurements that are, unfortunately, insensitive and unreliable. Despite this limitation in measurement capability, articular reduction has been demonstrated to be an important factor in PTOA outcomes of acetabular fractures, with step-offs greater than 1 mm having fewer good clinical results[29]. By comparison, tibial plateau fractures are very tolerant of reduction inaccuracy with step-offs greater than 10mm showing acceptable functional results[3]. In other IAFs, like those of the tibial plafond, the impact of reduction is less clear with reduction being closely associated with injury severity. The fractures subjectively judged as most severe were considered to have the worst reductions while the cases that were least severe had the best reductions[55, 56]. This makes the impact of reduction challenging to disentangle from the injury severity. Therefore, in order to understand the development of PTOA and identify optimal strategies to treat it in each joint, careful, objective measurements are required along with knowledge of the general idiosyncrasies of each joint's characteristic tolerance to injury and reduction.

Radiographic grading of PTOA

Radiographic grading of osteoarthritis is also necessary in the study of PTOA development. The Kellgren-Lawrence (KL) classification system is a common scale used for grading osteoarthritis in articular joints. It is a widely accepted measure of arthrosis and has been shown to have good inter-observer reliability[57]. The KL classification is graded from 0 to 4 with grade 0 showing no signs of osteoarthritis, grade 1 having doubtful presence of joint space narrowing and osteophytes, grade 2 with definite narrowing and osteophytes, grade 3 with multiple osteophytes, definite narrowing, some sclerosis and possible deformity, and grade 4

presenting as large osteophytes, marked narrowing of the joint space, and severe sclerosis with definite deformity of the bone (Figure 1). Grades 2 and above are typically considered to mark the presence of PTOA development after injury.

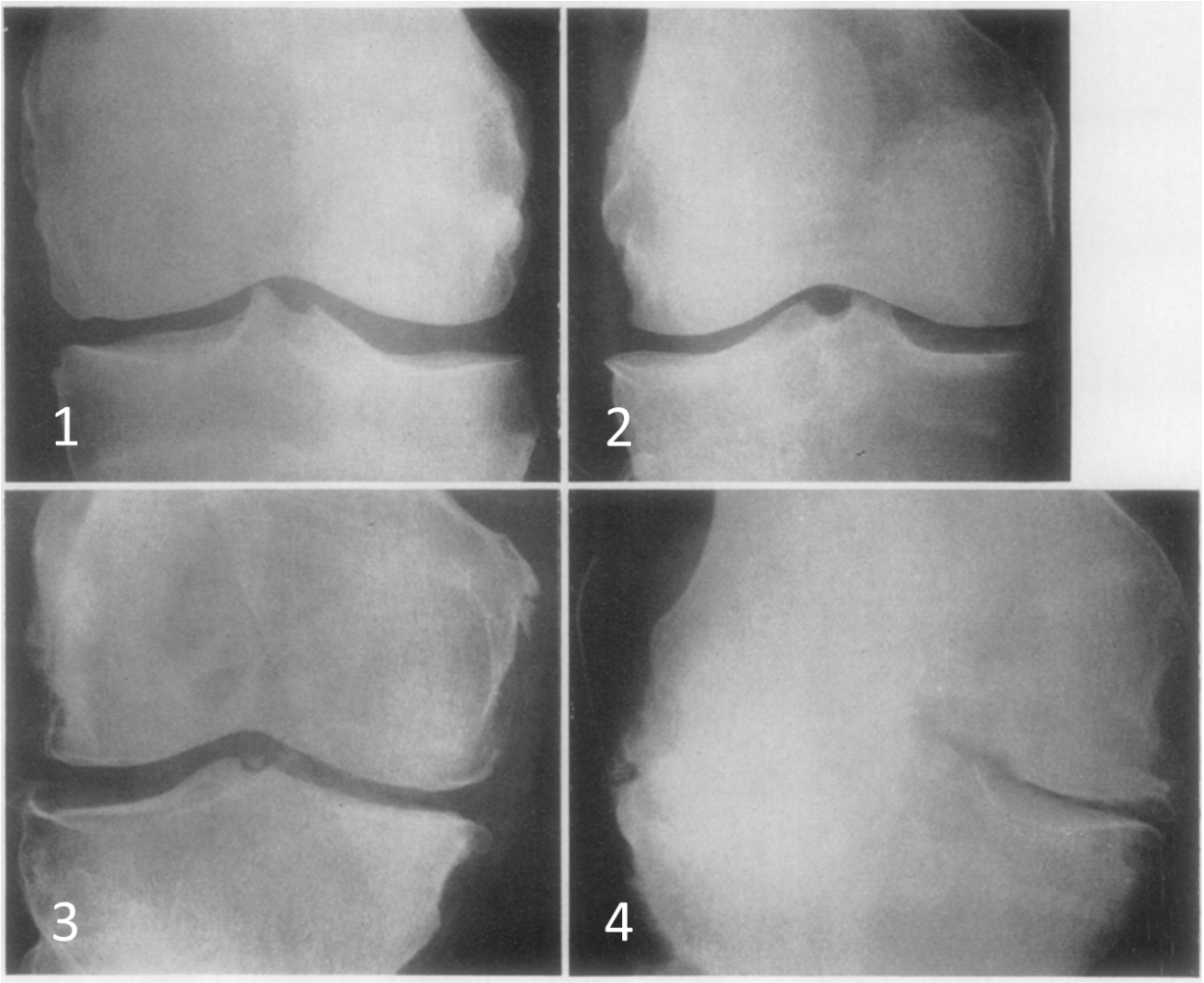

Figure 1. Kellgren-Lawrence classification grades 1-4 demonstrated in the tibial plateau (modified from original to label different grades)[57].

The Tönnis classification is another commonly used measure of radiographic arthritis that was specifically created for the hip. It is graded from 0 to 3 with grade 0 having no arthritis, grade 1 having increased sclerosis, minor joint space narrowing and no or minor loss of head sphericity, grade 2 having small bone cysts, moderate joint space narrowing and moderate loss of head sphericity, and grade 3 representing severe arthritis with large bone cysts, severe joint space

narrowing/obliteration and severe deformity of the femoral head[58, 59] (Figure 2). Grades 2 and above are considered to indicate the presence of PTOA development but, occasionally, grade 1 has also been used.

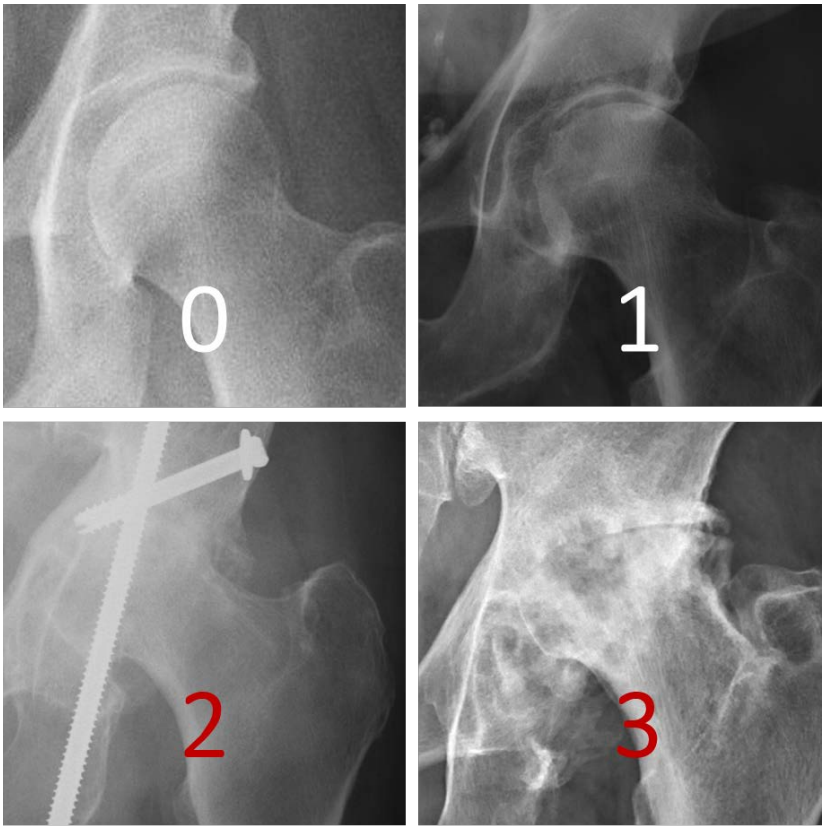

Figure 2. Tönnis grades 1-3 from the upper right to the lower right with grade 0, a normal hip, shown in the upper left.

PTOA in calcaneal fractures

Perhaps in no other joint is injury severity considered as central to PTOA outcomes as in the hindfoot after displaced intra-articular calcaneal fractures (DIACFs). Sanders et al. developed a classification for DIACFs based on evaluation of the number of fracture lines traversing the posterior facet[60]. In the original study, this Sanders classification was demonstrated to have a strong correlation with outcomes, with 73% of type II fractures repaired by open reduction and

internal fixation having good clinical results compared to only 9% of type IV fractures that were similarly treated. A subsequent study of long-term follow-up found significant differences in rates of subtalar fusion between type II and III fractures with 47% of type III fractures requiring fusion compared to only 19% of type II fractures[38]. Comparing radiographic grading of arthritis, 70% of type II fractures and 90% of type III fractures had the highest two grades of arthritis. These findings are of particular interest as 95% of fractures were reported as having anatomic reduction postoperatively, defined as a step-off between 0 and 1 mm, indicating that differences in long term outcomes were due to differences in the initial injury. A study by Rao et al. found similar correlations in percutaneously reduced fractures with 46% of patients having Sanders type I or II fractures and 77% of those having type III and IV fractures developing PTOA. In this study, however, positive correlations that trended toward significance were observed between post-reduction step-off and both KL grade and Sanders classification. This could implicate surgical reduction as contributing to at least a small component of PTOA risk in DIACFs.

PTOA in tibial plafond fractures

Contributors to the development of PTOA after IAF in the tibial plafond are more complicated. Some clinical evidence has found reduction accuracy to be strongly correlated with PTOA development[61]. Mechanical studies have also found elevated contact stresses from mal-reduced fractures to be predictive of PTOA development[25]. Other clinical studies by DeCoster et al. found no difference in outcomes of patients with good and poor reductions[55]. A study by Etter and Ganz suggests that there are other factors at play as perfect reductions did not guarantee good outcomes[52]. But, as Marsh et al. noted, “one of the biggest challenges for research on the effect of articular reduction is to disentangle the effect of injury to the articular

surface from … the reduction."[62] This is particularly true in the tibial plafond where there also exists a significant correlation between initial injury and outcomes. Studies of rank ordering of reduction quality and initial severity, and PTOA grade found significant correlations with both [55, 56]. Therefore, without the ability to accurately assess the degree of initial injury or the degree to which loading characteristics have been altered, it will not be possible to determine the influence of reduction quality on PTOA risk in fractures of the tibial plafond.

PTOA in acetabular fractures

Acetabular fractures, like calcaneal fractures, have a much clearer association between outcomes and predictors. In acetabular fractures, the literature provides a significant amount of evidence that accurate reduction is paramount in forestalling PTOA development[29, 63-66]. Matta was the first to classify acetabular reduction by measuring the residual incongruity between fragments as a step-off. His work established anatomic reduction as ≤1 mm of maximal articular displacement on any plain radiograph[65]. Reduction between 1 and 3 mm was considered satisfactory while reduction >3mm was unsatisfactory. For these three grades, he observed that anatomic reduction had 83% good clinical results while satisfactory had 68%; unsatisfactory reduction achieved good clinical results only 50% of the time. Subsequent studies found similar results with poor reductions strongly correlating to poor outcomes[27, 29, 66-68].

Despite significant study of reduction and outcomes in acetabular fractures, the effect of injury severity on acetabular fracture outcomes independent of reduction is unclear. Tannast, Najibi, and Matta studied the survivorship of 810 patients with operatively treated acetabular fractures but did not find significant differences in the survivorship by fracture type[27]. They did, however, find lower survivorship for cases having greater than 20 mm of initial displacement but did not report a correlation between reduction and displacement that may

confound these results. Briffa, Pearce, Hill, and Bircher reported certain fracture types, specifically posterior column and T-shaped fractures, to have a statistically significant negative impact on outcomes[68]. Combined posterior wall and T-shaped fractures fared the worst. They claimed "[W]e may be reaching the limit of our operative capabilities, suggesting that the biology of the fracture (primary articular cartilage damage) has now become the limiting factor." However, they again did not report correlations between injury type and reduction in their series highlighting the need for objective measurement of both injury and reduction in clinical series to definitively determine their relative contributions.

Objective measures of acute severity

As detailed in the previous sections, PTOA risk is widely held to relate to fracture type and its severity, even across joints and different surgical approaches. However, none of the clinically available methods for assessing IAF injury objectively assess the severity of fracture. Instead, clinical fracture severity assessment has relied upon joint-specific categorical classification systems that have poor inter-observer reliability. As such, they fail to provide a consistent and continuous contextual indication of fracture severity as it relates to PTOA risk. To remedy these shortcomings, previous work was undertaken to objectively quantify IAF severity in a continuous manner. The methods were based upon the principle that mechanical energy is required to create new free surface area when fracturing a brittle solid and that the amount of energy required is directly related to the amount of de novo surface area. This approach was originally developed using laboratory models (first, a dense polyether-urethane foam bone surrogate material[17, 18] and then bovine bone segments[16]) and subsequently extended it to use in human clinical cases[15]. Over the past decade, these techniques have been further developed to enable larger-scale study of fracture severity in the clinical setting[1, 19, 20, 37].

Methods for computing fracture energy were originally developed using pre-operative CT scans of articular fractures along with their intact contralateral bones[1, 14, 20]. Idiopathic OA is rare in the ankle whereas PTOA commonly presents within a few years of tibial plafond fracture. This high propensity for PTOA makes study of these plafond fractures ideal for identifying factors that predispose joints to degeneration while avoiding potential confounding variables. These methods, therefore, segmented the boundary of all tibial fragments and on the intact contralateral to compute the surface area difference between them (Figure 3). The fracture energy was quantified by relating the energy absorbed to this computed fracture-liberated surface area and scaling it to account for variation in bone density. Articular comminution was quantified by determining the amount of inter-fragmentary surface area present within 1.5mm of the articular surface expressed as a percentage of the intact area on the same region of the contralateral distal tibia.

In these original studies, Thomas et al. found that fracture energies ranged from 5.2 to 27.2 Joules, and the articular comminution from 51 to 156%[1]. There were significant differences in fracture energy and articular comminution between the 11 patients that developed moderate to severe OA (KL≥2) and the 9 who did not (KL≤1). A combined injury severity score of both fracture energy and articular comminution was found to be highly correlated with PTOA development (R^2=0.70, Figure 4).

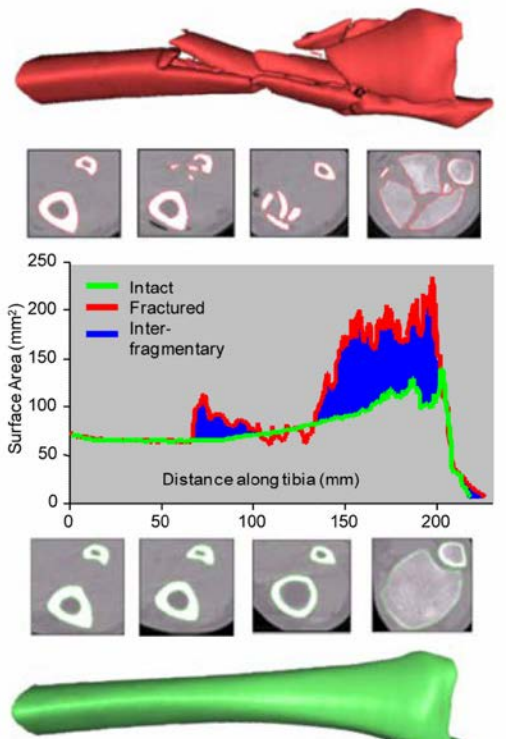

Figure 3. The surface area for the fractured (red) and intact contralateral (green) are plotted along the length of the tibia. The total inter-fragmentary surface area is graphically represented by the blue area between the intact and fractured curves. The severe disruption and fragmentation visible in the fractured metaphysis illustrate comminution[1].

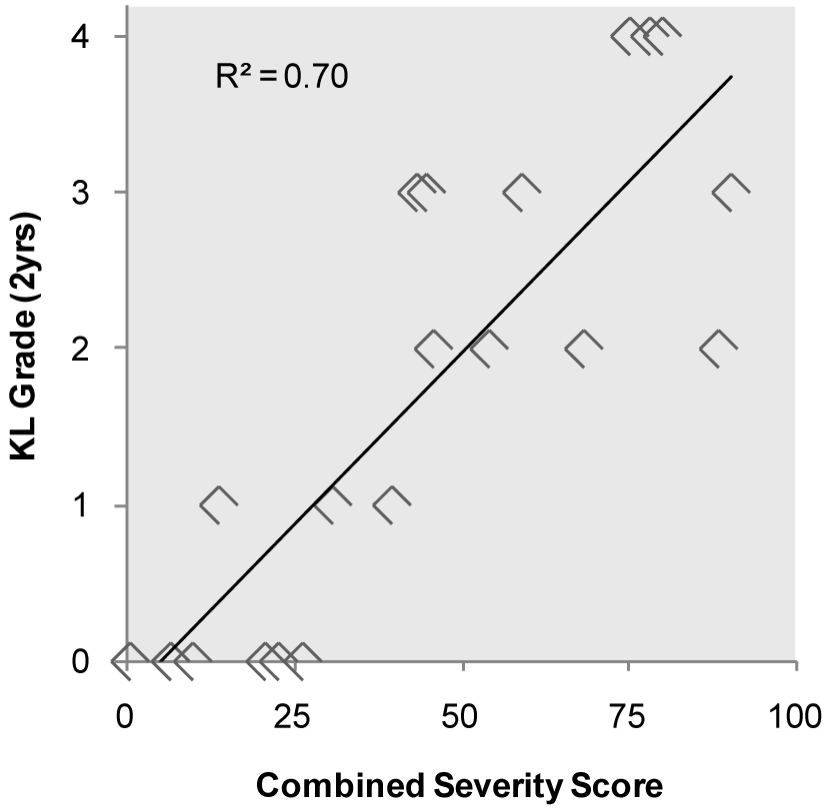

Figure 4. Linear regression modeled Kellgren-Lawrence (KL) arthrosis scores as a function of a combined severity score[1].

These results established fracture energy as an objective tool through which injury severity can be assessed. However, though their general concepts are translatable, the methods employed for measuring fracture energy and articular comminution were joint specific. They required an intact contralateral datum with which to compare liberated surface areas. Therefore, additional development was required to enable objective assessment of severity through fracture energy and articular comminution in joints outside of the tibial plafond.

Objective measures of surgical reduction

Though the pathogenesis and etiology of PTOA is not well understood, chronic exposure to elevated contact stresses resulting from residual articular surface incongruity have been

implicated as an important mechanical factor. Surgical reduction is frequently assessed in literature by measuring the step-off or gapping left after fixation. These measures are understood to merely be surrogates for assessing the altered mechanical environment of the joint. Hadley, Brown, and Weinstein were among the first to report the adverse effects of elevated contact pressure on long term outcomes of hips[69]. Maxian, Brown, and Weinstein followed these results and were the first to establish preliminary thresholds for contact stress tolerance in cartilage of the human hip[70].

Anderson et al.'s work was the first to attempt quantification of these deleterious contact stress over-exposures using patient-specific finite element analysis (FEA)[71, 72]. Again, this work used IAFs of the ankle as a useful model due to the joint's low incidence of idiopathic PTOA and high incidence of PTOA within a few years of injury. This work quantified differences in contact stress exposures for fractured and intact contralateral ankles, identifying a strong correlation between the development of radiographic PTOA, as measured by KL grading two years postoperatively, and contact stress exposure.

Contact stress exposure was calculated across the tibial articulating surface using the following equation:

$$\hat{P}_{cumulative} = \sum_{i=1}^{13}((\hat{P}_i - P_d)\Delta t_i)$$

where $\hat{P}_{cumulative}$ was the spatial distribution of per-gait cycle cumulative contact stress over-exposure, expressed in MPa-seconds; $\hat{P}_i$ were the computed contact stress magnitudes at each node, with i varying across 13 loading increments over the stance phase of gait; $P_d$represented the scalar contact stress damage threshold taken only from those nodes where $\hat{P}_i$ was greater than

P_d, nodes where $\hat{P}_i$ was less than P_d where excluded from analysis; and Δt_i was the time, in seconds, associated with a given increment in the gait cycle.

In these studies, however, it has remained unclear whether injury severity remains linked to poor reductions or whether accurate reduction of the articular surface can improve patient outcomes. Larger cohorts of subjects are required to sufficiently answer these questions but model building in FEA is cumbersome and articular contact remains a challenge. This is especially true in cases where residual incongruities of the articular surface require substantial effort to be expended in mesh generation. To resolve these problems, Kern and Anderson developed a discrete element analysis (DEA) contact model of articular fractures[33].

DEA models contact between cartilage surfaces as a bed of compressive-only springs distributed over an implicit (not explicitly included in computation) rigid bony surface. While FEA runs take on the order of hours, run time for DEA models take on the order of minutes, facilitating patient-specific modeling. Kern and Anderson expanded its use to report contact in both intact and fractured human ankles. In this DEA formulation, surfaces were triangulated and springs along the contact surface were oriented along each triangular face's surface normal, with an un-deformed length equal to its associated cartilage thickness. The cartilage surface was modeled as a bed of compressive springs spanning from the articular surface to a rigid attachment at the implicit underlying subchondral bone surface. Contact was defined between intersections of apposed surfaces. Within intersecting regions, compound springs were created across the total cartilage thickness of the joint. Each spring responds according to Hooke's law:

$$f = kd$$

where f is the force exerted by the spring along its normal direction, d is the spring deformation, and k is the spring constant as a function of the cartilage Young's Modulus, E, Poisson's ratio, v,

the length of the spring created from combined articular cartilage thicknesses, *l*, and the area of the spring's associated triangular surface, *a*, where

$$k = \frac{(1-v)E}{(1+v)(1-2v)}\frac{a}{l}$$

They validated DEA-computed contact stress using previously reported human cadaveric data[73]. Finally, they confirmed the utility of DEA contact stress computation in place of FEA for determining PTOA risk from contact stress over-exposures. A subsequent validation study was also performed for a model of contact stress in acetabular fractures by Townsend et al.[74].

Summary

Up to now, study of the interplay between acute and chronic mechanical factors has been limited due to the lack of ability to rapidly and objectively assess the pre-operative severity of the fracture and the postoperative mechanical environment of the joint. Fractures of the tibial plafond have proven useful in establishing objective methods that can achieve this goal by analyzing both acute and chronic mechanical contributors to PTOA development on a patient-specific basis. With the advent of fracture energy analysis and patient-specific discrete element analysis, we are now able to more comprehensively evaluate the interplay of these factors and to determine their relative contributions to patient outcomes across joints. This offers the unique opportunity to answer lingering questions posed in each joint as to the relative role that initial injury severity vs. surgical reduction quality play in PTOA risk. Specifically, we will seek to address two hypotheses: that severity of IAF fracture correlates with reduction quality and, subsequently, that the acute mechanical damage more greatly influences PTOA. To test these hypotheses, we will expand upon previous methods to create DEA models with relevant boundary conditions in the hip, ankle, and hindfoot as well as to develop and implement measures of fracture severity that can be utilized in all these joints. In conjunction with the recent investigations elucidating the pathobiological changes and mechanisms of PTOA development, this work aims to leverage patient-specific assessment capabilities toward a unifying understanding of all mechanical aspects of PTOA development.

CHAPTER 3 - METHODS

Improving measures of intraarticular injury severity

Fracture energy and articular comminution were previously established as objective measures of injury severity in the tibial plafond that are predictive of PTOA risk. It remained to be determined, however, whether these injury severity measures are likewise predictive of PTOA risk in other joints. To answer this question, major limitations of the previous analysis methods had to be addressed. Specifically, this involved eliminating the need for an intact contralateral datum and expediting the analysis time. Methods from work detailed below formed the foundation for establishing a fracture energy measure that could be extended to any joint. The following section will detail these methods and how they were expanded upon.

Fracture energy computation

The fracture energy computation requires 3d surface models of fractured bone. This involves segmenting CT scans of the fractured limbs to identify and separate bone fragments. Individual bone fragment volumes were identified using a semi-automated watershed transform-based algorithm implemented in MATLAB (The Mathworks, Natick, MA, USA) from purpose written code originally developed by Thomas, Kern, and Anderson [75]. Errors in separation of fragments were corrected using a custom graphical user interface written in MATLAB. From these segmentations, 3d models were produced and analyzed to identify new surfaces of bone liberated by the fracturing process. The procedure for identifying these surfaces relied heavily upon a surface classification algorithm trained to recognize fracture liberated surfaces based upon geometric and image intensity features (detailed below).

After segmenting bone fragments from CT scans, the resulting segmentations, stored as NIFTI files, were loaded into ITK-SNAP to correct errors and inconsistencies in the segmentation. After corrections were completed, ITK-SNAP was utilized to export all fragments as individual binary STL models, the 3d model format later used in delineating intact and fractured surfaces so that the interfragmentary fracture-liberated area could be quantified (Figure 5).

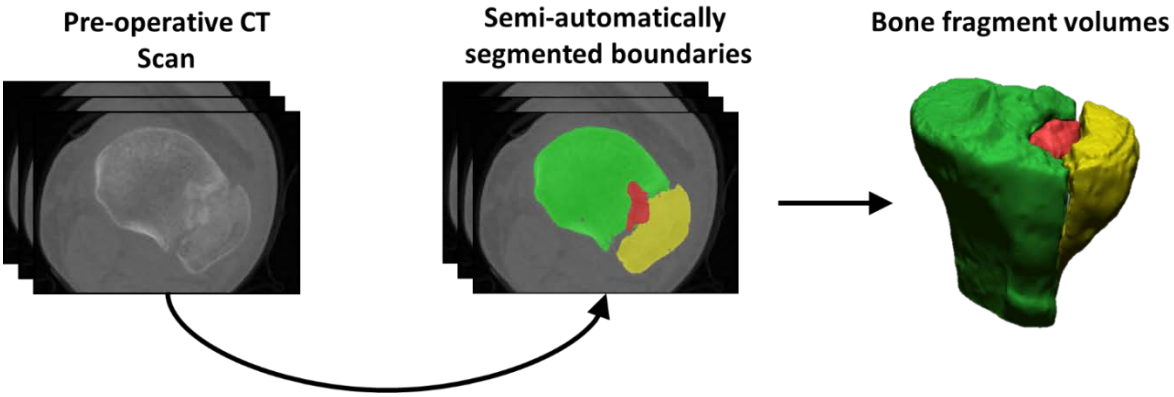

Figure 5. Semi-automated identification of bone fragments from preoperative CT imaging (colors represent each individually identified fracture fragment).

STL models were then imported into Geomagic Design X (3DS Systems, Rock Hill, SC), where a smoothing process was used to remove stair-step artifacts from the voxellated segmentations and a decimation routine was used to attain a more accurate representation of the bony surface in preparation for subsequent fracture severity computation. Each properly prepared STL surface file of a fracture fragment was then saved to be imported into the MATLAB bone surface classification algorithm (Figure 6 and Figure 7).

The classification of separate bone surfaces was performed to distinguish inter-fragmentary bone from intact bone to use in the subsequent computation of severity. Several optimally segmented and prepared sets of intact and fractured bone were painstakingly manually

identified to be used in training a classifier implemented through the MATLAB function 'predict'. This function implements the results of several machine learning classification strategies and options after training. Specifically, an ensemble of bagged decision trees was eventually used based on the promise it exhibited in preliminary studies. Bootstrap aggregation (bagging for short) is a powerful ensemble method that combines predictions from different machine learning models together to make a more accurate prediction than the constituent individual models. Bootstrap aggregation is generally applied to reduce the variance for algorithms that have high variance like the decision trees implemented herein. Initial training of the models was also performed in MATLAB using the 'fitensemble' function with the 'bag' option for classification using more than three predictors.

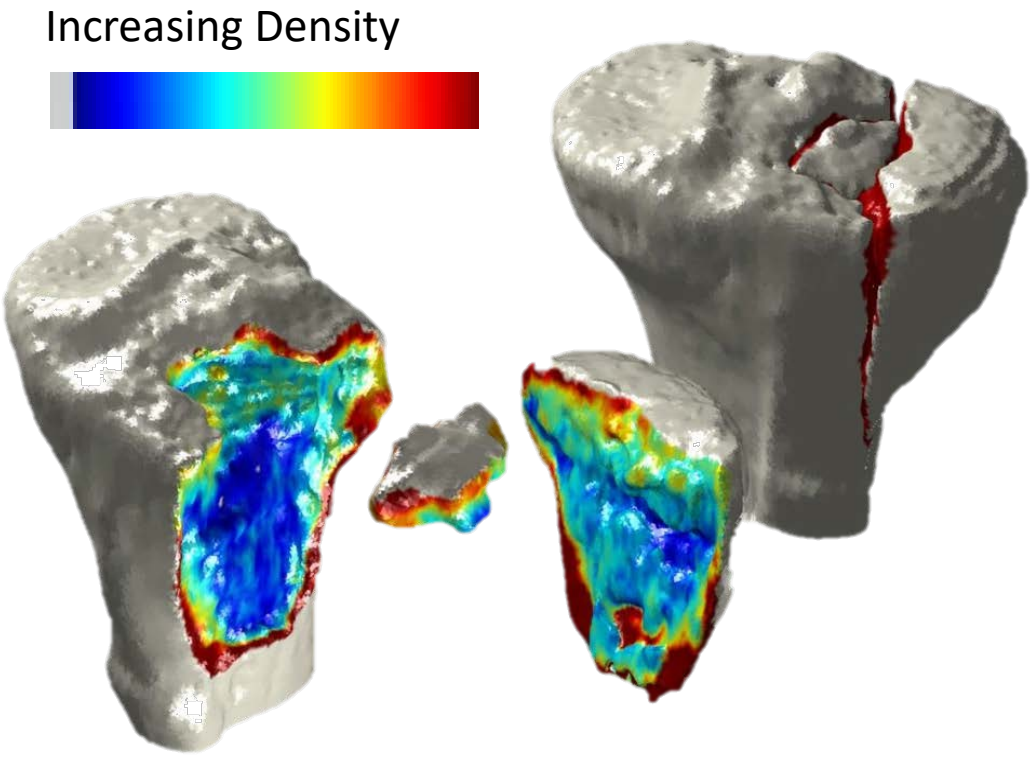

Figure 6. 3D surface models of the fractured bone for use in delineating intact and fractured surfaces so the interfragmentary fracture-liberated area could be quantified.

There were eight features selected for the classifier training task to aid in the optimal separation of intact and fractured bone surfaces. There were six image intensity-based features and two geometry-based features. The image intensity-based features were CT Hounsfield units, the image sheetness (second derivative of image intensity), and variations of the two at different depths from the normal direction of the bone model surface. The image sheetness is capable of detecting both direction and magnitude of edges, contrasted against original CT data. Obtaining the CT Hounsfield units was accomplished by sampling into the CT image at five depths along the normal direction of the surface of the STL model from 0mm to 2mm at 0.5mm intervals at each vertex. The mean, standard deviation, and difference in HU between the 0mm and 2mm depths were computed on the normal image and sheetness image and constituted the six image intensity-based features used in classification.

The geometry-based features were obtained purely from the STL model vertices without relation to the image intensity data. Minimum, maximum, and Gaussian curvatures were computed for each vertex. The Gaussian curvature is computed from a multiplication of the minimum and maximum curvatures, and only the maximum and Gaussian curvatures were used for classification purposes. They were selected to help the classifier better detect regions as intact bone when they have lower curvatures, because fractured bone surfaces tend to have much higher curvatures.

These features were then passed to the classifier which, based on the training data cases, computed the probability of a surface element as being from a fractured surface. The classifier was retrained for each different joint as needed to provide optimal identification of differences in intensities of fracture-liberated surfaces across highly varied bones like the dense, highly curved acetabulum from the flatter, less dense subchondral bone of the tibial plateau.

After classification of each vertex is computed, the identification of fracture-liberated surfaces was completed by a minimum-cut/maximum-flow graph cut algorithm. If this step was not included, the surface would be divided into heterogeneous regions of improperly classified vertices scattered throughout. Therefore, to achieve homogenous intact and fracture-liberated regions, the graph cut was performed. For the edge costs of the graph to decide where the cut should be made, predicted classification probabilities and surface curvatures were used (normalized between 0 and 1).

After the graph cut was performed to obtain a preliminary separation of the fracture-liberated surface regions, any spurious region classifications were manually corrected through a 3d user interface programmed in MATLAB. The interface consisted of a window displaying all fragments in their classified forms with the ability to select misclassified fragments. Selected fragments could then be independently opened to correct errors in classification. Errors in classification frequently occurred in cortical regions of high curvature.

Severity computation

Once fracture-liberated surfaces were identified, they could then be utilized to create an estimate of the energy involved in creating the fracture. The faces of each bone fragment that contained two or more vertices classified as fractured (after the graph cut) were included in the fractured area computation. The CT Hounsfield Unit (HU) intensity previously sampled at each of the three vertices in each face classified as fractured were averaged to obtain an approximation of bone density at the area of that face. Fracture energy was determined from these data using the following equation:

$$Energy(J) = \frac{1}{2} * [SA_{liberated}(m^2)] * \left[\left(\frac{HU}{10^{2.87}}\right)^{\left(\frac{1}{1.45}\right)} \left(\frac{g}{m^3}\right)\right] * \left[\frac{12000}{1.98}\left(\frac{J * m}{g}\right)\right]$$

where the first term, SA, is the liberated surface area, here scaled by $\frac{1}{2}$ to account for only the new surface area generated along the plane of fracture and not counting both sides of the fracture plane as it is segmented; the second term in brackets represents the density derived from the CT Hounsfield Unit intensity, HU in the equation, as empirically derived by Snyder et al. in 1991; the third bracketed term is the strain energy release rate, or the density-dependent energy scaling factor, empirically determined by Beardsley and first implemented by Thomas[1, 15, 17, 76]. The interfragmentary bone demonstrated in Figure 8 is shown with the densities mapped in color. The density, calculated in the second portion of the equation, is reported in grams/meter^3. The energy release rate is the same across all cases and the density does not account for patient factors such as age or gender. While this is a limitation, it has been established in prior work that such differences were relatively minor in the context of the articular fractures studied.

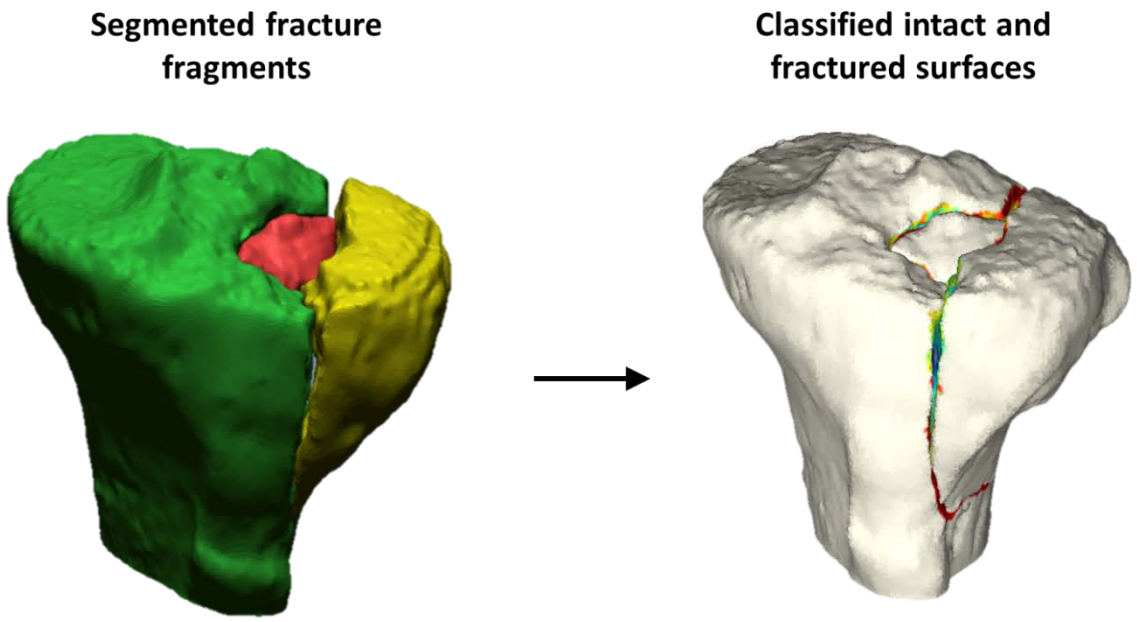

Figure 7. 3D models of the bone fragments are classified into intact and fracture liberated surfaces.

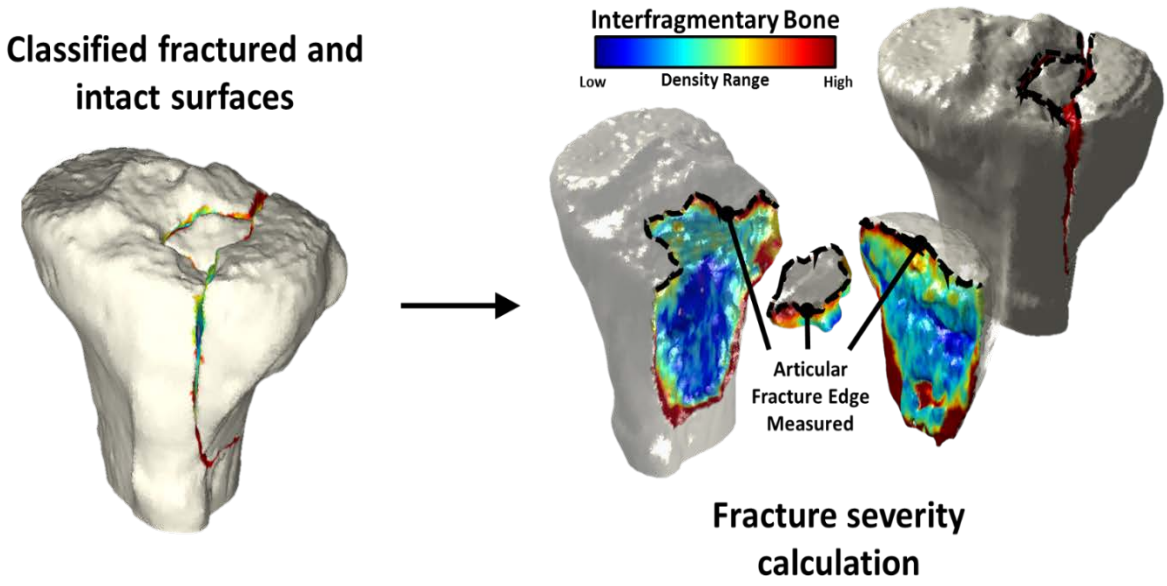

Figure 8. A graph cut was implemented to define the boundary between intact and fractured bone on each fragment so the fracture energy and articular fracture edge length could be computed.

Articular comminution and area measurement

Developing a new metric for computing articular comminution that can be applied in different joints was a priority of this work. Previously, the articular comminution measure had been computed as the interfragmentary surface area present within 1.5mm of the articular surface, expressed as a percentage of the surface area over the same portion of the intact datum tibia. It was only slightly correlated with the fracture energy measure (R^2=0.20) but when combined with it, yielded a significant correlation with outcomes. Therefore, keeping with these principles, but removing the requirement for the intact datum, a technique to examine the fracture energy within 1cm of the articular surface was developed. This necessitated the identification of the subchondral bone surface from the rest of the interfragmentary and intact bone. To accomplish this, a classifier was trained on subchondral bone surface geometries.

The classifier for identifying the subchondral bone surface regions utilized the same image intensity- and geometry-based features that had been previously used to aid in the identification of fracture-liberated bone area. The image-based features were the mean, standard deviation, and difference in intensities sampled at 0 mm and 2 mm into the bone surface from the STL models of the fragments for both the standard HU values and the sheetness image intensity values. The geometry-based features were the maximum and Gaussian curvatures. More so than for the interfragmentary bone surface classifier, the subchondral bone surface classifier required training for each individual joint to account for large differences in articular features across joints (Figure 9).

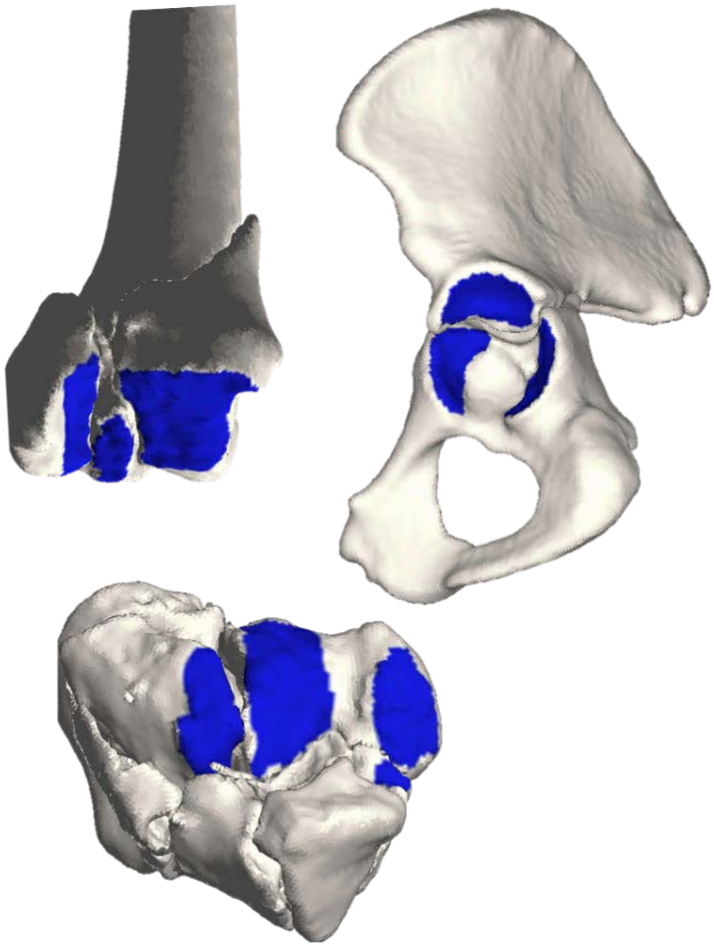

Figure 9. Vastly different articular geometries of articular surface that required classifier re-training.

A manual editing process of the subchondral bone surface classification was implemented in a similar manner to what was done for the interfragmentary bone surface classification. A key difference was that computation of the subchondral bone surface classification was limited to only fragments that were identified as containing components of the articular surface. This expedited computational efficiency and enabled for more rapid computation of the fracture energy within 1 cm of the subchondral bone surface.

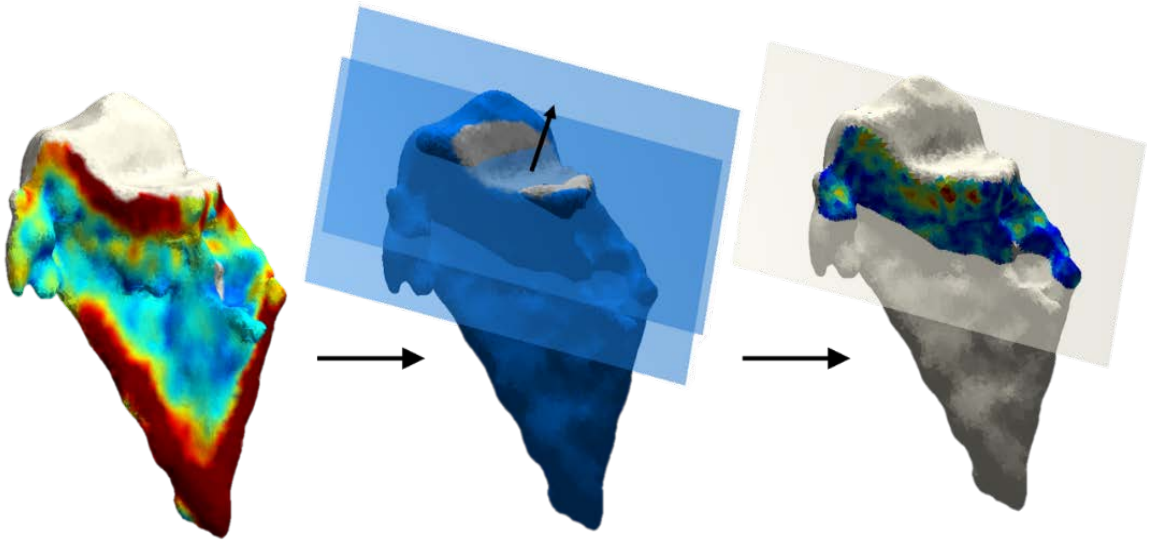

Figure 10. Subchondral energy measurement process. Previously classified (as intact or fracture liberated surface) articular fragments (left) have their subchondral surfaces identified through classification (middle), and subchondral energy is measured 10mm into the surface (shown in color on the right down to a plane marking 10mm into the bone) from the inverse of the average normal plane direction (shown with the arrow and two planes in the middle) of the articulation.

This articular comminution energy, or the subchondral energy, was computed after the finalized classification of both interfragmentary bone and subchondral bone surfaces. The subchondral energy was computed along the average normal of the subchondral bone surface pointing away from the articular surface as demonstrated in Figure 10. Liberated areas above the

plane were also included in the computation to ensure that all energy was captured. This would be expected to lead to a slight overestimation of the subchondral energy but ensures that all energy is captured along curved surfaces.

A secondary benefit to the computation of subchondral bone surface energy is the implicit task of identifying the articular surface. This enables a trivial computation of the articular surface area to provide an area-normalized comminution metric. When axial fracturing impacts are delivered to a joint, energy transfer is distributed over the articular surface through the contact area. A metric of fracture energy scaled by area, therefore, is appealing in the context of assessing likely cartilage insult at the tissue level. As contact areas are more challenging to obtain but are related to joint size and surface area, this articular area measure could provide a reasonable estimate to control for differences in damage caused by differences in energy distribution (i.e. energy per unit area). The correlation between contact area and surface area for each joint studied is explored in the following sections. Fracture energy itself is a representation of how badly the bone in its entirety was disrupted, i.e. the damage at the bone level. As the energy of articular fractures necessarily must involve the articular surface, it is likely also distributed over that articular surface area. Therefore, to control for variable joint sizes both within and between bones and to provide an estimate of the damage done to the cartilage tissue by the energy passing through it, the area over which that energy passes can be used to normalize energy and potentially provide an improved estimate of IAF damage.

Normalized fracture severity study

The ability of the new fracture energy measure to explain differences in PTOA rates across fractures of five different joints (subtalar, ankle, knee, hip, and wrist) was studied. To enable comparisons of the fracture energies across different joints, we normalized by

characteristic joint-specific contact areas. For this study a database of 319 patients having sustained IAFs that had been originally enrolled for fracture energy study without normalization were examined. Patients were selected for having pre-operative CT scans available for IAFs of the distal radius (n=22), acetabulum (n=79), proximal tibia (n=88), distal tibia (n=82), and calcaneus (n=48). An Institutional Review Board approved use of the imaging and patient data collected in the course of their standard-of-care clinical treatment.

Fracture energy was obtained for all fractures included in the study using previously validated, objective analysis methods working from preoperative CT scans [1, 14, 19]. In lieu of patient-specific contact areas that were not estimated, peer-reviewed literature was queried for generally accepted averages of the relevant contact areas (Table 2). Similarly, in lieu of appropriate duration longer-term clinical follow-up data for each individual patient, we again turned to the published literature to find average rates of PTOA development for each of the joints as a point of comparison. For consistency across the studies, we defined PTOA as being present in joints when the Kellgren-Lawrence radiographic grade was greater than or equal to two[3]. A summary of the PTOA rates for each joint and the source papers can be found in Table 2.

Table 2. PTOA rates and contact areas in the upper and lower extremity

	PTOA Rates	Contact Area (cm^2)
Calcaneus[36-38, 77-79]	85.7 (60.4-95.4%)	3.90 (3.10-5.36)
Distal Tibia[39-41, 80-82]	48.1 (40.8-74.0%)	6.28 (4.40-7.34)
Proximal Tibia[42-45, 83, 84]	24.5 (11.0-36.5%)	11.08 (10.65-11.50)
Acetabulum[29, 46, 74, 85-87]	27.9 (12.0-39.5%)	19.03 (14.70-26.77)
Distal radius[47-49, 88, 89]	43.4 (35.0-73.0%)	1.87 (1.00-2.74)

Finally, to explore how acute fracture severity influences PTOA risk after IAF, we first examined correlations between the computed fracture energies and published PTOA rates. Then

an additional data analysis step involved likewise examining correlations between contact area-normalized fracture energies and PTOA rates. Pearson's correlations were computed to determine the significance of the relationships between joints.

Surface area-normalized fracture energy as a patient-specific predictor of PTOA risk in individual joints

After completing the previous study, the next logical step was to test patient-specific correlations between surface area-normalized fracture energy and actual (rather than prior published group average norms for) PTOA outcomes. This involved the analysis of 190 patients having sustained IAFs in a multi-institutional study. Patients were selected for having pre-operative CT scans and a minimum of 12-month radiographic follow-up available for IAFs of the calcaneus (n=48), distal tibia (n=71), and acetabulum (n=71). An Institutional Review Board approved the use of the imaging and patient data collected during the course of their standard-of care clinical treatment.

Fracture severity was analyzed for all fractures included in the study using previously validated, objective analysis methods on pre-operative CT scans. During axial fracturing impacts, energy transfer is distributed over the articular surface through the contact area. In lieu of computing patient-specific contact areas for such circumstances and to enable comparisons across joints, we normalized to patient-specific joint surface areas. Therefore, the first step in this study was to determine how well correlated average contact areas were with joint surface areas. This was completed by comparing the results of the literature review for contact area (as reported in the previous study above) with the average surface areas for these calcaneal, distal tibial, and acetabular fracture cases. Table 3 shows a comparison of these averages. As might be anticipated due to highly varied loading and geometric characteristics across joints, joint classified surface

areas did not directly correspond to the literature reported values of contact area. The acetabulum and plafond showed surface areas were around 125-135% of the literature reported contact areas while the calcaneus was over 200% the size. The larger difference in the calcaneus is partially attributable to how it was measured. Literature only reported contact areas of the posterior facet of the calcaneus while the classifier described herein was also trained to identify the middle facet. The surfaces included for each joint are shown classified in blue in Figure 9. Of note is the inclusion of the entire sourcil in the acetabulum, the exclusion of the medial malleolus in the distal tibia, and the inclusion of the middle facet in the calcaneus. The criteria for inclusion was straightforward: all potential axial load bearing regions that frequently contained primary fracture lines were included in the surface area computation as these were the regions most likely to have the energy of impact transferred through them and damage is assumed to result from this energy transfer.

Table 3. Comparison of surface areas and average contact areas in the lower extremity.

	Surface Area(cm^2)	Contact Area (cm^2)
Calcaneus[36-38, 77-79]	8.11±1.24	3.90 (3.10-5.36)
Distal Tibia[39-41, 80-82]	8.06±1.94	6.28 (4.40-7.34)
Acetabulum[29, 46, 74, 85-87]	25.09±4.44	19.03 (14.70-26.77)

Follow-up was defined by radiographic measures of PTOA. In the calcaneus and distal tibia, the Kellgren-Lawrence (KL) radiographic grade was used, while in the acetabulum, the Tönnis grade was used. This was done because the joint-specific Tönnis grade has been shown to better reflect OA status in the hip than does the KL grade. The KL scale is graded from 0 to 4, where grades 2 and above are generally considered to represent the presence of arthritis. The Tönnis scale is graded from 0 to 3 where grades 2 and 3 are generally considered to represent

arthritis. For consistency, analyses across joints were completed using only the binary PTOA status (i.e. presence or absence as defined radiographically above).

To explore how acute severity influences PTOA risk after IAF, Spearman correlations between fracture energy and the radiographic measures of PTOA for each joint. Finally, to determine if there exists a unified threshold above which joints progress to PTOA, logistic regressions were performed for each joint.

Discrete element analysis

Discrete element analysis (DEA) modeling, as described in the literature review, is a technique that models cartilage as a deformable bed of springs over an implicit rigid bone surface. The specifics of the computational implementation are described in the literature review and are performed in Matlab on the order of seconds rather than the hours required for finite element analysis (FEA)[33]. DEA was first implemented to study a limited series of fractures in the tibial plafond as a proof-of-concept and to get a general idea of the stresses seen in articular cartilage after fracture reconstruction. Building from these studies, several important considerations also hold true for DEA modeling in reconstructed IAFs across different joints. Due to the large amount of metal near the articular surfaces of reconstructed IAFs, MRI is precluded from providing measurements of local cartilage thickness. In the ankle, a uniform cartilage thickness assumption proved adequate for generating DEA models of contact stress that were similar to a physical validation model. This assumption is carried forward to models of the subtalar joint, where accurate identification of the articular cartilage thickness is not possible from post-operative CT scans but prior studies have established normative values of the cartilage thickness. Additionally, DEA contact patches are very similar in size and shape to those produced via FEA but they tend to produce consistently higher contact stress values. Therefore,

the magnitudes of contact stress results should be interpreted with caution in a relative fashion, with DEA models being compared only with DEA models in the same joint or potentially by scaling them to comparable FEA models.

Analysis of results and PTOA development

Contact stress over-exposure

DEA-computed contact stress distributions are obtained throughout the stance phase of gait as implemented. In an effort to link contact stress to PTOA risk after IAF, a previously developed paradigm for evaluating the contact stress over-exposure was used. As contact stresses are not all deleterious in nature, this paradigm implements a threshold to exclude healthy stresses so that a potentially harmful per gait cycle over-exposure can be computed. The threshold was selected by performing a parameter sweep of all reasonable cutoffs for over-exposure, from 0 to 15 MPa. The optimal cutoff was selected by determining the highest number of correct selections for cases that developed PTOA. The results were then reported as MPa*s exposures, deriving from the equation described in the literature review on pages 15 and 16 where the amount of time (in seconds) joints were exposed to suprathreshold stresses was multiplied by magnitude of the stresses (MPa) to obtain the exposure (MPa*s). The P_d cutoff described in this equation as the damage threshold was then used for later statistics and comparisons.

Injury severity comparison

To better understand potential connections between injury severity and reduction accuracy, injury severity assessments were performed on all cases from pre-operative CT scans. The fracture energy, articular comminution energy, and joint area were analyzed. The fracture energy was normalized to joint area as an estimate of energy per unit area dissipated over the articular surface. The articular comminution energy, as described above was then combined with

the normalized fracture energy to test if a composite score was more predictive of PTOA development. A final composite measure was created by combining the injury severity and reduction accuracy components of composite severity and contact stress over-exposure, respectively. The composite scores were then analyzed using receiver operating characteristic (ROC) curves to assess sensitivity and specificity and the area under the curve (AUC) was measured to provide metric of performance.

Contact stress over-exposure in the tibial plafond after IAF

Prior studies have examined the contact stresses as a measure of both the surgical reduction's ability to restore the mechanics of the joint after IAFs of the tibial plafond and how they relate to PTOA development. Those studies examined a series of 11 cases where 10 had sufficient follow-up and DEA results while nine had adequate pre-operative CT for fracture severity to be measured. This study expanded to 16 cases with pre- and post-operative CT scans to enable objective measurement of both IAF injury and reduction for comparison to PTOA.

Patient Selection and outcomes data

After obtaining IRB approval, cases selected for analysis were drawn from a clinical series of 36 patients sustaining unilateral tibial plafond fractures. Patients were chosen to represent the spectrum of severity from partial articular fractures to highly comminuted fractures involving the entire joint surface. Fractures were initially treated using a spanning external fixator and subsequent screw fixation of the articular surface. They were assessed as having varying degrees of residual incongruity.

Model generation

The cartilage geometries from the first nine cases with adequate imaging and follow-up reported from previous studies were utilized in this study[33, 90]. These cases were previously segmented from post-operative CT using iso-surfacing in OsiriX (Osirix software, www.osirixviewer.com) and repaired and smoothed using Geomagic Studio (Geomagic Studio; Geomagic, Research Triangle Park, NC)[90]. For the other seven cases, bony geometries of the tibia and talus were segmented from the post-operative CT scans using a semi-automated watershed transform-based algorithm implemented in MATLAB (The Mathworks, Natick, MA, USA) from purpose written code originally developed by Thomas, Kern, and Anderson.[87] Errors in separation of the bones were corrected using a custom graphical user interface written in MATLAB. The resulting NIFTI files were then loaded into ITK-SNAP to correct minor errors in the subchondral regions of the tibia and talus. Geomagic Design X (3D Systems Inc., Rock Hill SC) was used to repair and smooth the final bone models. As contrast-enhanced post-operative CT arthrographic imaging failed to reliably provide adequate cartilage imaging, a uniform 1.7mm cartilage projection was made by extrusion from the subchondral bone along the normal direction of the smoothed surfaces.

Anatomical alignment

CT data were acquired with patients supine and their ankle joints planar-flexed and externally rotated. Therefore, their posture was not a functionally neutral pose for the stance phase of walking and required alignment. The first nine cases were previously aligned by an experienced ankle surgeon to a neutral weight-bearing apposition using a procedure that involved working from weight bearing radiographs when available. A local coordinate reference frame was defined based on anatomical landmarks and centered in the talus. The flexion/extension axis

of the ankle was defined along a line connecting the centers of the circles fitted to the condylar arcs of the talar dome. The origin was along this line splitting the distance between the two arcs of the talus. A projection of the primary axis onto a plane normal to the flexion/extension axis was used to define a second axis. Tibial and talar surfaces were translated together to ensure the talus' anatomic coordinate system was appropriately aligned to the global reference frame. The flexion/extension axis was defined as the global x direction and was sued to align the talus with the first metatarsal at 15° below horizontal. The tibia was then aligned so the angle between the shaft and the floor was 85°. The second 9 cases were aligned to the results of this robust initial alignment in Geomagic Design X. The medial-lateral x-axis was defined via the central axis of a fitted cylinder and the origin and second axis were defined as previously described. The final orientations of the bones were obtained by aligning them to one of the first 9 cases that they best matched anatomically.

Boundary conditions

Boundary conditions for the models were chosen to replicate the original DEA and FEA studies[33, 90]. The simulations were performed over the stance phase of gait using 13 quasi-static loading steps in which the ankle undergoes a flexion/extension arc ranging from 5° of plantar-flexion to 9° of dorsiflexion (Figure 11). During each quasi-static step in the flexion/extension arc, the tibia is axially loaded according to the forces reported for post-operative patients and proportional to the subject body weight and constrained in all directions except superior and inferior translation along its long axis. The talar rotations were free except flexion-extension, which was constrained to maintain the appropriate position for that stage of gait. Talar translations were free in all directions except for superior and inferior movement to resist the forces applied by the tibia. In every stage of the stance phase of gait the simulation

prescribed the flexion-extension of the talus beneath the tibia as dictated by its position within gait. A fibular restraint was added to emulate the ankle mortise, modeled as a linear spring acting laterally on the talus, resisting medial-lateral translation from the initial position of the talus (spring constant = 100N/mm)[33, 90].

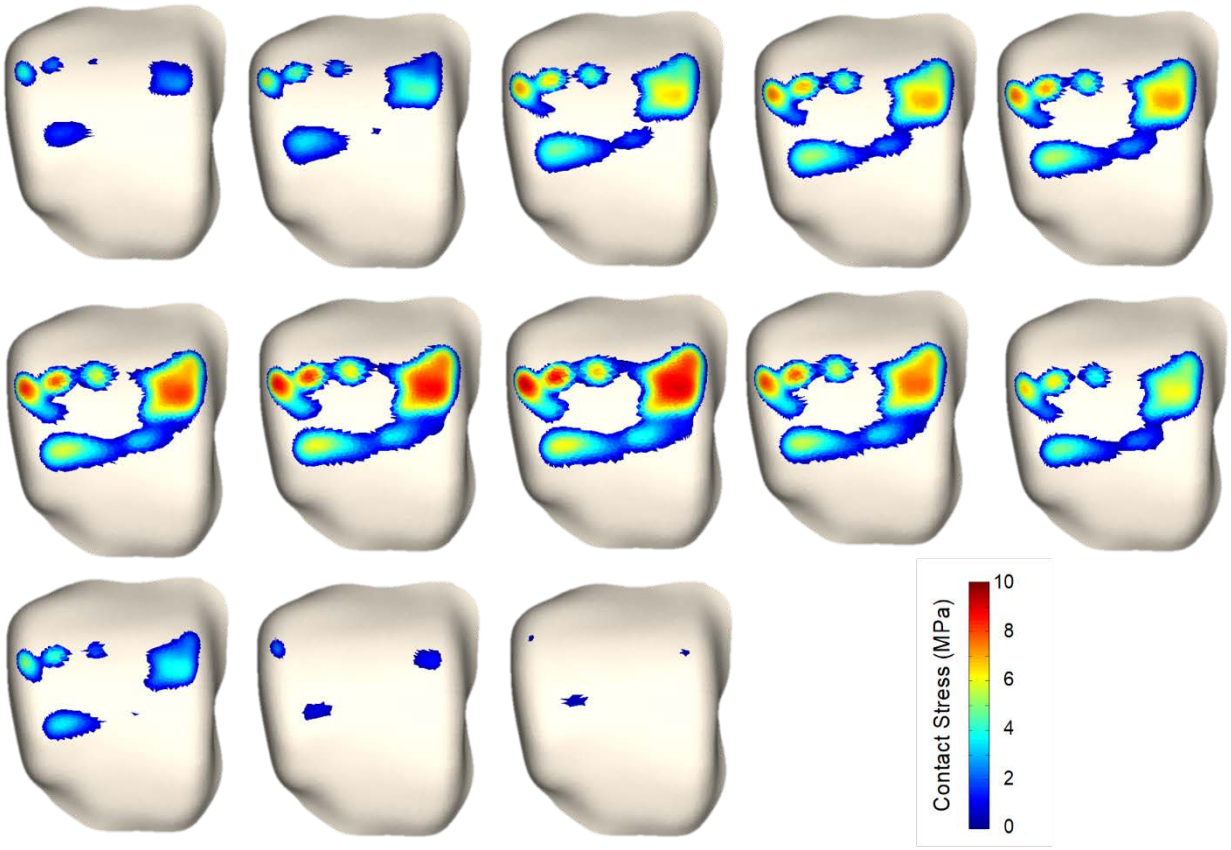

Figure 11. Contact stress (pressure) distributions on the superior dome of the talus after IAF of the tibial plafond. From the top left to the bottom right is heel-strike through toe-off of the 13 steps the stance phase of gait was discretized into. Top is anterior and left is lateral.

Contact stress over-exposure in the calcaneus after IAF

Patient Selection and outcomes data

To investigate the mechanical factors at play in the development of PTOA, contact stress was computed on patients with reconstructed intra-articular calcaneal fractures. Patients were chosen as a sample of convenience from a larger series of patients previously analyzed for fracture energy. Pre-operative scans were analyzed for fracture energy to determine the severity of the initial injury and post-operative CT scans were analyzed for contact stress to evaluate the joint mechanics after surgery. After obtaining Institutional Review Board (IRB) approval, thirty-six patients with 48 DIACFs were selected for study from among 153 patients that had been treated. The patients selected were age $\geq$ 18 years, had available electronic pre-operative and post-operative CT scans, and good quality post-op and follow up radiographs. Patients age < 18, extra-articular fractures, patients without pre-op CT scans, patients without post-op CT scans, and follow up < 18 months were excluded. Final selection for inclusion in this study was determined by convergence criteria in the contact stress modeling. Failed models were excluded.

Model Generation

Calcaneal and talar geometries for each patient were extracted from post-operative CT scans using the same semi-automated watershed-based algorithm from the plafond study (Figure 5). Errors in the automated surface detection and separation protocol were manually corrected using ITK-SNAP and STL models were exported. The triangulated surface models produced had residual artifact from voxelization of the anatomy, so they were subsequently smoothed and resampled to remove any errors and irregularities in the mesh (Geomagic Design X software, 3D Systems Inc., Rock Hill SC). Articular cartilage surfaces were approximated by projecting the calcaneal and talar subchondral surfaces of the posterior and middle facets a uniform distance of 1 mm. This projection was taken from literature values sampling from a healthy joint[91].

Therefore, cartilage in the fractured joints was assumed to be healthy at the time of injury with thicknesses maintained after surgical reduction. Additional considerations from these normative data are that the edges of the articular surfaces be tapered. Therefore, the cartilage surfaces were subsequently projected back toward the subchondral bone by 1 mm to simulate the natural tapering of cartilage thickness toward its outmost edges.

Anatomical alignment

The models were aligned to neutrally opposed bones in a weight bearing CT-scan of a well reduced calcaneal fracture not contained within the examined dataset. This case was selected to be representative of an average post-operative reconstruction from a series of 10 candidate cases. The alignment procedure was completed in Geomagic Design X by first aligning the talus of the representative bone to a global coordinate system centered at the subtalar joint [92]. The footpad of the WBCT was segmented and used to define the z-axis as orthogonal to it. The x and y planes were taken to be at the slot center of the subtalar joint. The y-axis was defined from the intersection of the plane defined by approximating the long axis of the third metatarsal (obtained with a cylinder fit) and a point passing through the center of the heel (taken from the mean of the heelpad segmentation) and orthogonal to the plane defined by the origin and orthogonal z-axis. The x-axis was orthogonal to this line and the z-axis defining and just

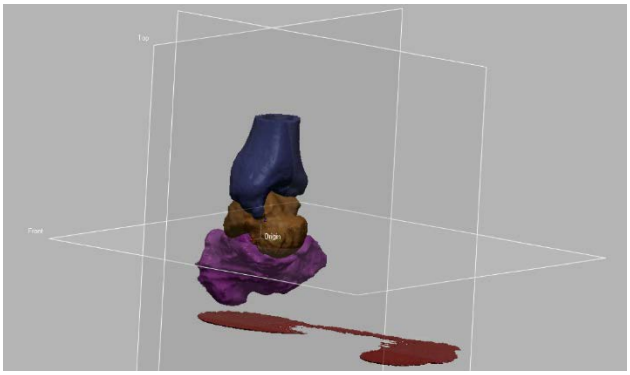

Figure 12. Alignment models segmented from weight-bearing CT with planes defining the appropriate alignment positions.

below the axis about which planar and dorsiflexion occur. The alignment models are shown in Figure 12.

Boundary conditions

Similar to the tibial plafond model, the boundary conditions were chosen to simulate the stance phase of gait in 13 quasi-static loading steps. Kinematics of the joint motion were defined by Arndt et. al.'s study using intracortical pins to assess relative talocalcaneal motion[92]. Talocalcaneal forces were defined from heel strike to toe-off from Giddings 2000 study of forces during walking[93]. As the Giddings study simulated healthy gait, a correction of the maximum forces was applied to reduce peak forces to 68% of their peak to match the post-operative forces observed in gait in the Stauffer et. al study(reported as over 500% of body-weight in the

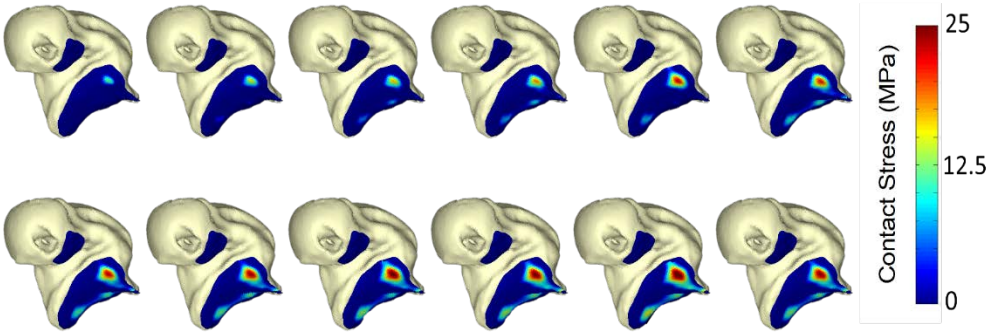

Figure 13. Inferior view of contact stresses on the talus after IAF of the calcaneus. From the top left to the bottom right are the 12 discretized steps of the gait cycle analyzed. The top is anterior and left is medial.

Giddings study)[94]. Patient-specific weights were utilized to be scaled by the percent of body-weight forces reported across the prescribed gait cycle. The talus was allowed to freely translate over the calcaneus with rotations rigidly prescribed in accordance with each quasi-static loading step. Anterior-posterior motion and medial-lateral motion were restricted with 350 N/mm springs to simulate the boney constraints of the navicular and forefoot as well as the strong ligamentous attachments. With these parameters the models were then analyzed using DEA to evaluate contact stress.

Contact stress over-exposure in the acetabulum after IAF

Patient Selection and outcomes data

After obtaining Institutional Review Board (IRB) approval, a series of 75 patients at a single institution who had undergone operative fixation of acetabular fractures between 2004 and 2016 were identified for having pre-operative and post-operative CT scans. Patients were excluded from study for having less than two-year radiographic follow-up, being under the age of 18 at the time of surgery, undergoing arthroplasty within the same hospital admission, or if they had associated femoral head fracture. Twenty-four patients declined to participate or were unreachable. Ten patients had undergone surgery within the past two years and thus did not have 2-year radiographic follow-up. One patient was 17 at the time of surgery. Of the remaining 40 patients, 22 patients had adequate imaging and follow-up available for contact stress analysis. A total of 19 had adequate imaging and follow-up for both fracture energy and contact stress analysis.

Radiographs obtained at a minimum of 12 months were evaluated for arthritic changes by two independent evaluators. Each evaluator assigned a Tönnis grade to each hip using the modified Tönnis grading description scale [95]. When there was disagreement between observers, an arbitrator (MW) reviewed the studies and determined Tönnis grade. Patients having Tönnis grades 0 and 1 were included in the no PTOA group and Tönnis grades 2 and 3 were included in the PTOA group. Those patients who went on to total hip arthroplasty were considered as Tönnis grade 3 equivalents for radiographic purposes.

Contact Stress Analysis

Femoral and pelvic geometries for each patient were extracted from post-operative CT scans using a semi-automated watershed-based algorithm (Figure 14). Errors in the automated surface detection and separation protocol were manually corrected, and triangulated surface models of the anatomy were generated and smoothed (Geomagic Design X software, 3D Systems Inc., Rock Hill SC). Articular surfaces were approximated by projecting the acetabular and femoral subchondral surfaces a uniform distance of 1 mm then subsequently smoothing the projected surfaces toward sphericity using a custom iterative smoothing algorithm[74]. The resulting approximations of the chondral geometries have been previously shown to yield accurate contact stress computations, even from fractured surfaces.

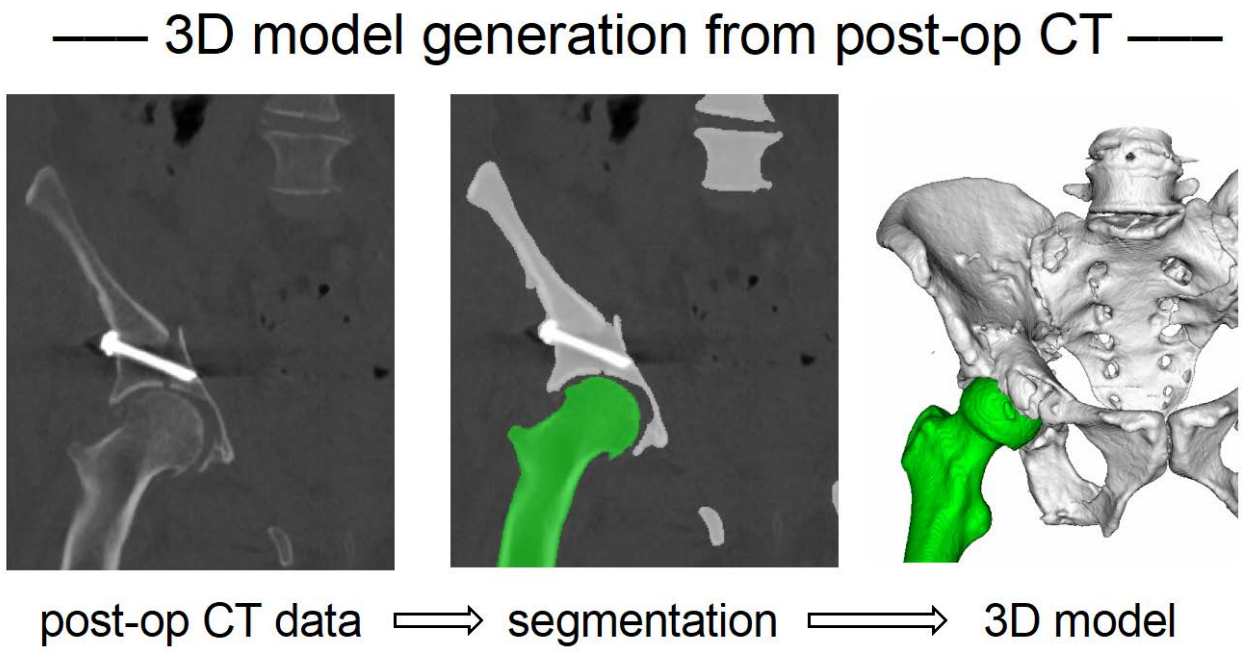

Figure 14. Patient-specific 3D models of the hip were generated from post-operative CT scans of the surgically reduced acetabular fractures.

The models were aligned to the hip joint coordinate system defined by Bergmann et. al. (2001) based on patient-specific anatomic landmarks on the bone surface models[2]. DEA was used to compute contact stress over an entire gait cycle for each case. Boundary conditions for

forces and rotations were based on patient-specific body weights and were defined by the Bergmann et. al. study (2001) from instrumented total-hips[2]. The stance phase of gait was discretized into 13 quasi-static time steps to facilitate direct comparison of the resulting contact

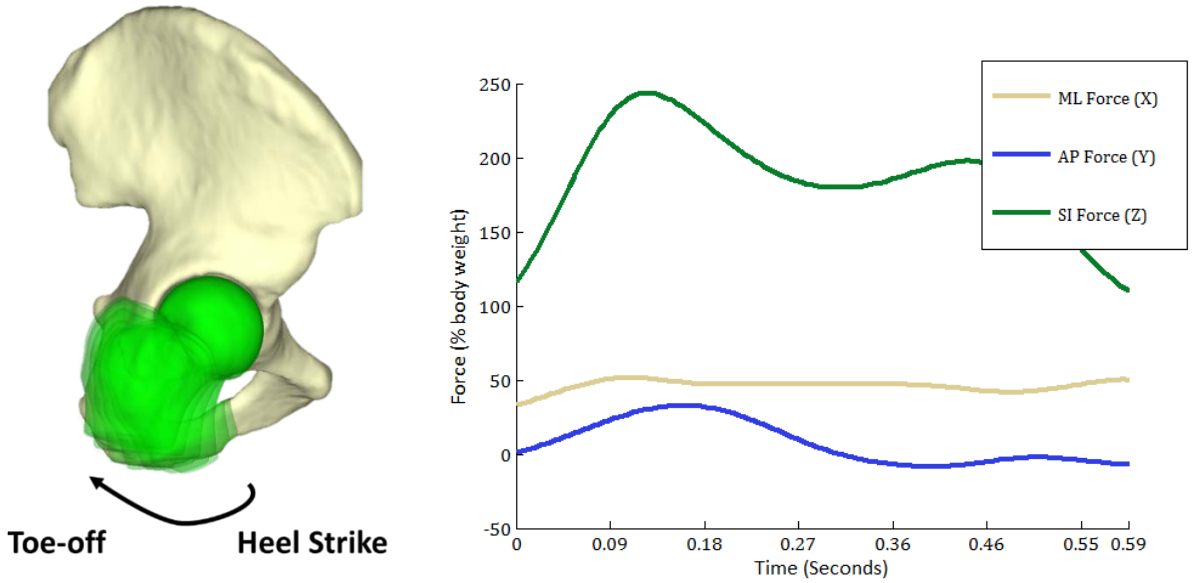

Figure 15. The gait cycle was discretized into 13 quasi-static time steps (shown overlaid on one another to the left) with forces and rotations obtained form the Bergman gait data (right) [2].

stress distributions (Figure 15 and Figure 16). Forces were applied to the femur and directed toward the hip as dictated by the Bergmann data. Cartilage was assigned isotropic linear-elastic material properties (E=8MPa, v= 0.42).

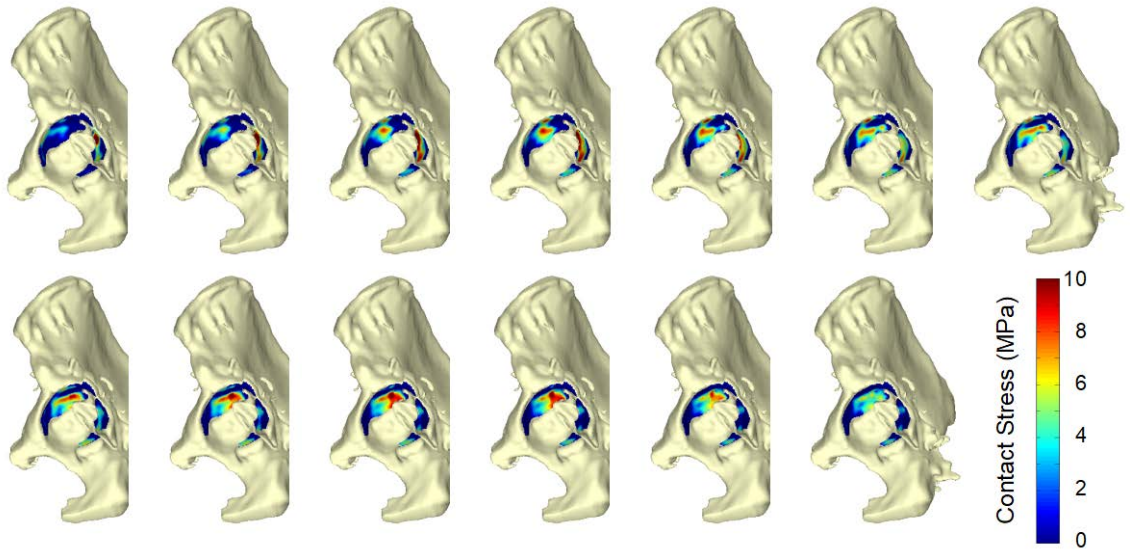

Figure 16. Contact stress distributions are computed at each of the 13 loaded poses to replicate the entire stance phase of gait.

Statistical Models of injury severity and reduction

The purpose of these studies was ultimately to determine the effect of articular reduction and injury severity on patient outcomes in various joints. Unpaired t-tests were used to compare results between the no PTOA and PTOA groups (defined as KL and Tönnis Grades ≥2). Spearman's rank-order correlations were computed to evaluate correlations between patient factors, predictors, and the ordinal radiographic outcomes. Spearman's correlations were used as the outcome variable was categorical in nature and therefore, not as amenable to study by Pearson's correlations which can consider continuous predictor and outcome variables.

CHAPTER 4 - RESULTS

Contact area-normalized fracture energy as a predictor of PTOA risk:

Initial data on contact area-normalized fracture severity was obtained from the literature normative reported values for contact area and PTOA rates across different joints. The fracture energies for all cases analyzed, measured as delineated in the methods above, ranged from 0.9 to 41.9 (J). The range of fracture energies for calcaneal fractures was 14.2 to 26.2J, for distal tibial fractures it was 0.9 to 38J, for proximal tibial fractures it was 3.2 to 33.2J, for acetabular fractures it was 4.5 to 41.9J, and for distal radial fractures it was 2.8 to 9.0J. The fracture energies (mean ± standard deviation) were 19.3±3.1J for calcaneal fractures, 15.3±7.3J for distal tibia fractures, 13.1±6.5J for proximal tibia fractures, 16.9±8.9J for acetabular fractures, and 4.9±1.8J for distal radius fractures. The distribution of energies was highly dissimilar between a number of these groups with no overlap whatsoever between the calcaneal and distal radius fractures (Figure 17).

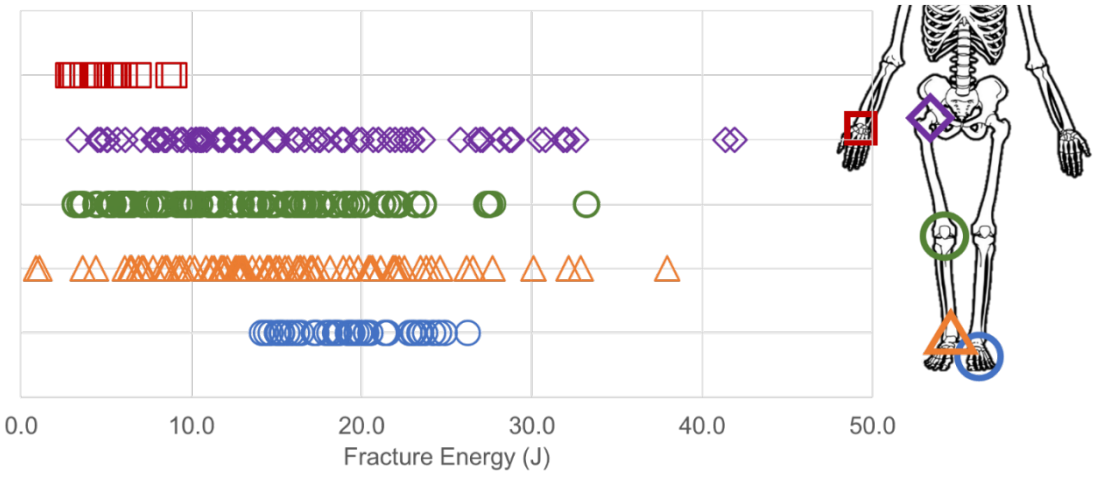

Figure 17. The distribution of fracture energies for calcaneal, distal tibial, proximal tibial, acetabular, and distal radial fractures.

The contact area-normalized fracture energies ranged from 0.14 to 6.73 J/cm^2 for all cases. The range of contact area-normalized fracture energies for calcaneal fractures was 3.63 to 6.73 J/cm^2, for distal tibial fractures it was 0.14 to 6.04 J/cm^2, for proximal tibial fractures it was 0.28 to 2.92 J/cm^2, for acetabular fractures it was 0.18 to 2.20J/cm^2, and for distal radial fractures it was 1.49 to 4.81 J/cm^2. The contact area-normalized fracture energies (mean ± standard deviation) were 4.94±0.79 J/cm^2 for calcaneal fractures, 2.44±1.17 J/cm^2 for distal tibia fractures, 1.16±0.57J/cm^2 for proximal tibial fractures, 0.89±0.47 J/cm^2 for acetabular fractures, and 2.59±0.94 J/cm^2 for distal radius fractures. There was a trend toward decreasing energy in joints going from distal to proximal in the lower extremity with distal radial fractures having energies in the middle of the range (Figure 18).

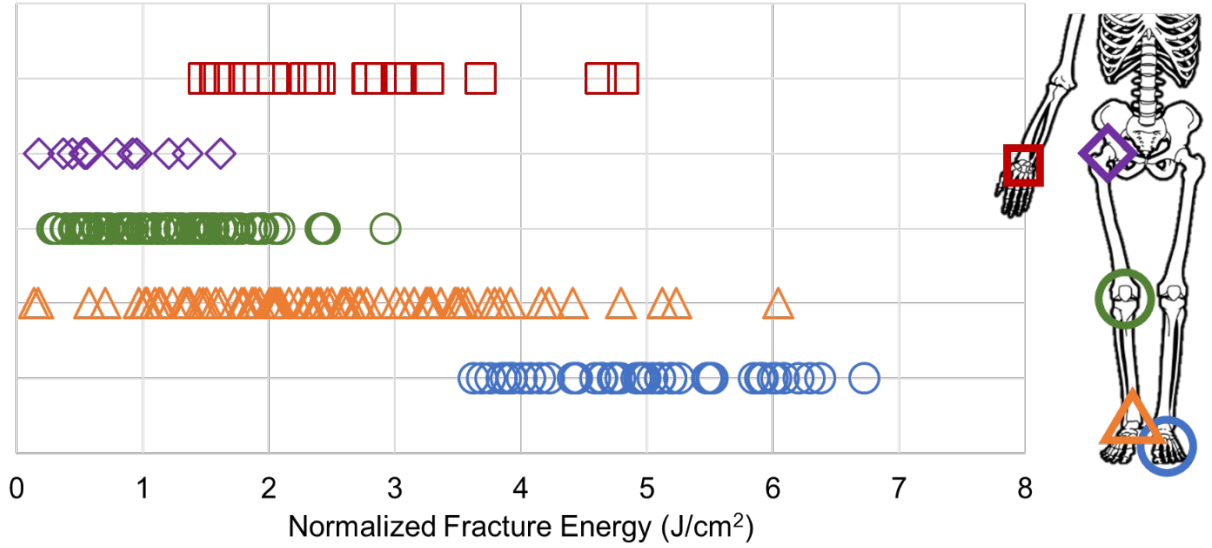

Figure 18. The distribution of fracture energies for calcaneal, distal tibial, proximal tibial, acetabular, and distal radial fractures scaled by the average contact area for each joint.

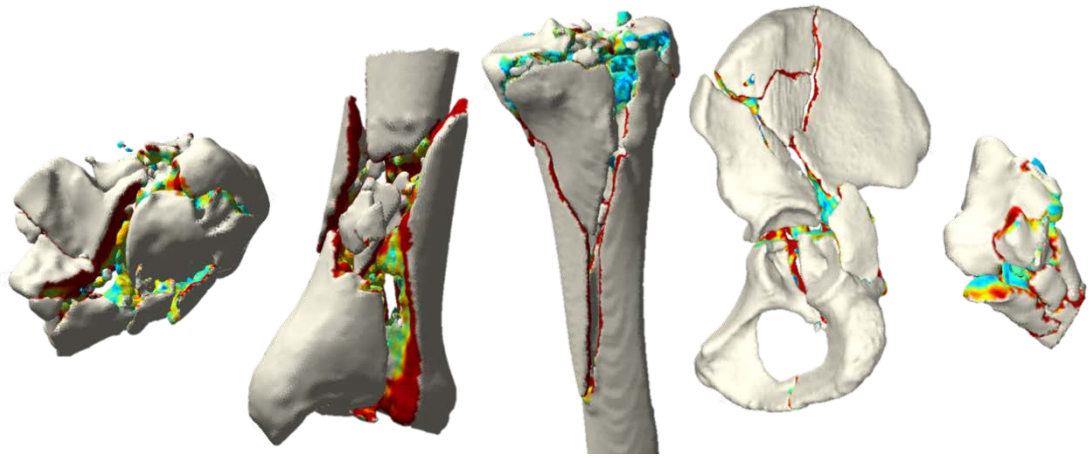

Figure 19. High energy fractures have similar characteristics across joints with many fragments, significant comminution, and disruption of the articular surface.

Qualitatively, high energy fractures in all five joints shared similar characteristics having similar size, number, and dispersion of fragments (Figure 19). Fractures at the lower energy end of the spectrum, however, did not demonstrate such similarities. When comparing fractures of similar energy across joints, there were perceptible differences in their appearance. An 8J fracture in the ankle can appear relatively minor while an 8J fracture of the distal radius can have a highly comminuted joint space with large diaphyseal extensions. Comparing joints with similar contact area-normalized fracture energies showed more consistent appearance across joints. A 4.29 J/cm^2 fracture of the distal radius is similarly comminuted with diaphyseal extension as is a 4.19 J/cm^2 fractures of the distal tibia (Figure 20).

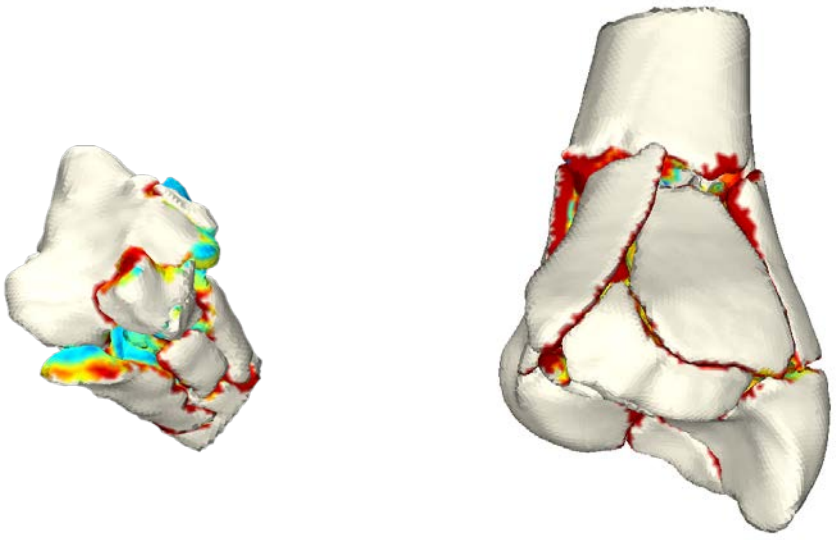

Figure 20. A 4.29 J/cm^2 fracture of the distal radius and a 4.19 J/cm^2 fracture of the distal tibia. Similar scaled fracture energy values tend to have visually similar degrees of damage.

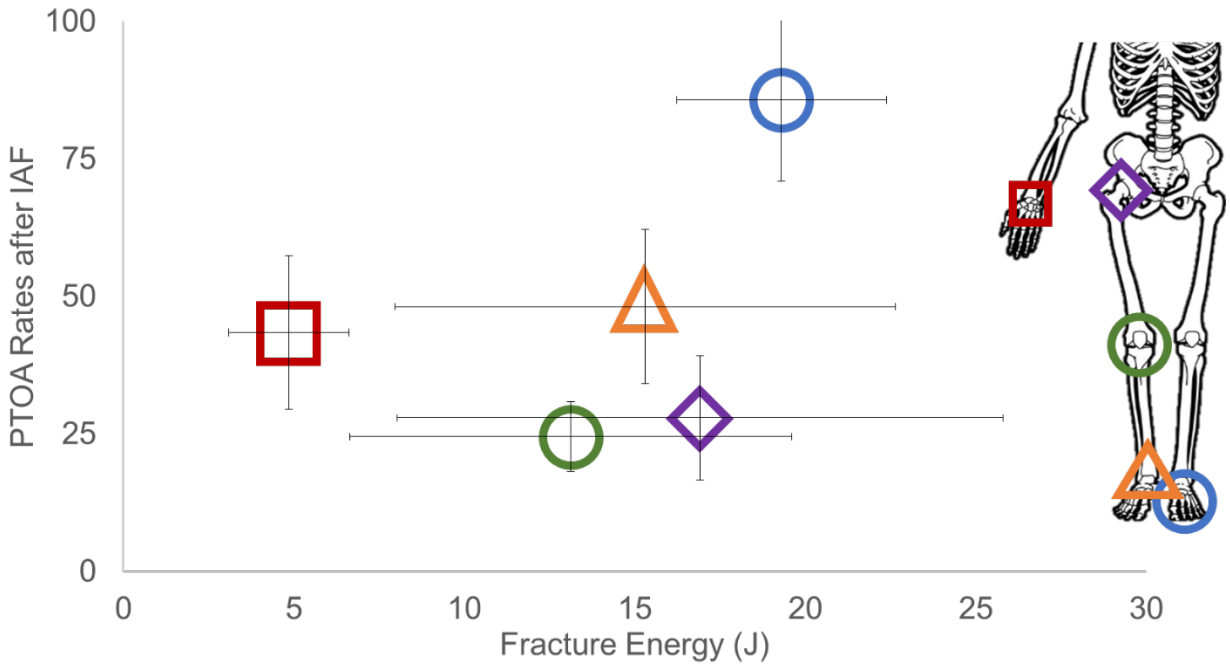

Figure 21. Fracture energies do not correlate with published rates of PTOA across the joints studied.

The computed fracture energies showed no correlation whatsoever with the published rates of PTOA across the joints studied (Figure 21). However, there was a highly significant correlation between contact area-normalized fracture energies and the rates of PTOA (Figure 22). The primary limitation to this study's results is that it is based on normative values of contact area and therefore cannot be interpreted on a patient-specific basis. Interpretation of these results is also limited by fact that it did not differentiate between groups for age, size, and gender differences.

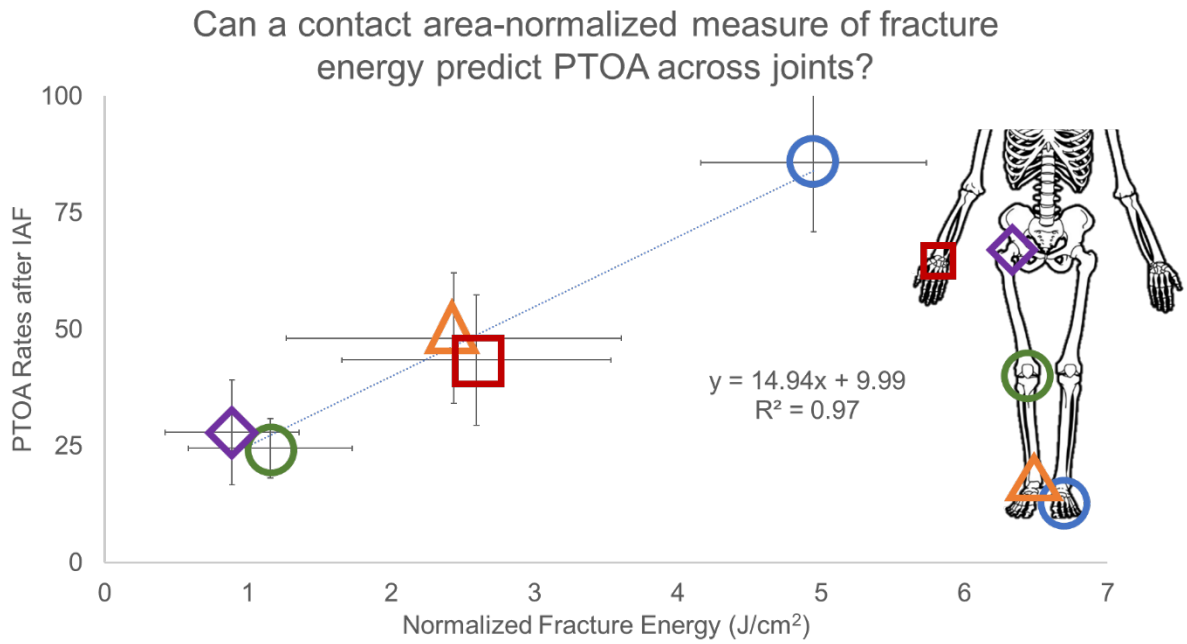

Figure 22. Area-normalized fracture energies have a highly significant correlation with rates of PTOA.

Articular surface area-normalized fracture energy as a predictor of patient-specific PTOA development in individual joints

Overall, 56.8% (108/190) of the patients studied developed PTOA by the time of their last radiographic follow-up. The PTOA rate in the plafonds studied was 52.1% (37/71), in the calcaneus it was 60.4% (29/48), and in the acetabulum it was 59.1% (42/71); PTOA rate was determined by a KL grade and Tönnis grade cutoff of ≥2 indicating the development of radiographic arthritis. The cases reported were not consecutive series and may have some selection bias, as the PTOA rates observed for them are not consistent with those previously reported in literature: 70-75% in the plafond[39], 83-92% in the calcaneus[38, 60], and 11-38% in the acetabulum[85].

As noted above, fracture energy ranged from 0.9 to 41.9J (17.7±7.5 J) for all cases. Fracture energies in patients who developed PTOA were significantly higher than those in the patients who did not (19.3±7.3 vs 15.5±7.1, $p<0.001$). Fracture energy in the tibial plafond ranged from 0.9 to 30.1J (14.6±6.5 J), in the calcaneus it ranged from 14.1J to 26.2J, and in the acetabulum it ranged from 4.5 to 41.9J (19.7±9.3J). Fracture energy was significantly higher in patients that developed PTOA in the plafond ($p=0.011$) and acetabulum ($p=0.021$), but not in the calcaneus ($p=0.51$).

Patient-specific contact area-normalized fracture energy ranged from 0.09 to 3.57 J/cm^2. The normalized fracture energies in patients who developed PTOA were significantly higher than in those who did not (17.5±8.8 vs 13.9±8.1, $p=0.004$). Normalized fracture energies ranged from 0.09 to 3.42 J/cm^2 (1.84±0.76 J/cm^2) in the tibial plafond, 1.24 to 3.56 J/cm^2 (2.42±0.47 J/cm^2) in the calcaneus, and 0.14 to 1.95 J/cm^2 (0.79±0.36 J/cm^2) in the acetabulum. The normalized fracture energy was significantly higher in patients that developed PTOA in the

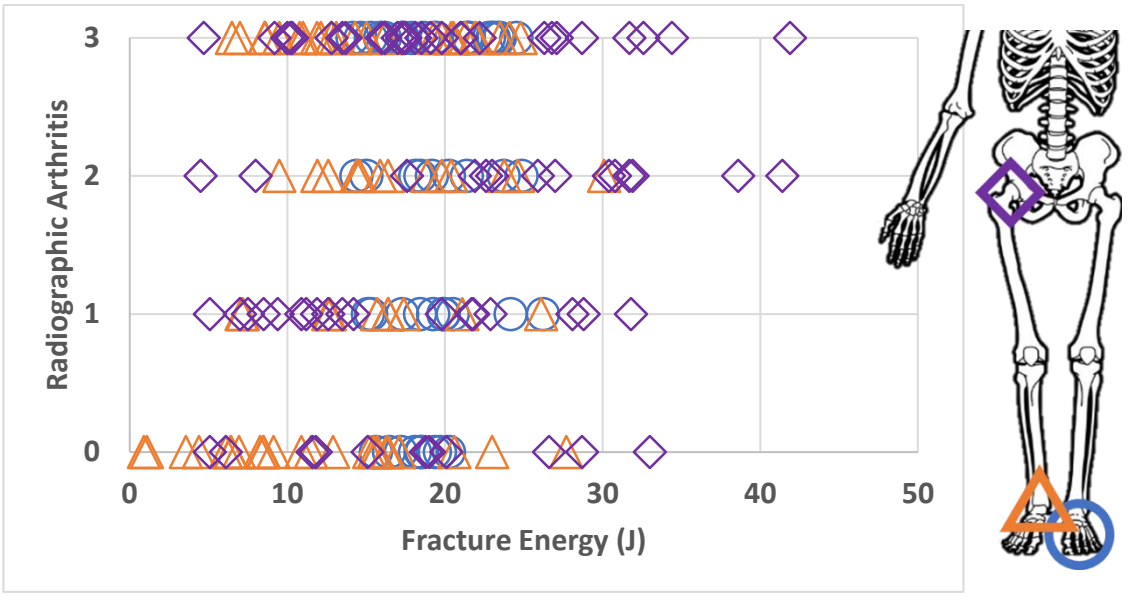

Figure 233. Fracture energy and grade of radiographic arthritis. The Tönnis grade was used for the acetabulum and a truncated Kellgren-Lawrence grade (where grades 3 and 4 were combined) was used for the calcaneus and tibial plafond.

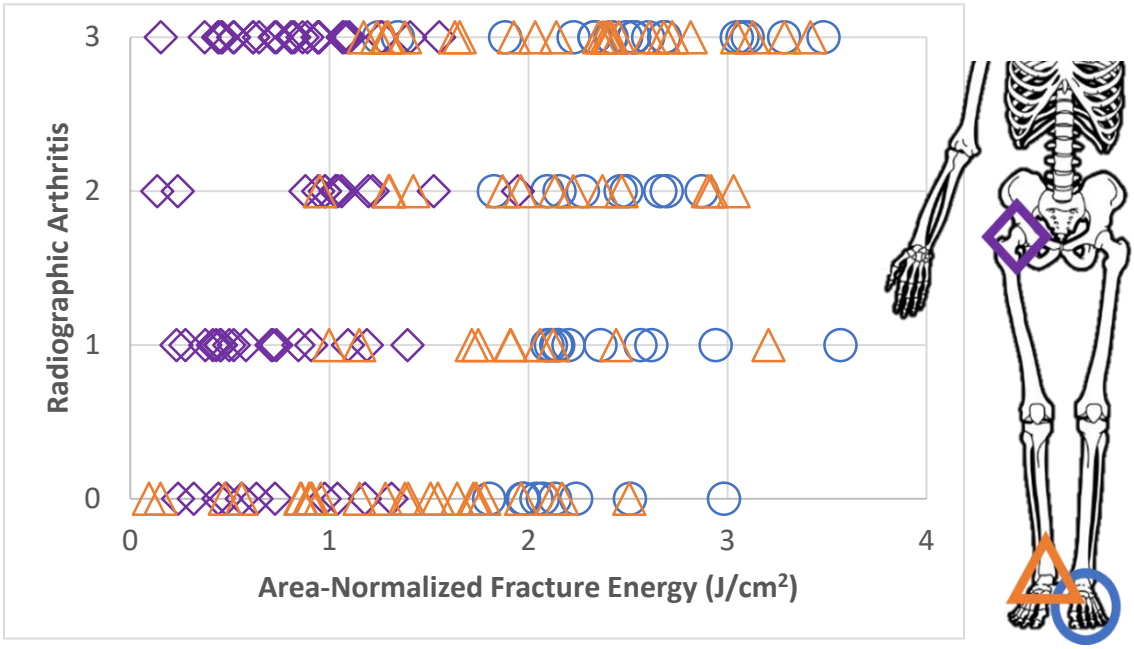

Figure 244. Area-normalized fracture energy and grade of radiographic arthritis. The Tönnis grade was used for the acetabulum and a truncated Kellgren-Lawrence grade (where grades 3 and 4) were combined was used for the calcaneus and tibial plafond.

plafond (2.18 vs 1.47 J/cm^2, p<0.001) and acetabulum (0.87 vs 0.68 J/cm^2, p=0.031), but not in the calcaneus (2.48 vs 2.12 J/cm^2, p=0.33). Figure 23 and Figure 24 show the distributions of fracture energy and normalized fracture energy, respectively versus radiographic grade for each joint.

Spearman's correlations between fracture energy, area, normalized fracture energy, radiographic OA grade, and OA status across all joints are shown in Table 4. Table 5, Table **6**Table 7 show Spearman's correlations between fracture energy, area, normalized fracture energy, radiographic OA grade, and OA status for the calcaneus, tibial plafond, and acetabulum, respectively. Across all cases, fracture energy had a small, but significant correlation with degree of OA development as well as OA status. Comparatively, normalized fracture energy had a slightly stronger correlation with degree of OA development that was highly significant. Broken down by joint, the fracture energy was significantly correlated with OA status in the plafond and acetabulum, but not the calcaneus. The degree of OA present was only significantly correlated with fracture energy and normalized fracture energy in the plafond. Normalized fracture energy was also significantly correlated with OA status in the plafond and acetabulum, but, once again, not in the calcaneus. In the calcaneus, the correlation appeared stronger but was not significant (p=0.062).

Logistic regressions of fracture energy, normalized fracture energy, and OA status across joints are shown in Table 8. Table 9, Table 10, and Table 11 show the results of these regressions for the calcaneus, tibial plafond, and acetabulum respectively. The confidence interval for the odds ratio across joints did not contain one, indicating that the results are significant for both the fracture energy and normalized fracture energy. They further revealed that for every Joule of increase in the fracture energy, there is an associated 3.2 to 12.6%

increased risk of PTOA development. Similarly, for each 0.1 J/cm^2 increase in area-normalized fracture energy, there was a corresponding 1.5 to 8.7% increase in PTOA risk. For individual joints, the odds ratios were also significant in the plafond and acetabulum, but not in the calcaneus. Additionally, the confidence intervals for the odds ratios were very large, indicating that more data is needed to reliably predict increased risk.

Table 4. Spearman correlations between objective measures of acute mechanical damage and PTOA status across fractures of the calcaneus, tibial plafond, and acetabulum. Significant correlations in bold. Coefficients are listed first followed by their p-value of significance.

All Cases Spearman Correlation Coefficients, N = 190 Prob > |r| under H0: Rho=0		
	Radiographic OA Grade	**OA**
Fracture energy	**0.189** **0.009**	**0.248** **<0.001**
Normalized Fracture Energy	**0.267** **<0.001**	**0.215** **0.003**

Table 5. Spearman correlations between objective measures of acute mechanical damage and PTOA status across fractures of the calcaneus. Significant correlations in bold. Coefficients are listed first followed by their p-value of significance.

Calcaneus Spearman Correlation Coefficients, N = 48 Prob > |r| under H0: Rho=0		
	KL Grade	**OA**
Fracture energy	0.102 0.491	0.090 0.547
Normalized Fracture Energy	0.271 0.062	0.248 0.090

Table 6. Spearman correlations between objective measures of acute mechanical damage and PTOA status across fractures of the tibial plafond. Significant correlations in bold. Coefficients are listed first followed by their p-value of significance.

Tibial Plafond Spearman Correlation Coefficients, N = 71 Prob > |r| under H0: Rho=0		
	KL Grade	**OA**
Fracture energy	**0.264** **0.026**	**0.286** **0.016**
Normalized Fracture Energy	**0.51749** **<.0001**	**0.466** **<.0001**

Table 7. Spearman correlations between objective measures of acute mechanical damage and PTOA status across fractures of the acetabulum. Significant correlations in bold. Coefficients are listed first followed by their p-value of significance.

Acetabular Spearman Correlation Coefficients, N = 71 Prob > |r| under H0: Rho=0		
	Tönnis Grade	**OA**
Fracture energy	0.129 0.282	**0.252** **0.033**
Normalized Fracture Energy	0.136 0.256	**0.257** **0.030**

Table 8. Results of logistic regressions of PTOA risk as predicted by the fracture energy in the top division in each table and by surface area-normalized fracture energy in the bottom division for all cases. For each regression, their respective parameter and odds ratio (OR) estimates are reported as well as a confidence interval of the OR.

Parameter	**Estimate**	**Standard Error**	**Wald Chi-Square**	**Prob > ChiSq**	**OR Point Estimate**	**95% Wald Confidence Limits**	
Constant	-1.025	0.405	6.409	0.0114			
Fracture energy	0.075	0.0221	11.5589	<0.001	1.078	1.032	1.126
Parameter	**Estimate**	**Standard Error**	**Wald Chi-Square**	**Prob > ChiSq**	**OR Point Estimate**	**95% Wald Confidence Limits**	
Constant	-0.493	0.310	2.529	0.1118			
Normalized Fracture Energy	0.049	0.018	7.704	0.006	1.050	1.015	1.087

Table 9. Results of logistic regressions of PTOA risk as predicted by the fracture energy in the top division in each table and by surface area-normalized fracture energy in the bottom division for the calcaneus. For each regression, their respective parameter and odds ratio (OR) estimates are reported as well as a confidence interval of the OR.

Calcaneal							
Parameter	Estimate	Standard Error	Wald Chi-Square	Prob > ChiSq	OR Point Estimate	95% Wald Confidence Limits	
Constant	-0.789	1.892	0.174	0.677			
Fracture energy	0.063	0.098	0.418	0.518	1.065	0.880	1.289
Parameter	Estimate	Standard Error	Wald Chi-Square	Prob > ChiSq	OR Point Estimate	95% Wald Confidence Limits	
Constant	-1.071	1.584	0.457	0.499			
Normalized Fracture Energy	0.062	0.065	0.911	0.340	1.064	0.937	1.209

Table 10. Results of logistic regressions of PTOA risk as predicted by the fracture energy in the top division in each table and by surface area-normalized fracture energy in the bottom division for the tibial plafond. For each regression, their respective parameter and odds ratio (OR) estimates are reported as well as a confidence interval of the OR.

Tibial Plafond							
Parameter	Estimate	Standard Error	Wald Chi-Square	Prob > ChiSq	OR Point Estimate	95% Wald Confidence Limits	
Constant	-1.366	0.640	4.556	0.033			
Fracture energy	0.100	0.0411	5.957	0.015	1.106	1.020	1.198
Parameter	Estimate	Standard Error	Wald Chi-Square	Prob > ChiSq	OR Point Estimate	95% Wald Confidence Limits	
Constant	-2.721	0.823	10.943	<0.001			
Normalized Fracture Energy	0.154	0.042	12.845	<0.001	1.166	1.072	1.269

Table 11. Results of logistic regressions of PTOA risk as predicted by the fracture energy in the top division in each table and by surface area-normalized fracture energy in the bottom division for the acetabulum. For each regression, their respective parameter and odds ratio (OR) estimates are reported as well as a confidence interval of the OR.

Acetabular							
Parameter	Estimate	Standard Error	Wald Chi-Square	Prob > ChiSq	OR Point Estimate	95% Wald Confidence Limits	
Constant	-0.847	0.5916	2.0474	0.1525			
Fracture energy	0.064	0.0289	4.8539	0.028	1.066	1.007	1.128
Parameter	Estimate	Standard Error	Wald Chi-Square	Prob > ChiSq	OR Point Estimate	95% Wald Confidence Limits	
Constant	-0.792	0.605	1.716	0.190			
Normalized Fracture Energy	0.151	0.073	4.217	0.040	1.162	1.007	1.342

Contact stress over-exposure in the tibial plafond after IAF

A total of 17 unilateral fractures of the tibial plafond were studied. For those included in the final analyses, the average age of the patients was 37.9±10.4 at the time of surgery (40.2±12.3 years in the OA group and 36.7±9.0 years for the no OA group, p=0.59). The average weight was 101.8±27.9 kg for the OA group and 85.0±8.6 kg in the normal controls. There were 10 males and 7 females in the patient group (7 males and 4 females in the OA group).

Fractured tibiotalar joints experienced an average maximum contact stress over-exposure of 0.69±0.17 MPa*s. Patients that developed PTOA had significantly higher maximum contact stress over-exposures in the tibiotalar joints than patients that did not (0.77±0.16 MPa*s in the OA group and 0.55±0.03 MPa*s in the No OA group, $p < 0.001$). Examining plots of the contact stresses, contact patches appeared more focal with higher peak contact stresses in cases that developed PTOA compared to more diffuse regions of lower contact stresses in the no PTOA groups (Figure 25).

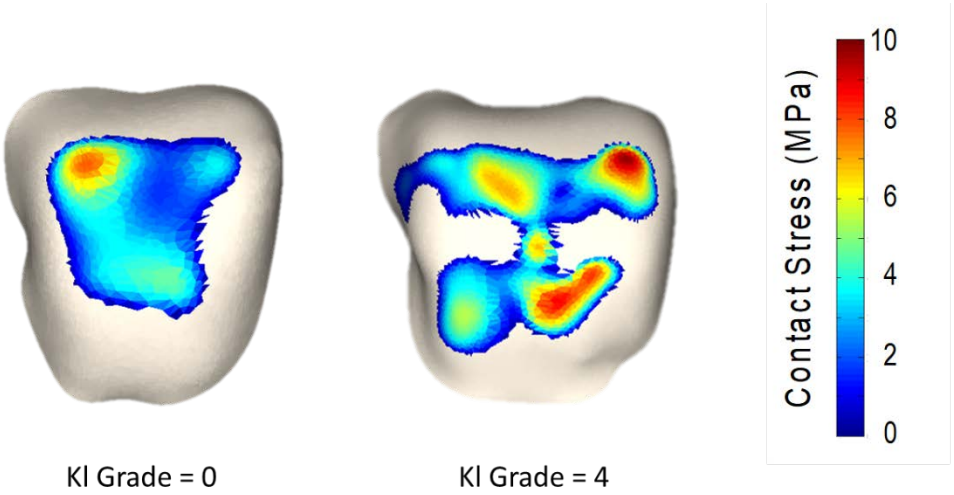

Figure 25. Contact stress distributions on the talar dome after tibial plafond IAF reconstruction. Cases that developed PTOA tended to have more focal and higher peak contact stresses than cases that did not.

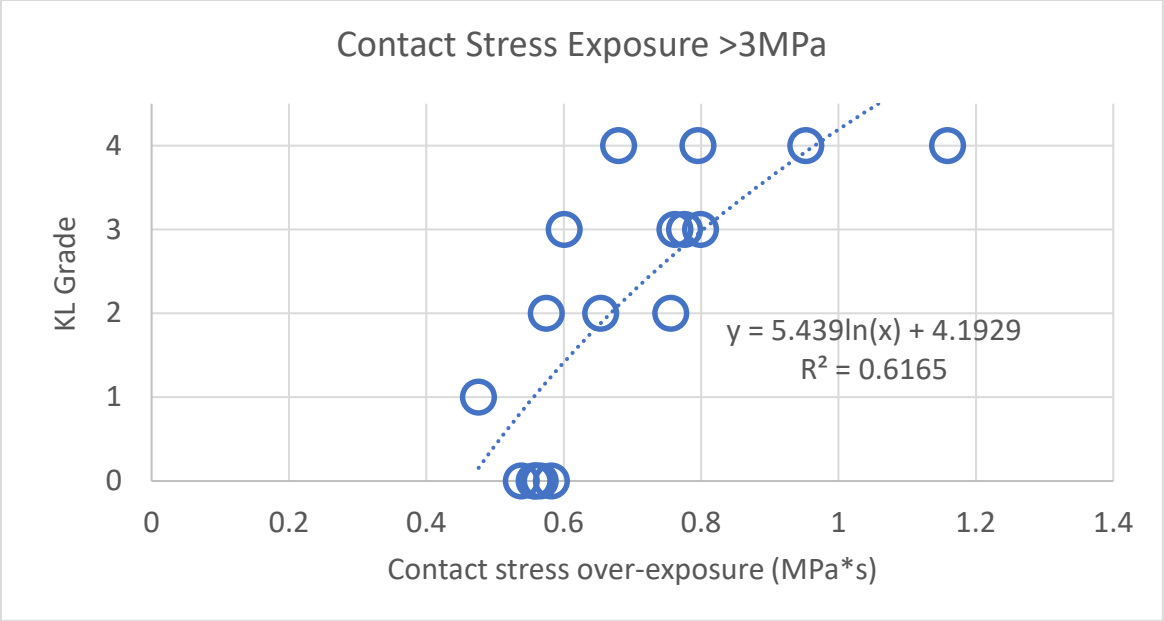

Figure 26. Contact stress over-exposure is highly correlated with PTOA outcomes in the tibial plafond after IAF reconstruction.

Contact stress over-exposure was found to be best correlated with patient outcomes when using a damage threshold of 3 MPa. The resulting exposures for each case are plotted above in Figure 26. There appears to be a clear delineation between exposures that develop PTOA and those that do not. Exposures above 0.6 MPa*s appear to predictably progress to PTOA development. There is also a strong correlation between the degree of radiographic arthritis and the quantity of over-exposure. It is important to note here that, as might be expected, the correlations reported do not directly explain the amount of variance in arthritis development as might be expected. This is because the KL grade is a categorical variable such that each grade will contain a range of continuous predictor values. The effect of this is that it will skew the assessment of variance toward a lower range and prevent it from having a directly interpretable meaning. Therefore, the R^2 values are merely included and discussed to generally assess each predictor against one another. Statistical evaluations of these correlations are performed with the Spearman's correlations as reported below in Table 12.

The measures of injury severity, as seen in the previous section, are also correlated with PTOA outcomes in this series of patients. The fracture energy and articular comminution energy are both moderately correlated with patient outcomes. The area-normalized fracture energy demonstrated a slightly stronger correlation with outcomes. It also demonstrated a potential cutoff above 1.5J/cm^2 that clearly demarcates the boundary between cases that did and did not develop radiographic PTOA above KL grade 2. The articular comminution energy, the energy absorbed within 10mm of the joint space, was the most highly correlated predictor. When combined with the normalized fracture energy, the results improved even further where a potential threshold at 0.2 would only misclassify one case.

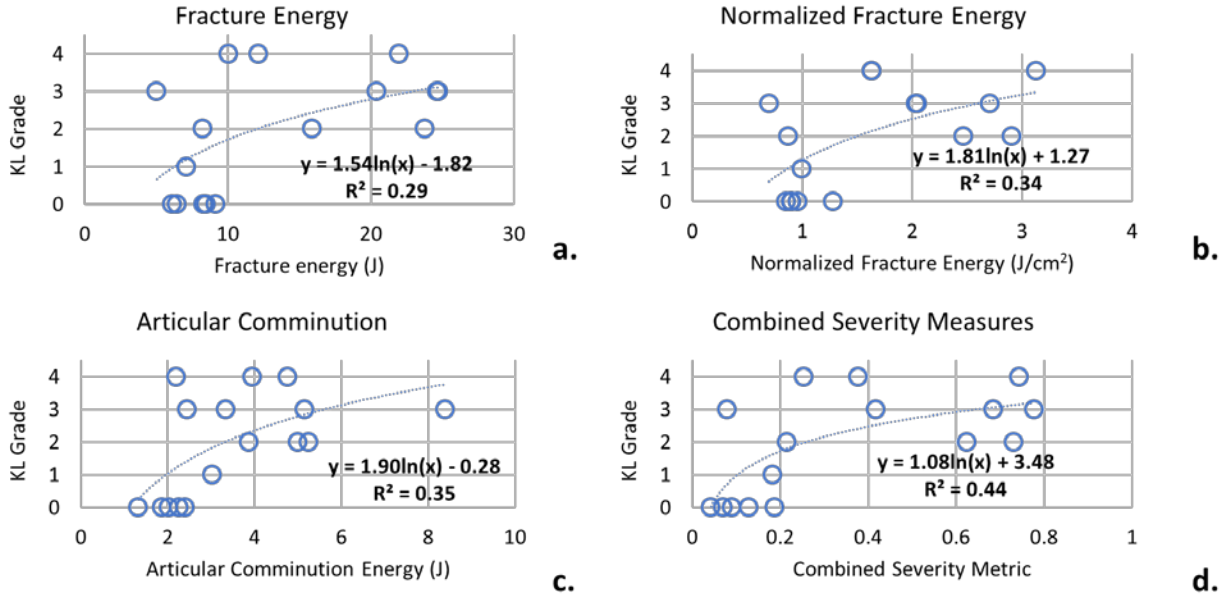

Figure 27. Correlations between measures of injury severity and radiographic outcomes in the tibial plafond. The area-normalized fracture energy, c, and the articular comminution, b, were normalized and combined equally to create the combined measure shown in d.

A further equally combined model of the composite injury severity measures shown in Figure 27d and the reduction accuracy (as quantified by the contact stress over-exposure in Figure 26) was created and is shown in Figure 29. This combined model explains over 70% of the variance in the degree of radiographically measured arthritic degeneration, further improving

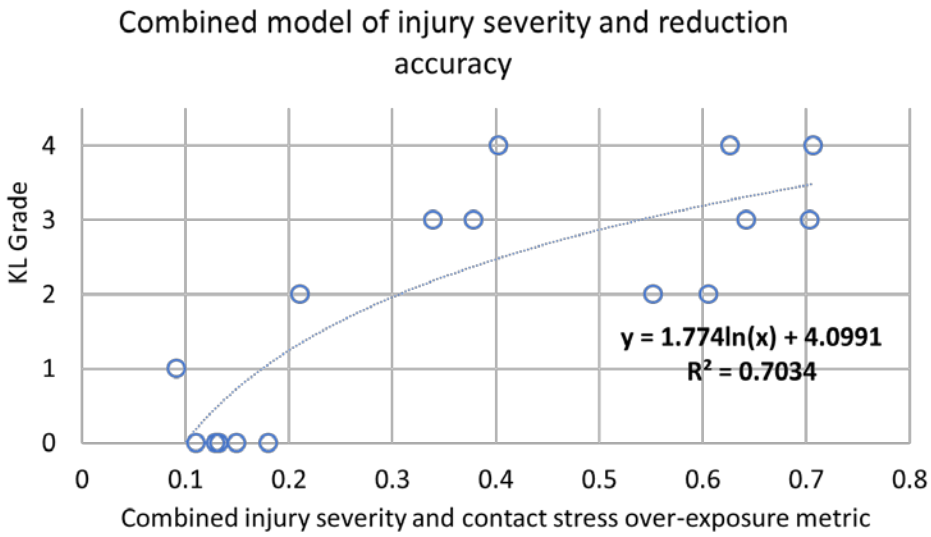

Figure 29. Combined model of the best objective measures of injury severity and reduction accuracy in the tibial plafond.

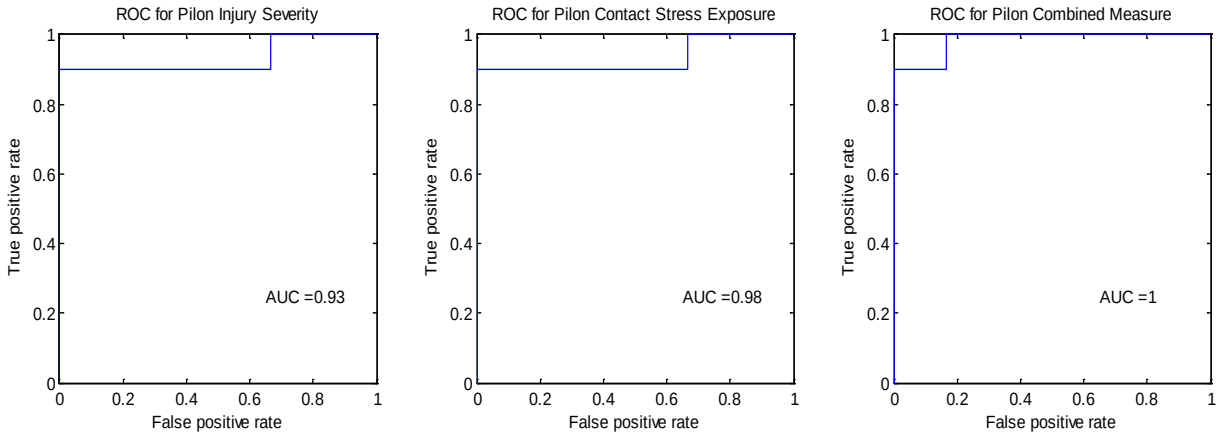

Figure 28. ROC curves for the tibial plafond of the combined injury severity measure, contact stress over-exposure, and the combined measure of injury severity and contact stress over-exposure. The AUC for each case is displayed on each graph.

upon its constitutive components. If a threshold were applied around 0.2, it would also achieve perfect delineation between cases that did and did not develop arthritis.

The accuracy of the model was demonstrated by the receiver operating characteristic (ROC) curves shown in Figure 28. The injury severity had excellent accuracy with an area under the curve (AUC) of 0.93 while the contact stress exposure measure had even higher accuracy with an AUC of 0.98. The combined measure of injury severity and contact stress over-exposure provided the best results with a perfect accuracy demonstrated by its AUC of 1.00.

To examine the relationships between the objective measures of injury severity and reduction accuracy, area-normalized fracture energy was plotted against contact stress over-exposure in Figure 26 and the combined severity metric from Figure 27d was plotted against the contact stress over-exposure above 3 MPa in Figure 31. Neither figure evinces a strong correlation between the injury severity and the reduction accuracy in these cases. Comparing the small blue bubbles that indicate KL grades of 0 and 1 to the large red bubbles indicating PTOA development of grades 2 through 4, we note that the former are clustered in the lower left-hand corner, indicating that cases that did not develop PTOA tended to have lower objective measures of injury severity and better reduction accuracy. Conversely, cases that had poor reductions and high injury severity predictably (found in the upper right corner) progressed to PTOA.

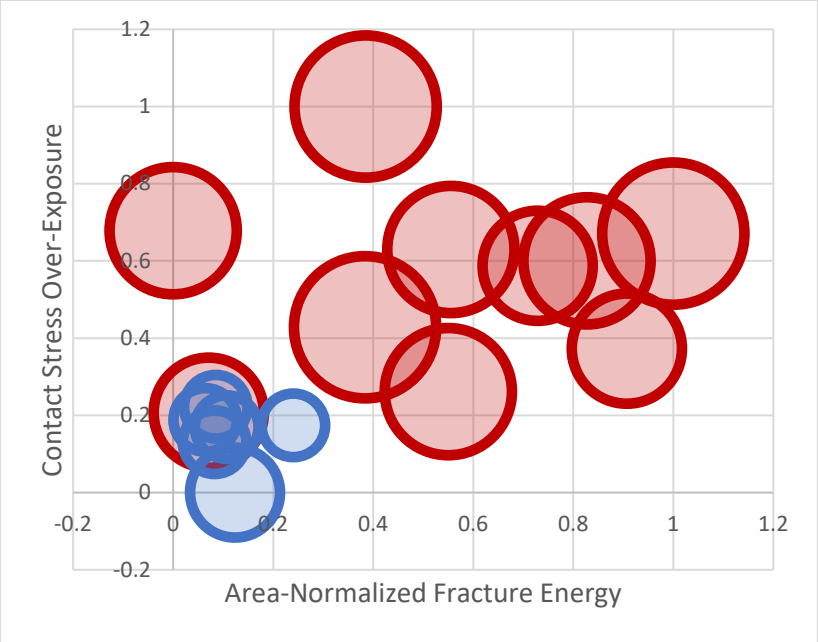

Figure 30. Normalized fracture energy is not correlated with contact stress over-exposure in fractures of the tibial plafond. High levels of contact stress over-exposure and area-normalized fracture energy are associated with higher grades of radiographic arthritis (KL 0-1 are shown as small blue bubbles and KL 2-4 are shown as larger red bubbles).

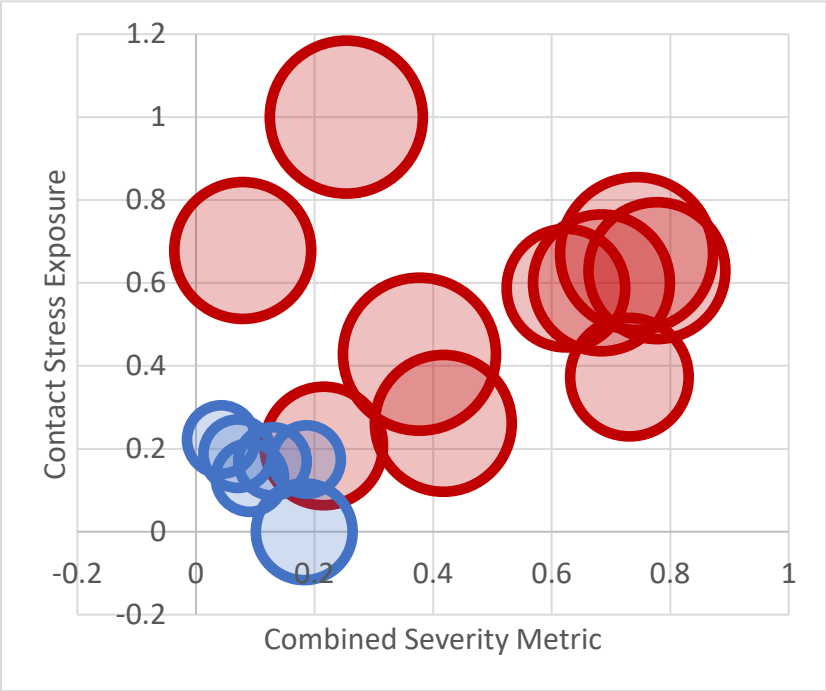

Figure 31. A combined metric to estimate the severity of articular injury is not correlated with contact stress over-exposure in the tibial plafond. Low levels of contact stress over-exposure and injury severity are associated with forestallment of PTOA (small blue bubbles) while high levels of both either or both were associated with PTOA development (large red bubbles).

The results of the Spearman's rank order correlations also demonstrated significant correlations between predictors and outcomes (Table 12). The two potential confounders, age and sex, were not significantly correlated to any of the predictors or outcomes. Fracture energy, articular comminution, area-normalized fracture energy, the injury severity composite, and stress and severity combined measures were all significantly correlated with radiographic outcomes of arthritis.

Table 12. Spearman's correlations of all predictors and radiographic outcomes in the tibial plafond. Significant correlations in bold.

Spearman Correlation Coefficients, N = 16									
	Fracture energy	Articular comm	Area norm energy	Contact Stress Exposure	Injury Severity Composite	Stress & Severity	Age	Sex	KL
Fracture energy	1.00000	**0.78824 0.0003**	**0.91471 <.0001**	0.42059 0.1048	**0.93529 <.0001**	**0.76471 0.0006**	-0.26510 0.3211	-0.44809 0.0817	**0.52064 0.0387**
Articular comm	**0.78824 0.0003**	1.00000	**0.72353 0.0015**	0.42941 0.0969	**0.89412 <.0001**	0.71765 0.0017	-0.16200 0.5489	-0.36407 0.1657	**0.54788 0.0280**
Area norm energy	**0.91471 <.0001**	**0.72353 0.0015**	1.00000	0.44412 0.0848	**0.89706 <.0001**	**0.74706 0.0009**	-0.15758 0.5600	-0.19604 0.4668	**0.51761 0.0400**
Contact Stress Exposure	0.42059 0.1048	0.42941 0.0969	0.44412 0.0848	1.00000	**0.51471 0.0413**	**0.87647 <.0001**	-0.02946 0.9138	0.08402 0.7571	**0.82636 <.0001**
Injury Severity Composite	**0.93529 <.0001**	**0.89412 <.0001**	**0.89706 <.0001**	**0.51471 0.0413**	1.00000	**0.83235 <.0001**	-0.18704 0.4879	-0.36407 0.1657	**0.64626 0.0068**
Stress & Severity	**0.76471 0.0006**	**0.71765 0.0017**	**0.74706 0.0009**	**0.87647 <.0001**	**0.83235 <.0001**	1.00000	-0.12960 0.6324	-0.16803 0.5339	**0.79912 0.0002**
Age	-0.26510 0.3211	-0.16200 0.5489	-0.15758 0.5600	-0.02946 0.9138	-0.18704 0.4879	-0.12960 0.6324	1.00000	**0.67313 0.0043**	-0.20993 0.4352
Sex	-0.44809 0.0817	-0.36407 0.1657	-0.19604 0.4668	0.08402 0.7571	-0.36407 0.1657	-0.16803 0.5339	**0.67313 0.0043**	1.00000	-0.12970 0.6321
KL	**0.52064 0.0387**	**0.54788 0.0280**	**0.51761 0.0400**	**0.82636 <.0001**	**0.64626 0.0068**	**0.79912 0.0002**	-0.20993 0.4352	-0.12970 0.6321	1.00000

Contact stress over-exposure in the calcaneus after IAF

A total of 41 fractures from 32 patients were studied. Of the 41 patient-specific fracture models created, 33 reached convergence and were included in final analyses. There was no significant difference in KL graded outcomes between the patients whose models converged and those that did not. Both normal controls also reached convergence. For those included in the final analyses, the average age of the patients was 43.3 at the time of surgery (42.2±7.7 years in the OA group and 44.5±13.4 years for the no OA group, p=0.56). The average BMI was 26.7±4.0. There were 30 males and 3 females in the patient group (16 males and 1 female in the OA group).

The subtalar joints in the PTOA group were exposed to an average maximum contact stress over-exposure of 1.22±0.45 MPa*s (mean ± standard deviation). Fractured subtalar joints experienced an average maximum contact stress over-exposure of 0.99±0.19 MPa*s. This difference was highly significant (p=0.005). Examining plots of the contact stresses, contact patches appeared more focal with higher peak contact stresses in cases that developed PTOA compared to more diffuse regions of lower contact stresses in the no PTOA groups (Figure 32).

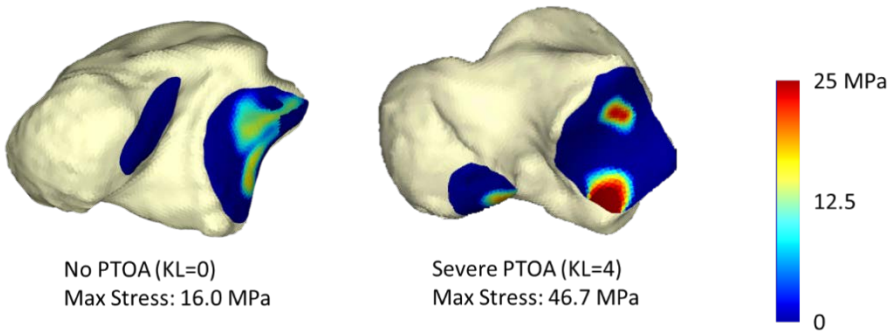

Figure 32. Differences in the maximum contact stress patches shown between a case that did not develop PTOA and a case that developed severe PTOA.

The results of the fracture energy analysis were similar to what was previously reported on the entire series of 48 fractures, fracture energy in the subgroup of 33 that reached convergence was not significantly correlated with PTOA outcomes (p=0.08). When considering the area-normalized fracture energy, differences were significant (2.54±0.40 MPa*s in the OA group versus 2.24±0.38 MPa*s in the no OA group, p=0.04).

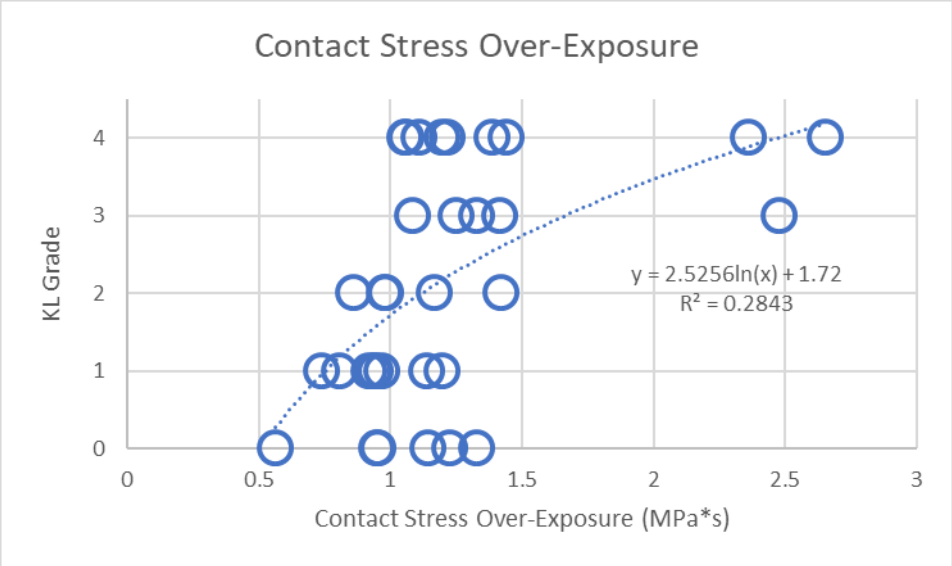

Figure 33. Contact stress over-exposure is correlated with PTOA outcomes after IAF in the calcaneus.

Contact stress over-exposure was found to be best correlated with patient outcomes when using a damage threshold of 10MPa. This is significantly higher than the 3MPa found in the tibiotalar joint in the previous section. The resulting exposures for each case are plotted above in Figure 33. There is not a clear delineation between exposures that develop PTOA and those that do not in the subtalar joint. Exposures above 1.25 MPa*s appear to be more likely to progress to PTOA development. There is also a small to moderate correlation between the degree of radiographic arthritis and the quantity of over-exposure with the over-exposure potentially explaining 28.4% of the variance in arthritis development. As noted in the discussion of the

plafond results, it is important to note that these variances are skewed low by the comparison of a categorical and continuous variables and have no directly interpretable meaning. Therefore, they are merely reported as a reference for comparison across predictors. Statistical analysis of correlations was performed using Spearman's correlations in Table 13.

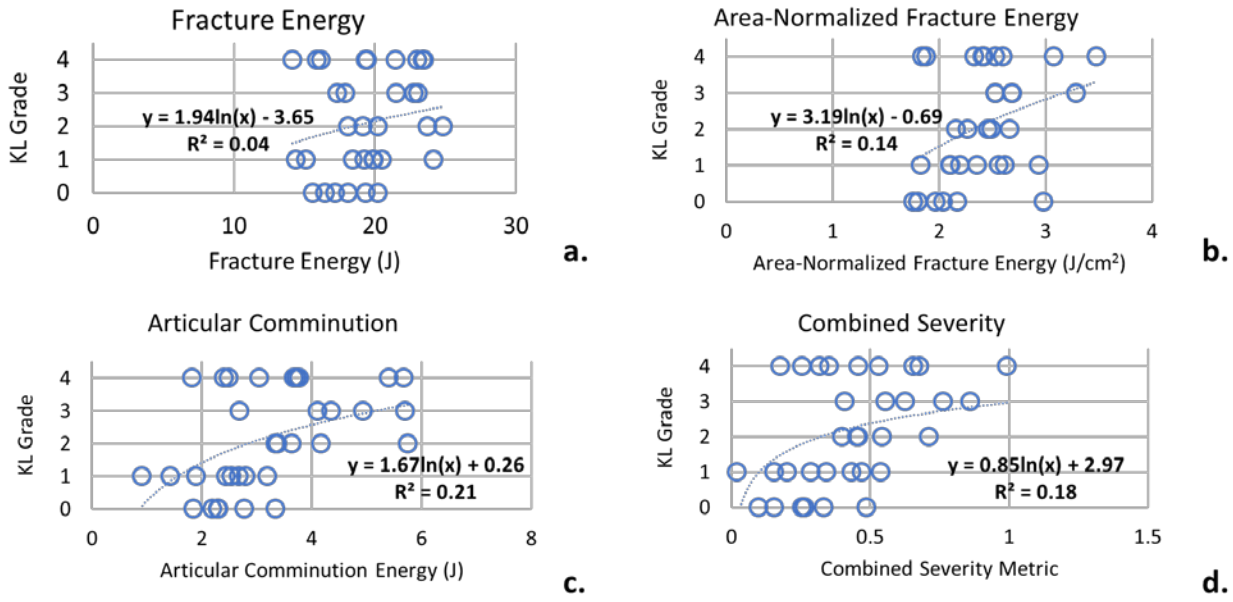

Figure 34. Correlations between measures of injury severity and radiographic outcomes in the calcaneus after IAF. The area-normalized fracture energy, c, and the articular comminution, b, were normalized and combined equally to create the combined measure shown in d.

Some measures of injury severity, as seen earlier in this document, are also correlated with PTOA outcomes in this subset of that prior series of 48 patients. The fracture energy was not correlated with outcomes ($R^2 = 0.04$, Figure 34a). The area-normalized fracture energy demonstrated a slightly stronger correlation with outcomes ($R^2=0.14$, Figure 34c), but was still not significant. The articular comminution as a measure of injury severity was the most correlated with patient radiographic outcomes, but its association was still rather modest. The articular comminution energy also appeared to demonstrate a potential cutoff around 3.5J, above

which cases were likely to degenerate to PTOA. Correspondingly, the average differences in articular comminution energy were also highly significant (3.90±1.15J in the OA group vs 2.33±0.64J in the no OA group, $p<0.001$). When combined with the normalized fracture energy, the correlation with degree of arthritic outcomes improved slightly, but did not demonstrate as clear of a threshold above which cases predictably progressed to PTOA as was seen previously in the plafond.

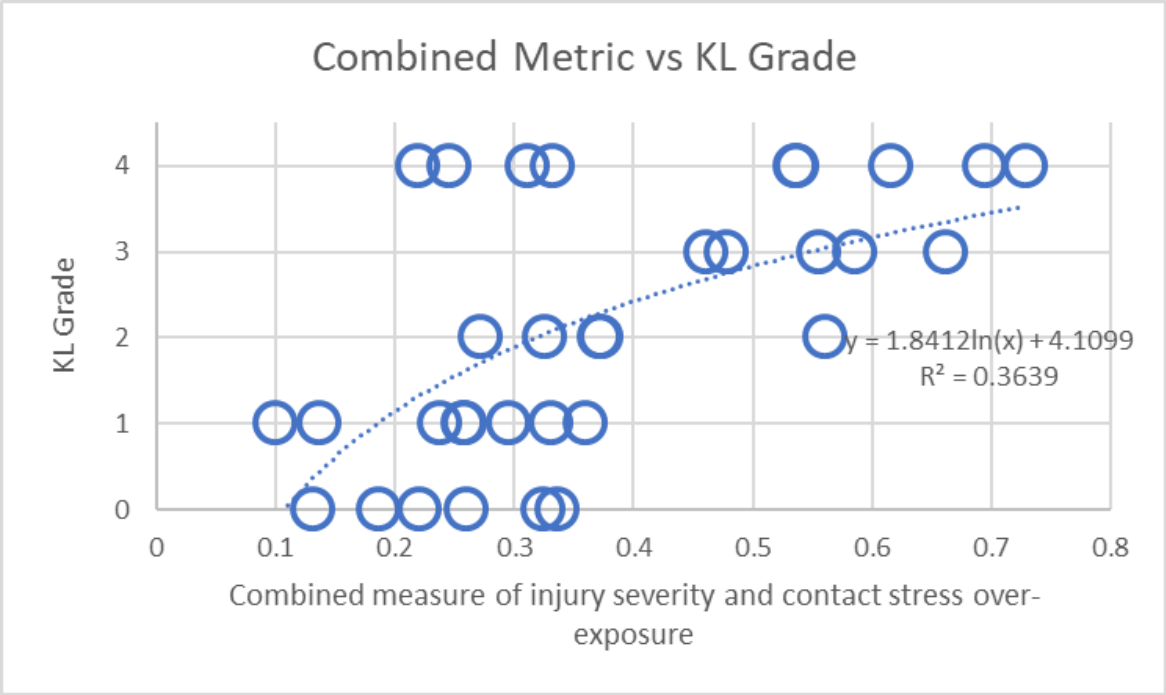

Figure 35. Combined model of the best objective measures of injury severity and reduction accuracy in reconstructed IAFs of the calcaneus.

A second combined model, this time of equal parts composite injury severity score (figure 34d) and contact stress over-exposure (Figure 33), was created (Figure 35). It demonstrated improved correlation with KL graded degree of radiographic arthritis over both of its constitutive components explaining over 36% of the variance in PTOA development. The metric also had a clear threshold around 0.4 above which cases predictably progressed to PTOA development.

The ROC curves, as shown in Figure 36, demonstrate the relative predictive accuracy of each measure. The combined injury severity measure provided equivalent predictive accuracy to that of the contact stress over-exposure measure, though both were slightly less predictive in this joint than in the plafond. Again, the combined measure of injury severity and contact stress over-exposure provided the best predictive accuracy of any model.

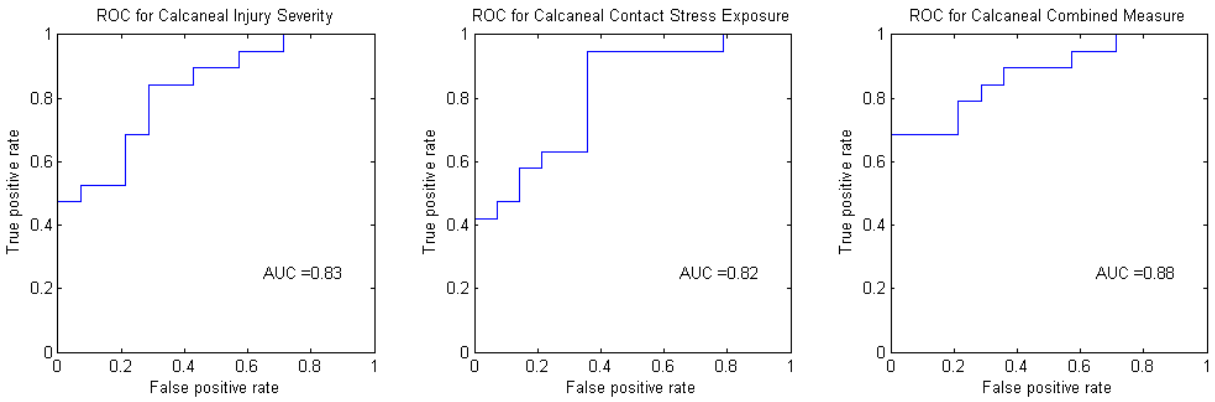

Figure 36. ROC curves for the calcaneus of the combined injury severity measure, contact stress over-exposure, and the combined measure of injury severity and contact stress over-exposure. The AUC for each case is displayed on each graph.

Examining the relationships between the objective measures of injury severity and reduction accuracy, area-normalized fracture energy was plotted against contact stress over-exposure in Figure 37 and the combined severity metric from Figure 34d was plotted against the contact stress over-exposure above 10 MPa in Figure 37. Neither finds a correlation between the injury severity and the reduction accuracy in these cases. Looking at the small blue bubbles that indicate KL grades of 0 and 1 in relation to the large red bubbles indicating PTOA development of grades 2-4, cases that did not develop PTOA tended to have lower objective measures of injury severity and better reduction accuracy, showing them clustered in the lower left-hand

corner. This is more apparent in the combined measure of severity in Figure 38. Conversely, cases that had poor reductions and high injury severity predictably progressed to PTOA in the upper right.

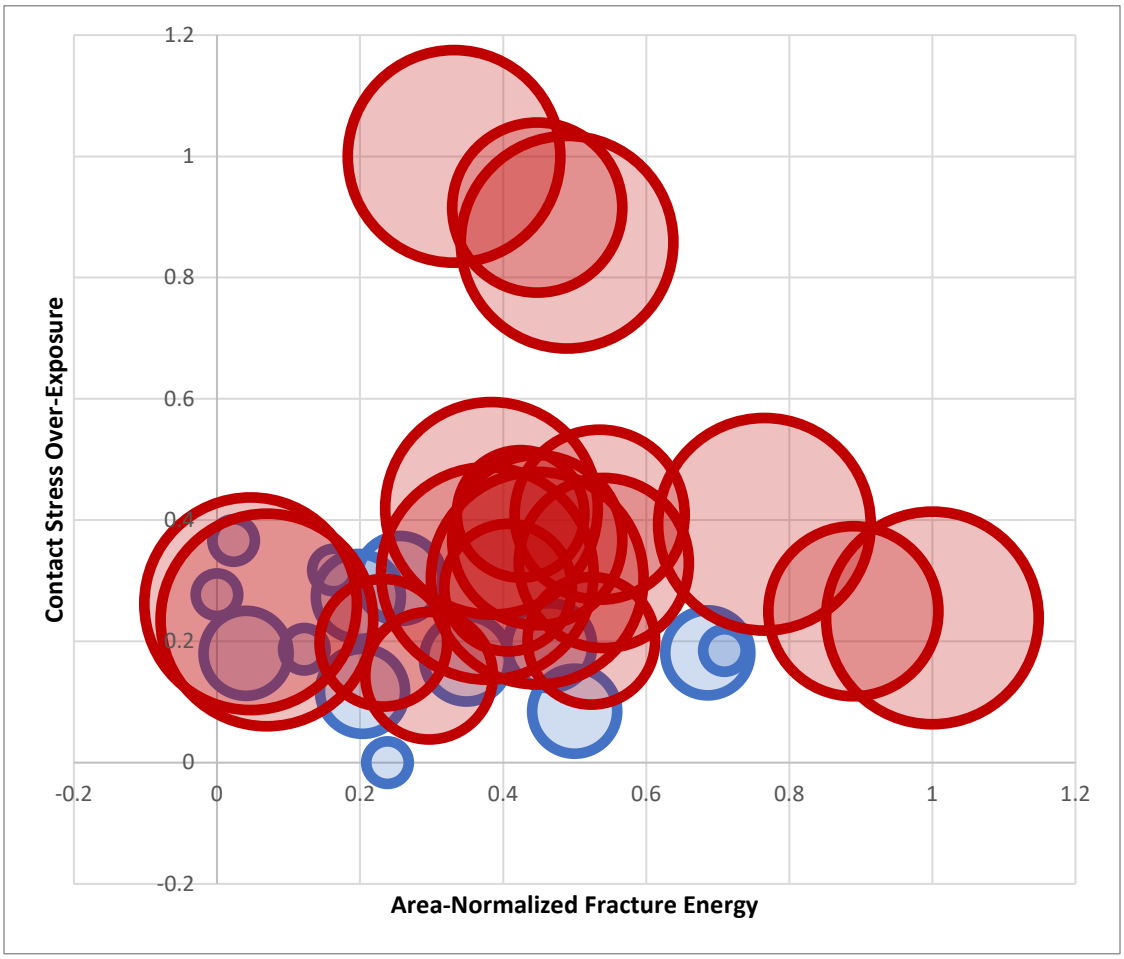

Figure 37. Normalized fracture energy is not correlated with contact stress over-exposure in the calcaneus. Cases that have low contact stress over-exposures demonstrate a lesser degree of radiographic arthritis (demonstrated by the larger red bubbles).

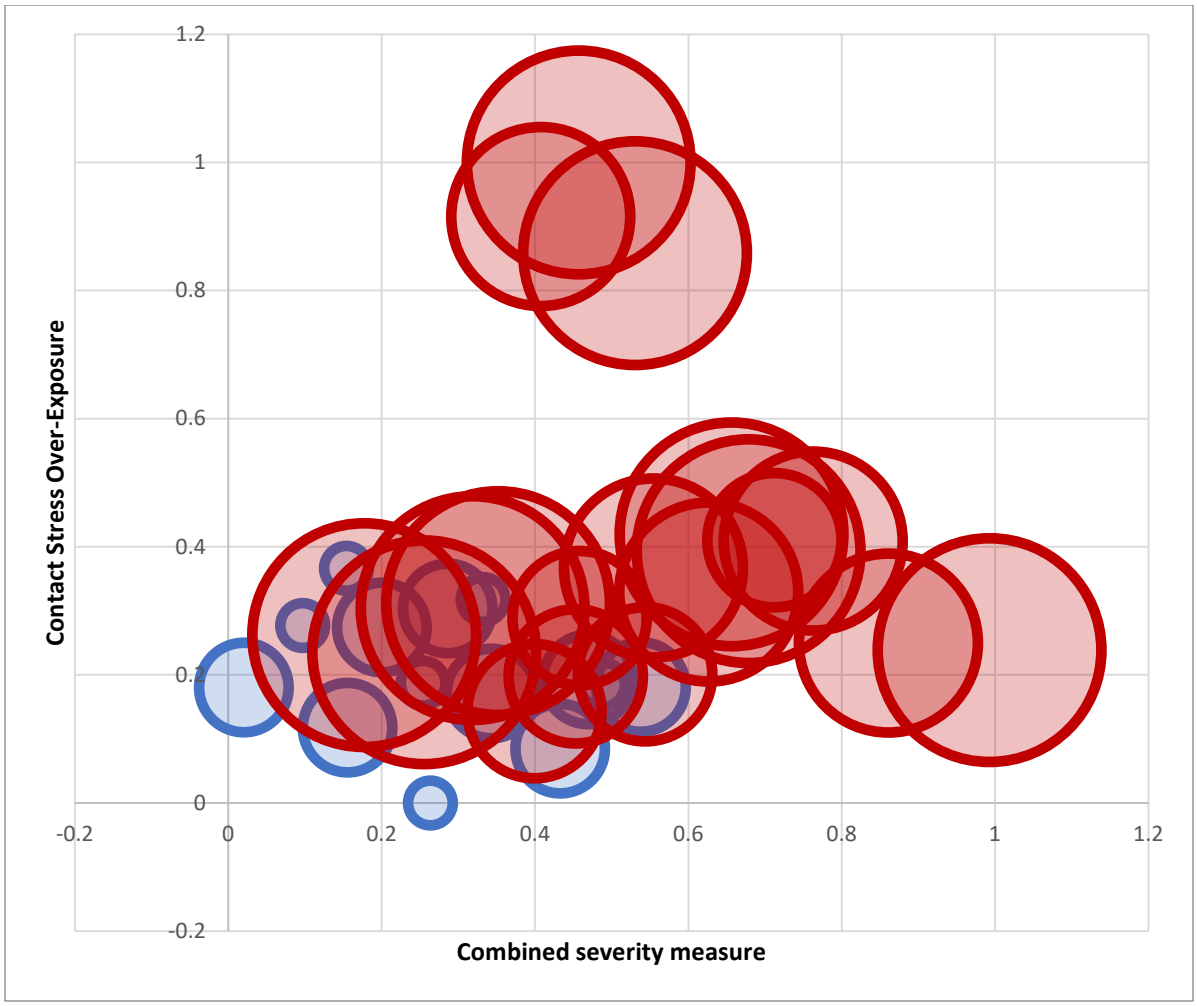

Figure 38. Combined severity measure is not correlated with contact stress over-exposure in the calcaneus. Cases that have low severity and contact stress over-exposures demonstrate lesser degrees of radiographic arthritis (demonstrated by larger red bubbles).

The results of the Spearman's rank order correlations found significant correlations between some of the predictors and outcomes (Table 13). The two potential confounders, age and sex, were not significantly correlated to any of the predictors or outcomes. Fracture energy by itself was not a significant predictor of outcomes but was significantly associated with Sanders classification, the gold standard clinical assessment of injury severity in the subtalar joint. Measures of contact stress exposure, articular comminution, the injury severity composite score, and stress and severity combined measures were all significantly correlated with radiographic outcomes of arthritis. The articular comminution energy and injury severity

composite were even more strongly predictive of the degree of arthritic development than the Sanders classification.

Table 13. Spearman correlation coefficients for predictors of PTOA in the subtalar joint after IAF of the calcaneus.

Spearman Correlation Coefficients										
	Contact Stress Exposure	Fracture Energy	Articular Comm	Area norm energy	Injury Severity Composite	Stress& Severity	Sanders	Age	Sex	KL
Contact Stress Exposure	1.00000	-0.04546 0.8017	**0.44472** **0.0095**	0.13574 0.4513	**0.34592** **0.0486**	**0.68549** **<.0001**	0.05781 0.7493	-0.112 0.4636	0.06642 0.7134	**0.52030** **0.0019**
Fracture Energy	-0.04546 0.8017	1.00000	0.520 0.0565	**0.68361** **<.0001**	**0.56973** **0.0005**	**0.45107** **0.0084**	**0.44250** **0.0099**	-0.09051 0.6164	0.09410 0.6024	0.20942 0.2421
Articular Comm	**0.44472** **0.0095**	0.520 0.0565	1.00000	**0.53900** **0.0012**	**0.85853** **<.0001**	**0.77463** **<.0001**	0.20482 0.2529	-0.26601 0.1346	0.22142 0.2156	**0.48516** **0.0042**
Area norm energy	0.13574 0.4513	**0.68361** **<.0001**	**0.53900** **0.0012**	1.00000	**0.87362** **<.0001**	**0.71615** **<.0001**	0.26449 0.1369	-0.285 0.1102	0.02215 0.9026	**0.35936** **0.0400**
Injury Severity Composite	**0.34592** **0.0486**	**0.56973** **0.0005**	**0.85853** **<.0001**	**0.87362** **<.0001**	1.00000	**0.85227** **<.0001**	0.22580 0.2064	-0.31095 0.0782	0.07749 0.6682	**0.45646** **0.0076**
Stress& Severity	**0.68549** **<.0001**	**0.45107** **0.0084**	**0.77463** **<.0001**	**0.71615** **<.0001**	**0.85227** **<.0001**	1.00000	0.21224 0.2357	-0.26206 0.1407	0.06642 0.7134	**0.57250** **0.0005**
Sanders	0.05781 0.7493	**0.44250** **0.0099**	0.20482 0.2529	0.26449 0.1369	0.22580 0.2064	0.21224 0.2357	1.00000	-0.13558 0.4519	0.10604 0.5570	**0.41419** **0.0166**
Age	-0.112 0.4636	-0.09051 0.6164	-0.26601 0.1346	-0.285 0.1102	-0.31095 0.0782	-0.26206 0.1407	-0.13558 0.4519	1.00000	-0.028 0.8541	-0.16129 0.3699
Sex	0.06642 0.7134	0.09410 0.6024	0.22142 0.2156	0.02215 0.9026	0.07749 0.6682	0.06642 0.7134	0.10604 0.5570	-0.028 0.8541	1.00000	0.30612 0.08
KL	**0.52030** **0.0019**	0.20942 0.2421	**0.48516** **0.0042**	**0.35936** **0.0400**	**0.45646** **0.0076**	**0.57250** **0.0005**	**0.41419** **0.0166**	-0.16129 0.3699	0.30612 0.08	1.00000

Contact stress over-exposure in the acetabulum after IAF

A total of 22 patients were included in the final analysis. Fifteen out of 22 patients developed OA. The mean follow-up time for joints that developed PTOA was 33.1 (12.8-69) months. The mean follow-up time for joints that did not develop OA was 31.6 (12.2-76) months. Follow-up time was not significantly associated with PTOA (p=0.82). The average age of the patients was 39.7 ± 16.2 years at the time of surgery (42.7 ± 16.6 years in the OA group and 33.3 ± 13.1 years for the no OA group, p=0.19). The average BMI was 30.4±6.4 for the patients (29.7 ± 7.0 in the OA group and 32.7 ± 3.1 in the no OA group, p=0.24). There were 18 males and 4 females in the patients studied (2 females in the OA group).

Qualitatively, the contact stress over-exposure distributions in the cases that did not develop OA were smaller and varied more gradually over the surface than those in the OA group (Figure 16). For those in the PTOA group, there were much more focal contact stress elevations that led to higher regions of over-exposure and varied in location over the gait cycle, attributable to larger local articular surface incongruities. All hips from patients with acetabular fractures experienced an average maximum contact stress exposure of 4.41 ± 1.53 MPa*s. Patients that developed PTOA had significantly higher maximum contact stress exposures in their hips than patients that did not (5.00 ± 1.38 MPa*s vs. 3.15 ± 0.96 MPa*s; p=0.003).

The range of fracture energies for the 19 cases on which it was computed was 7.0-41.4 J (18.3 ± 9.6 J). As was found in the larger study of injury severity reported earlier in this document, for the cases that developed PTOA, fracture energy was significantly higher than for those that did not (22.2 ± 9.2 J in the OA group and 10.0±3.1 in the group that did not develop OA, p<0.001).

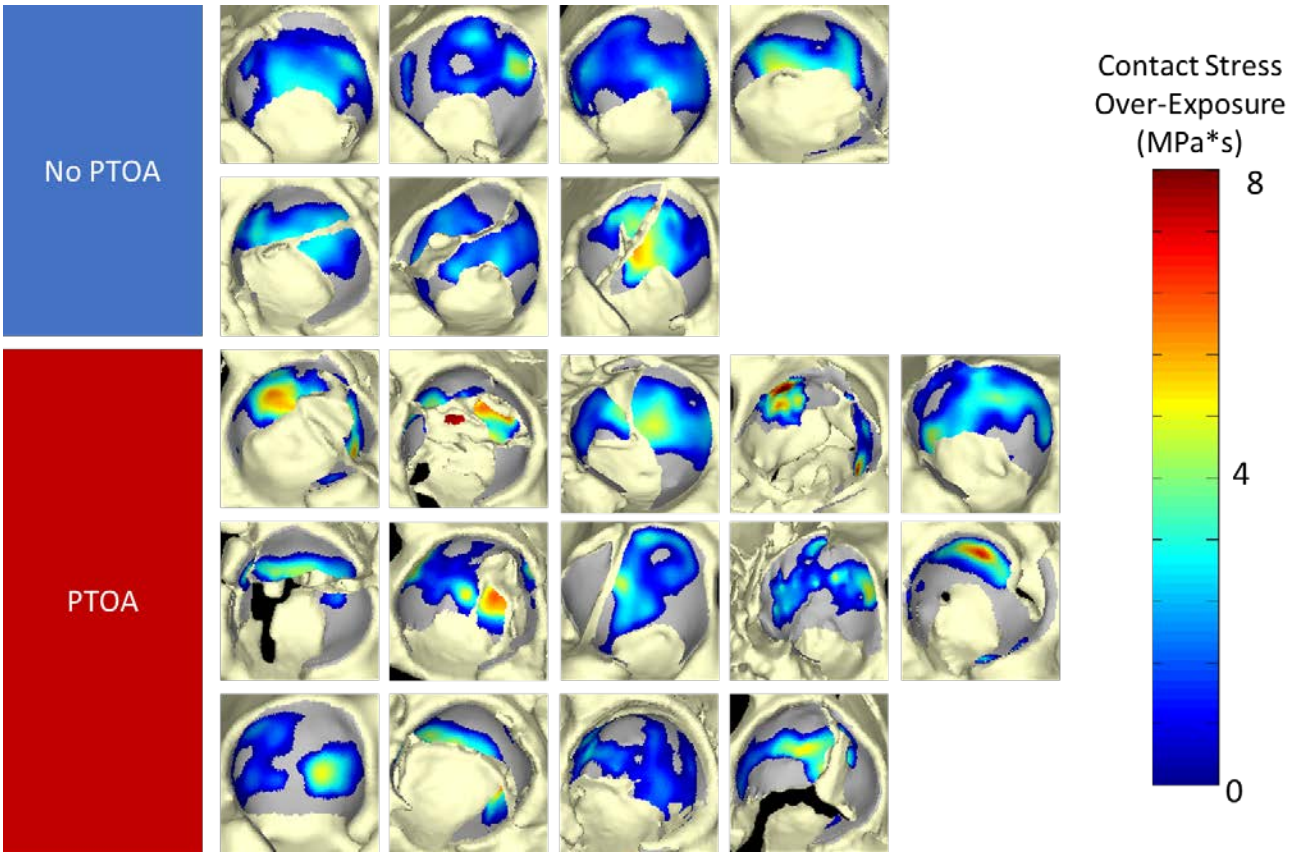

Figure 39. The contact stress over-exposure distributions for the patients who had developed PTOA at two years after surgery were substantially more focal and had significantly higher peak values.

Contact stress over-exposure was found to be best correlated with patient outcomes when using a damage threshold of 1 MPa. This is lower than the 3MPa found in the tibiotalar joint and substantially lower than the 10MPa found for the calcaneal fractures in the previous section. The resulting exposures for each case are plotted above in Figure 399. There is delineation between exposures that develop PTOA in the acetabulum around 4 MPa*s. There is also a moderate correlation between the degree of radiographic arthritis and the quantity of over-exposure with the over-exposure potentially explaining 41% of the variance in arthritis development (Figure 4040). As noted in the discussion of the plafond and calcaneal results, it is important to be aware

that these variances are skewed low by the comparison of categorical and continuous variables and have no directly interpretable meaning. Therefore, they are merely reported as a reference for comparison across predictors. Statistical analysis of correlations was performed using Spearman's correlations in Table 14.

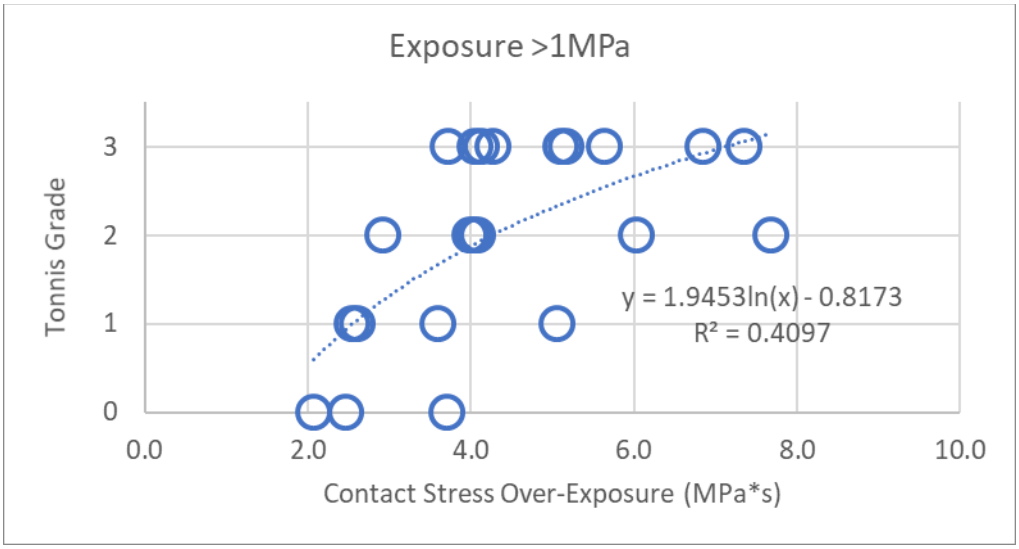

Figure 40. Contact stress over-exposure is correlated with PTOA outcomes after IAF of the acetabulum.

Measures of injury severity, as seen earlier in this document, are also correlated with PTOA outcomes in this subset of that prior series of 71 acetabular fracture patients. The fracture energy had a small correlation with outcomes ($R^2 = 0.23$, Figure 41a). The articular comminution and area-normalized fracture energy measures demonstrated similar small correlations with outcomes (R^2=0.20 and $R^2 = 0.22$, Figure 41b and 41c, respectively). The fracture energy appeared to demonstrate a potential cutoff around 15J; above this value, cases were likely to degenerate to PTOA. When the normalized fracture energy and articular comminution were taken in equal parts to form a combined model, the correlation with degree of arthritic outcomes improved substantially (R^2=0.36) and a clear threshold above which cases predictably progressed to PTOA emerged around 0.4.

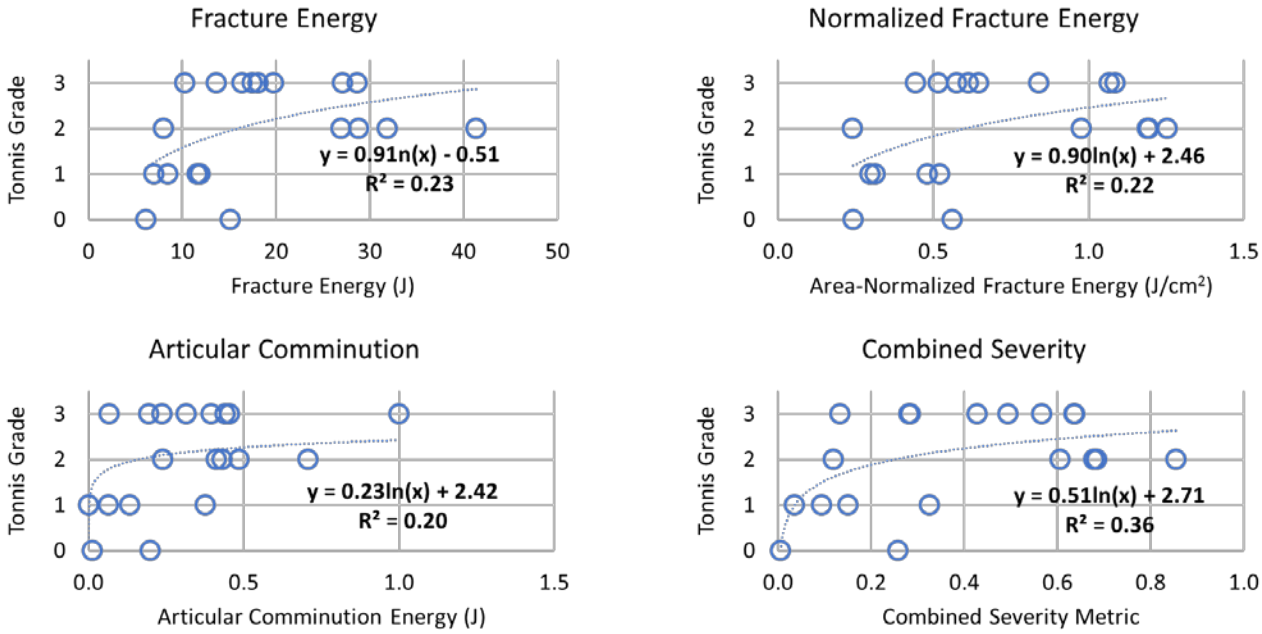

Figure 41. Correlations between measures of injury severity and radiographic outcomes in the acetabulum after IAF. The area-normalized fracture energy, c, and the articular comminution, b, were normalized and combined equally to create the combined measure shown in d.

Another combined model of equal parts composite injury severity score (Figure 41d) and contact stress over-exposure (Figure 40), was created (Figure 42). It demonstrated improved correlation with KL graded degree of radiographic arthritis over both of its constitutive components, explaining over 46% of the variance in PTOA development. The metric also had a clear threshold around 0.4 above which cases predictably progressed to PTOA development.

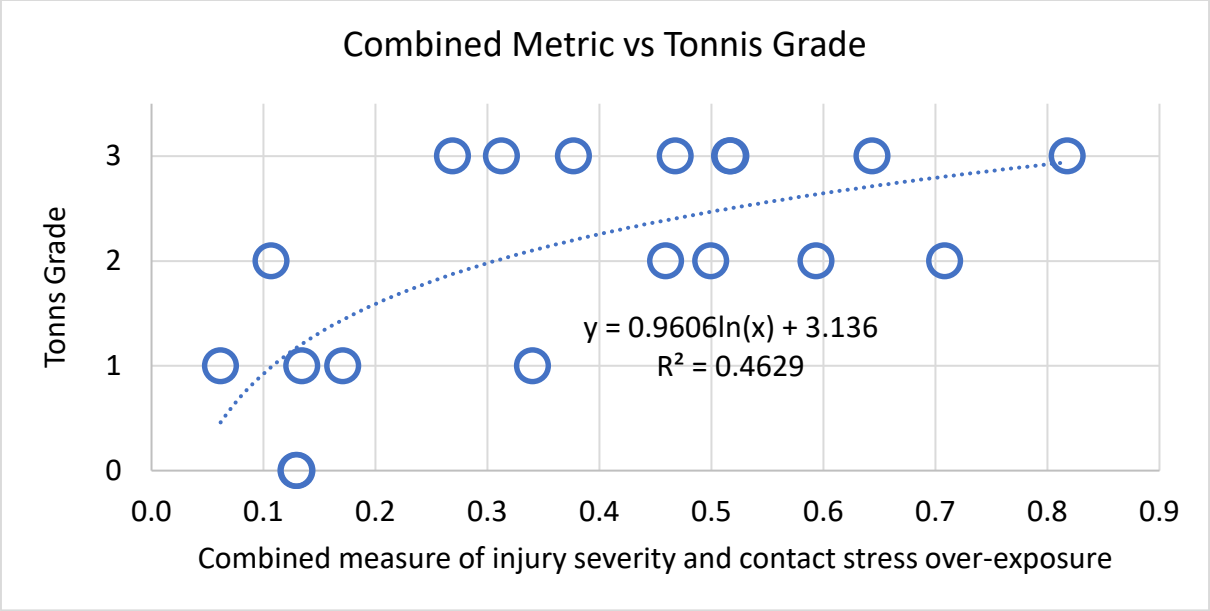

Figure 43. Combined model of injury severity and reduction accuracy predicts PTOA development in the acetabulum.

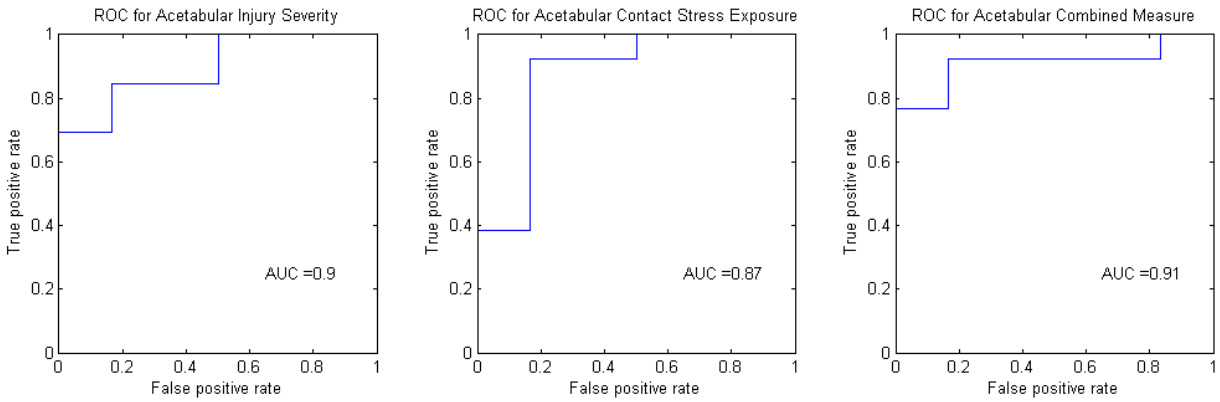

Figure 42. ROC curves for predictors of PTOA development in acetabular fractures. The combined measure of injury severity, the measure of contact stress over-exposure, and the combined measures of injury severity and contact stress over-exposure were plotted from left to right.

The ROC curves again demonstrated the predictive accuracy of each model for acetabular fractures in Figure 43. The combined measure of injury severity was slightly more predictive than the contact stress over-exposure measure while both had good to excellent accuracy. As

with the plafond and calcaneus, the combined measure provided the highest overall accuracy with an AUC of 0.91.

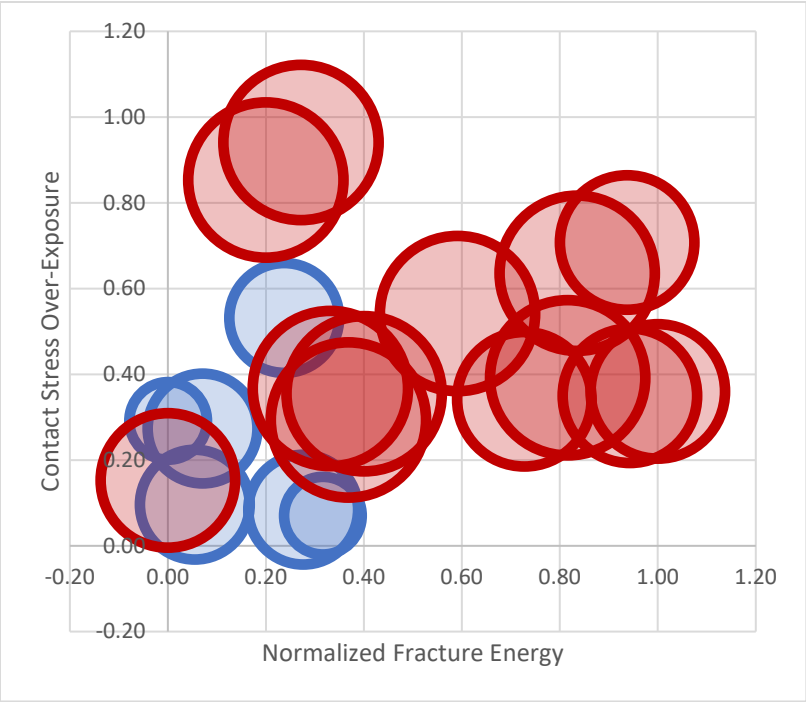

Figure 44. Normalized fracture energy is not correlated with contact stress over-exposure in fractures of the acetabulum. High levels of contact stress over-exposure and area-normalized fracture energy are associated with higher grades of radiographic arthritis (KL 0-1 are shown as small blue bubbles and KL 2-4 are shown as larger red bubbles).

Examining the relationships between the objective measures of injury severity and reduction accuracy, area-normalized fracture energy was plotted against contact stress over-exposure in Figure 44 and the combined severity metric from Figure 41d was plotted against the contact stress over-exposure above 1 MPa in Figure 45. Neither figure finds a strong correlation between the injury severity and the reduction accuracy in these cases. Noting the location of the small blue bubbles that indicate KL grades of 0 and 1 in relation to the large red bubbles indicating PTOA development of grades 2-4, cases that did not develop PTOA tended to have lower objective measures of injury severity and better reduction accuracy such that they were

clustered in the lower left-hand corner. Conversely, cases found in the upper right of the plot area had poor reductions, high injury severity, and consequently, predictably progressed to PTOA.

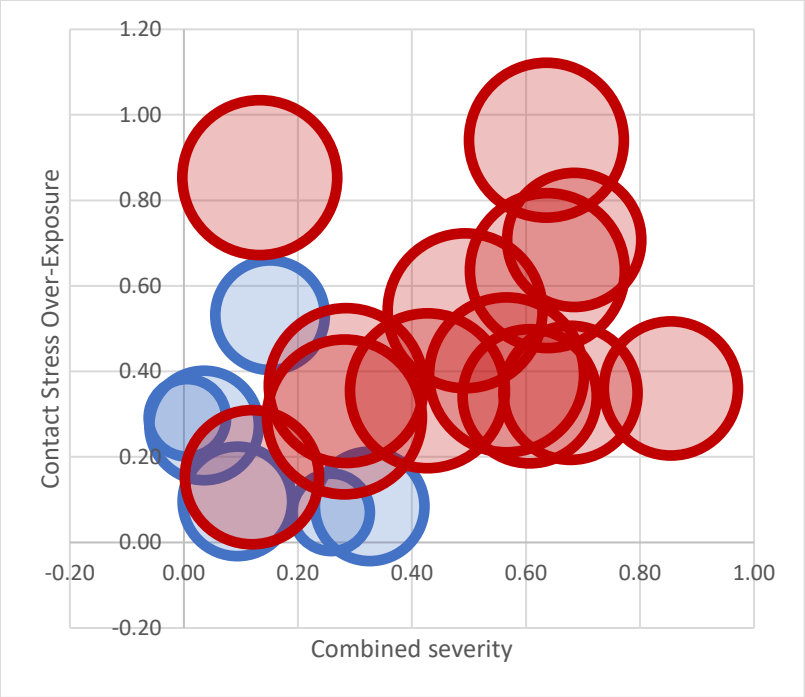

Figure 45. A combined metric to estimate the severity of articular injury is not correlated with contact stress over-exposure in the acetabulum. Low levels of contact stress over-exposure and injury severity are associated with forestallment of PTOA (small blue bubbles) while high levels of both either or both were associated with PTOA development (large red bubbles).

Table 14. Spearman Correlation Coefficients between mechanical predictors of PTOA and potential confounders.

Spearman Correlation Coefficients, N = 19									
	Contact Stress Exposure	Fracture Energy	Area norm energy	Articular comm	Injury Severity Composite	Stress& Severity	Age	Sex	Tonnis
Contact Stress Exposure	1.00000	0.40702 0.0837	0.37193 0.1169	0.37593 0.1127	**0.50175** **0.0286**	**1.00000** **<.0001**	0.12313 0.6155	-0.32998 0.1677	**0.67439** **0.0015**
Fracture Energy	0.40702 0.0837	1.00000	**0.92632** **<.0001**	**0.78173** **<.0001**	**0.91754** **<.0001**	0.40702 0.0837	-0.01671 0.9459	-0.21213 0.3833	0.43387 0.0635
Area norm energy	0.37193 0.1169	**0.92632** **<.0001**	1.00000	**0.69565** **0.0009**	**0.90877** **<.0001**	0.37193 0.1169	-0.05101 0.8357	-0.02357 0.9237	0.39131 0.0976
Articular comm	0.37593 0.1127	**0.78173** **<.0001**	**0.69565** **0.0009**	1.00000	**0.88450** **<.0001**	0.37593 0.1127	0.15103 0.5371	-0.05900 0.8104	0.44880 0.0539
Injury Severity Composite	**0.50175** **0.0286**	**0.91754** **<.0001**	**0.90877** **<.0001**	**0.88450** **<.0001**	1.00000	**0.50175** **0.0286**	0.00352 0.9886	-0.02357 0.9237	0.43294 0.0641
Stress& Severity	**1.00000** **<.0001**	0.40702 0.0837	0.37193 0.1169	0.37593 0.1127	**0.50175** **0.0286**	1.00000	0.12313 0.6155	-0.32998 0.1677	**0.67439** **0.0015**
Age	0.12313 0.6155	-0.01671 0.9459	-0.05101 0.8357	0.15103 0.5371	0.00352 0.9886	0.12313 0.6155	1.00000	0.02363 0.9235	0.22678 0.3505
Sex	-0.32998 0.1677	-0.21213 0.3833	-0.02357 0.9237	-0.05900 0.8104	-0.02357 0.9237	-0.32998 0.1677	0.02363 0.9235	1.00000	-0.16157 0.5087
Tonnis	**0.67439** **0.0015**	0.43387 0.0635	0.39131 0.0976	0.44880 0.0539	0.43294 0.0641	**0.67439** **0.0015**	0.22678 0.3505	-0.16157 0.5087	1.00000

The results of the Spearman's rank order correlations found significant correlations between some of the predictors and outcomes (Table 14). The two potential confounders, age and sex, were not significantly correlated to any of the predictors or outcomes. Fracture energy, area normalized fracture energy, and articular comminution were not significant predictors of the degree of arthritic development, but all trended toward significance, as was seen previously in the larger study of 71 acetabular fractures. Measures of contact stress exposure, and the combined measure of injury severity and contact stress exposure were significantly correlated with the degree of radiographic arthritis development indicated by the Tönnis grade.

CHAPTER 5 - DISCUSSION

Presently, clinical practice and research into optimal IAF treatment rely upon subjective measures of injury severity and reduction accuracy to control data and guide surgical management. However, such measures are inadequate to objectively characterize the degree of injury severity and to understand the accuracy of reduction required to optimally restore joint mechanics. Furthermore, due to this inability to fully understand the impact of injury severity on outcomes, the true effects of reduction are difficult to characterize. The only way to resolve these issues is through objective measurement of these pathomechanical factors within individual joints. The injury severity assessment and DEA contact stress models developed herein therefore hold great potential for improving research to better guide clinical practice.

Existing methods for objective measurement of injury severity and reduction accuracy after IAF had been developed in the tibial plafond. The plafond proved a useful model for establishing these objective methods due to its known tendency to degenerate quickly after injury and the relatively rare incidence of idiopathic PTOA development. Expansion of the severity and reduction analyses to include different joints in the body posed several challenges that were overcome in the course of the work described herein. Previously, the objective measures of injury severity had leveraged fracture energy and a measure of articular comminution to obtain estimates of severity. While these methods were expanded in earlier work to measure energy in other joints, they did not account for the significant differences in joint size and contact area through which the damage occurred across joints. Furthermore, development of a new articular comminution measure was also necessitated to better assess the damage to areas most critical for joint function. Finally, models of DEA in the calcaneus and acetabulum required development in order to assess reduction in the same cases where injury severity was measured and thereby

provide a complete and objective assessment of the pathomechanical factors underlying PTOA development.

Normalized Fracture Severity

Expansion of the fracture severity measure to additional joints brought about consideration of the effects of the vastly different anatomies being injured. One of the most prominent differences was the size of the articular contact across which injurious energy was transferred. This study leveraged significant prior efforts investigating the variance in fracture energies across joints to establish the potential impact of differences in contact area normalized fracture energy on PTOA outcomes. There was a strong correlation between the fracture energy per unit contact area, obtained from pre-operative data, and PTOA rates across 5 different joints without controlling for any operative factors. This provided strong evidence that differences in energy per unit contact area may be more predictive of PTOA development and should be further investigated on a joint specific basis.

Though PTOA is a known sequela of acute IAF, the exact mechanism and the contributions of acute injury to its development have remained unclear. In 2011, Tochigi et al made two major discoveries. Upon examination of debrided fragments containing cartilage from calcaneal fractures, they found significantly lower chondrocyte viability near fracture edges. Interestingly, they also found that chondrocyte death propagated from these fracture sites over the next several days [9]. This discovery is important because it demonstrates that acute damage likely has a long-term effect on cartilage health through decellularization of the tissue and that the acute effects of the injury progress after surgical intervention. From these findings, one might expect joints with more fracture edges to report higher rates of injury severity, however, a 2017

study by Dibbern et al found the opposite. They found that tibial plateau fractures had significantly higher fracture edge lengths than plafond fractures, despite plateaus reporting PTOA rates half those found in plafonds[19]. To explain this finding, they suggested that differences in the impact tolerance of some joints could be due in part to differences in the size of the articular surface. Distributing the impact over a larger area would effectively lessen the magnitude of the injurious event per unit area, like contact stress is reduced by increasing contact area. For our study, to approximate this effect, the contact area was used to scale fracture energy by the area through which it could be transferred.

Fracture energy scaled by contact area is appealing in the context of assessing cartilage and joint damage. The distribution of the energy over that joint, now quantified by the scaled fracture energy, gives further insight into the severity of damage in a consistent and objective manner. The joints studied herein differ significantly in bony morphology, cartilage thickness, the surrounding anatomy, loading conditions, reconstruction difficulty, and injury patterns. However, the results suggest that 97% of variance in PTOA rates between them may be due to the acute fracture severity scaled simply by contact area.

This elucidates a potential reason for the disconnect between advances in fracture management and the lack of improvement observed in PTOA prevention. Acute biological damage caused by fracture is not meaningfully treated presently but appears to be a significant contributor to PTOA development. It likely manifests in a consistent manner across joints, but over an extended period of time as the effects of alterations in chondrocyte function after injurious impact lead to joint degeneration. The fact that the altered chondrocyte function arises over the course of over several days presents an exciting opportunity for intervention. As >97% of the variance in PTOA rates may be due to the initial severity, novel biological interventions

may reduce PTOA development more substantially than previously estimated. It also suggests that less invasive surgical techniques may be preferred, especially when paired with interventions that can maintain chondrocyte viability in fractured joints.

Among the limitations of this study, the patients for whom fracture energies were computed were not all followed clinically. Therefore, rates of OA represent literature values derived from multiple patient populations. Similarly, PTOA was defined radiographically by the KL radiographic grade for studies that did not report OA development. However, the KL scale was not designed to consider symptoms when defining OA such that the relationships in this study represent radiographic, not necessarily symptomatic, OA. Finally, to be included in the study, CT scans had to be obtained during a standard of care protocol. As obtaining a CT scan does not necessarily fall under the standard of care for more minor fractures, it is possible the energy ranges are skewed toward the higher end and may not capture lower energy fractures.

Surface area-normalized fracture energy as a predictor of patient-specific PTOA development in individual joints

The purpose of this study was to improve our understanding of the influence of acute fracture severity on PTOA risk following IAFs across a variety of joints by implementing the contact area normalization within each joint. The primary hypothesis of this study was that normalized measures of acute severity would be predicted on a patient-by-patient basis was partially supported by the results. Two of the three joints examined, the tibial plafond in the ankle and the acetabulum in the hip, had significant correlations between fracture energy per unit joint surface area, obtained from pre-operative CT scans, and PTOA rates. The third joint, the calcaneus in the hindfoot, did not demonstrate these strong correlations between measures of

acute severity and PTOA outcomes, but trended toward significance (p=0.06). A previous study by Rao et. al. using these data found no correlation between fracture energy and PTOA outcomes[37]. Therefore, it is notable that when accounting for joint surface area, a small to moderate correlation is found when neither fracture energy nor joint surface area demonstrate independent correlations with outcomes. Taken with the results of the tibial plafond and acetabulum and the overall correlation between all joints considered together, it confirms that a relationship exists between surface area-normalized fracture energy and PTOA development.

Logistic regressions were computed for all cases and within each joint to establish the extent to which acute severity is predictive on a patient-specific basis. For all cases, the results of the regression for both fracture energy and normalized fracture energy produced significant models with odds ratios greater than 1. For the overall models, each 1J increase in fracture energy is expected to increase the risk of PTOA development by 7.8% or 5% for each 0.1J/cm^2. However, these numbers are likely skewed by the observed lack of a significant correlation found for the calcaneus, as independent regression models of fracture energy and normalized fracture energy for both the tibial plafond and acetabulum were highly significant. The models predict a 6.6% and 10.6% increase in PTOA risk for each 1J increase in fracture energy in the acetabulum and plafond, respectively. Even greater differences were seen for the normalized fracture energy, where a 0.1J/cm^2 increase would predict a 16.2% increase in risk of PTOA development in the acetabulum and 16.6% increase in risk in the tibial plafond.

These results provide further evidence that area-normalized fracture energy as an objective measure of injury severity can explain previously unaccounted-for variance in PTOA rates. As delineated above, normalizing joints by average contact area revealed that up to 97% of the variance in PTOA rates across joints could be explained by these previously unaccounted-for

differences in acute severity. This implied that there may be a consistent damage threshold across joints and led to a further hypothesis that there exists a unified damage threshold above which joints predictably progress to PTOA.

The results of this study, however, do not support that conclusion. It appears that even when controlling for the energy per unit area, joints have different impact tolerances. Despite each joint having relatively similar rates of PTOA development (for the cases included in our study this was 52-60%), joints had dissimilar average normalized fracture energies (acetabulum: 0.79 J/cm^2, tibial plafond: 1.84 J/cm^2, and calcaneus 2.42 J/cm^2). Additionally, average normalized fracture energies for the PTOA groups across joints were dissimilar (acetabulum: 0.87 J/cm^2, tibial plafond: 2.18 J/cm^2, and calcaneus 2.48 J/cm^2). Therefore, future studies are needed to establish thresholds of normalized fracture energies to best assess the contribution of initial severity to PTOA outcomes in each joint.

There are several limitations to this study. The surface areas measured may not be indicative of the areas through which energy is transferred. Contact areas through which the injurious forces are transferred will always be smaller than the surface area of the joints through which they are being transferred. Therefore, it is likely that the energy per unit area is underestimated in many cases leading to higher energies per unit area in joints with the large differences in contact versus surface area. Finally, to be included in the study, CT scans had to be obtained during standard of care protocol. It is possible then that the energy ranges are skewed toward higher energy fractures and may not capture the lower energy injuries.

PTOA development in the tibial plafond after IAF

The tibial plafond has served as the proving grounds for new objective measures of injury severity and reduction accuracy. It was therefore, used again to develop the new measures of articular comminution energy and area-normalized fracture energy as well as to compare them with the reduction. An additional seven cases were added to the nine that had both fracture severity and contact stresses reported previously. Highly significant differences were found in patients that developed PTOA from those that did not in fracture energy, normalized fracture energy, articular comminution, and contact stress over-exposure. Significant Spearman's rank order correlations were also found between all predictors and both KL graded degree of radiographic arthritis as well as OA status.

Articular comminution, in the preliminary studies on developing objective measures of injury severity, had been previously reported as the amount of surface area liberated within the first millimeter of the articular surface as a percentage of the intact area on the contralateral limb. The new measure of articular comminution was similar, but instead measured the energy absorbed within 1cm of the articular surface. The ability to measure energy without the constraint of needing an intact datum with which to compare enabled this measure to be directly applied to other joints as well. It is useful as it provides a direct measure of insult contained within the subchondral region.

The results of the new, normalized fracture energy measure appeared to modestly improve upon correlations with degree of PTOA development in the plafond when compared to the unnormalized energy (R^2=0.34 vs R^2 = 0.29). However, more significant improvements were noted when looking at the Spearman's correlations in the 71 patients reported earlier (ρ=0.52 vs ρ=0.26). On this basis, normalized fracture energy was selected as the measure to be combined

with the measure of articular comminution to create a composite metric to more fully describe the severity of injury. This combined injury severity measure was more predictive of PTOA development than either of its constitutive components, indicating the necessity of studying both the articular insult and the damage to the entire bone when assessing severity in the tibial plafond.

The reduction accuracy, as measured by the contact stress over-exposure was also significantly correlated with rates of PTOA development. These findings are consistent with those reported on the smaller subset of 10 cases reported earlier. It is interesting to note that in these plafond fractures up to 61.7% of the variance in PTOA rates could be explained by this objective predictor alone compared to 70% for the combined model. It suggests the accuracy of reduction is more important than the initial injury severity in plafond injuries.

Having established the objective measures of the degree of initial injury and the degree to which loading characteristics have been altered, it is now possible to examine the true influence of reduction quality of PTOA risk in fractures of the tibial plafond. In order to better assess which predictor is most important and how they might be associated, bubble plots were created of severity and reduction with the color and size of the bubbles indicating the presence and degree of PTOA development, respectively. As might be expected of good predictors of PTOA development, the good outcomes are clustered in the lower left corner of the plot indicating low severity, excellent reduction fractures. Interestingly, the two fractures with low severity that developed PTOA had two of the highest contact stress over-exposures. This fits with one portion of the contradictory literature that reduction accuracy is important in the plafond. Similarly, several fractures with good reductions that developed PTOA had relatively higher combined severity scores. This fits with the other side of the literature where the study by Etter and Ganz

suggested there may be other factors at play when good reductions result in poor outcomes with those factors now identified as the severity of injury.

The combined model demonstrated this improved understanding of PTOA development by identifying a threshold that has perfect sensitivity and specificity. It even demonstrates an highly significant correlation with the degree of PTOA severity ($\rho=0.80$, $p<0.001$). Therefore, in the plafond it appears likely that predicting PTOA development requires both assessment of injury severity and reduction accuracy. This refutes the hypothesis that acute severity more significantly contributes to PTOA in the plafond.

Examining these data in the context of our other hypothesis, that injury severity is correlated with reduction accuracy, they appear to support it. The most substantial corroborating data are the Spearman's correlations between contact stress over-exposure and measures of initial injury. Correlations between the contact stress over-exposure and each individual predictor of severity trended toward significance ($p=0.10$, $p=0.10$, $p=0.08$), while the combined measure was significantly correlated with reduction accuracy ($\rho=0.51$, $p=0.04$). However, from this limited dataset, it is difficult to determine conclusively whether the data are supportive of this hypothesis as none of the highest severity fractures achieved accurate enough reductions to have low contact stress over-exposures.

PTOA development in the calcaneus after IAF

Contrasting with the tibial plafond, PTOA development in the calcaneus is considered to result primarily from the severity of initial injury after IAF. The Sanders classification for displaced IAFs of the calcaneus is the present clinical gold standard for assessing injury severity and predicting outcomes. As prior studies have reported that up to 90% of Sanders class III

fractures degenerate to PTOA despite 95% of cases having an anatomic reduction (0-1 mm), this claim is well supported in the present literature[38]. However, a previous study by Rao et al. found that a new measure of post-reduction step-off was correlated with Sanders classification[37]. This implicated surgical reduction as a potential contributor to PTOA development in IAFs of the calcaneus. The study by Rao also included a measure of fracture energy that was not found to be associated with radiographic evidence of PTOA. This finding was particularly noteworthy as it may further suggest that Sanders classification is merely indicative of how well joints are able to be reduced. It also offered the unique opportunity to study the new methods for articular comminution and area-normalization of fracture energy as improvements over the existing methods for measuring acute injury.

While the fracture energy was not significantly correlated with PTOA outcomes as discussed previously, the area-normalized fracture energy was significantly, albeit weakly, correlated with PTOA (ρ=.36, p=0.04). There were also significant differences in the area-normalized fracture energy. Area-normalized fracture energy was significantly higher for patients that developed PTOA than those that did not (2.54±0.40 MPa*s in the OA group vs 2.24±0.38 MPa*s in the no OA group, p=0.04). The articular comminution was even more significantly correlated with PTOA development (ρ=.48, p=0.004). The combined severity metric of articular comminution further improved upon the correlation between severity and outcomes. The articular comminution energy and combined metric were both more significantly correlated with PTOA outcomes than the present gold standard, Sanders classification and represent a substantial advancement in predicting the degree of PTOA development in these fractures.

In stark contrast to the literature findings of no association between reduction accuracy and PTOA development, the reduction accuracy, as measured by the contact stress over-exposure, was significantly correlated with rates of PTOA development. Furthermore, in this subset of cases, contact stress over-exposure was even more significantly related to patient outcomes than both Sanders classification and the objective measures of severity (ρ=.52, p=0.002). It is worth noting, however, that there was a relatively wide range of over-exposures and no clear threshold delineating cases that developed PTOA from those that did not. This suggests that while reduction accuracy is clearly an important factor in outcomes, the initial injury severity as well as other patient factors may contribute significantly to outcomes.

After establishing the importance of these new objective measures of injury severity and reduction accuracy, it is possible to examine their relative influence on PTOA risk in IAFs of the calcaneus. Again, bubble plots of severity and reduction were used with the color and size of the bubbles indicating the presence and degree of PTOA development, respectively. The clustering of good outcomes in the lower left corner of the plot shows that these cases involved low severity, excellent reduction fractures. Despite this, however, a number of these fractures in this region still progressed to PTOA, indicating that there remain unaccounted-for components of the PTOA development mechanism in the calcaneus. As indicated in the literature, we also found a number of cases in the lower right corner that despite excellent reduction, cases still progressed to PTOA. Interestingly, in the 33 cases we examined, none of the lowest severity injuries had poor reductions, while none of the lowest severity injuries had poor reductions, the worst reductions among them did all progress to PTOA.

The combined model of injury severity and reduction accuracy again provided the best prediction of cases that will progress to PTOA with a clear threshold above 0.4 indicating

probable degeneration. It does not have the perfect sensitivity and specificity and specificity found in models of the plafond, however. It demonstrates a moderate correlation with the degree of PTOA severity (R^2=0.36), but is held back by four clear outliers. Therefore, it appears that predicting PTOA development in the calcaneus requires assessment of injury severity, reduction accuracy, and other unaccounted-for factors. Again, the clear, significant, contribution of reduction accuracy to PTOA development refutes the hypothesis that acute severity more significantly contributes to PTOA in IAFs of the calcaneus.

Finally, these data also appear to support the hypothesis that injury severity is correlated with reduction accuracy. Though fracture energy and area-normalized fracture energy are not associated with contact stress over-exposure, the articular comminution measure is highly correlated with it (ρ=.44, p=0.01). On the surface, this appears to be logical, as higher articular comminution energy fractures are more likely to have more fragments and be more difficult to reduce. However, the Sanders classification is a measure of the number of articular fragments and it was not associated with contact stress over-exposure or articular comminution energy. It is interesting to note that 3 of the 4 outliers mentioned previously were Sanders grade III fractures, suggesting that the objective measures of injury severity still lack some contextual information necessary to fully assess the injury. Therefore, while some key measures of injury severity are correlated with reduction accuracy, others are not, so the hypothesis can neither be refuted nor accepted. It is also worth noting that these fractures were all treated percutaneously at the University of Iowa. The percutaneous technique focuses on minimizing soft tissue damage, so surgery is performed through small incisions where the joint space is never visualized. Therefore, compared to extensile lateral approaches where a skin flap is created to fully visualize the joint in hopes of accurate restoration, the results may be skewed toward having poorer

surgical outcomes which may make the initial injury have greater influence on and correlation with the reduction.

Contact stress over-exposure in the acetabulum after IAF

As a foil to the calcaneus, PTOA in the acetabulum is thought to result not from the severity of initial injury, but from the accuracy of surgical reduction. Many past studies have cited anatomic reductions of less than 1 mm as being a key factor in preventing PTOA in acetabulum fractures[29]. However, there is some evidence that certain fractures like posterior column and T-shaped fractures have negative impacts on outcomes[68].

These findings were confirmed previously in the larger series of 71 fractures where the fracture energy and area-normalized fracture energy were significantly predictive of PTOA development after IAF of the acetabulum ($p<0.001$). Higher articular comminution energy was also significantly predictive of PTOA development($p<0.001$). All measures of severity demonstrated moderate Spearman's correlations with outcomes, but these correlations were not significant (fracture energy $\rho=0.43$ $p=0.06$, normalized fracture energy $\rho=0.39$ $p=0.10$, articular comminution $\rho=0.43$ $p=0.054$). The combined severity metric improved upon the correlation between severity and outcomes ($R^2=0.36$ vs $R^2=0.23$, $R^2=0.20$, $R^2=0.21$).

Confirming literature findings of significant association between reduction accuracy and PTOA development, the reduction accuracy, as measured by the contact stress over-exposure, was also significantly correlated with the degree of PTOA development ($\rho=0.674$ $p=0.0015$). The association between PTOA outcomes and contact stress over-exposure, however, does not well delineate which cases will develop PTOA; two cases are misclassified and six fall within 5% of the optimal cutoff around 3.9MPa*s. This suggests that while reduction accuracy is clearly

an important factor, the initial injury severity as well as other patient factors may contribute significantly to outcomes.

To examine the relative influence of injury severity and reduction accuracy on PTOA risk in IAFs of the acetabulum, bubble plots of severity and reduction were again used with the color and size of the bubbles indicating the presence and degree of PTOA development, respectively. The clustering of good outcomes in the lower left corner of the plot indicate these correspond to low severity, excellent reduction fractures. There are, however, two outliers to this trend: one developing PTOA while having low severity and an excellent reduction, while the other did not degenerate to PTOA despite having a poor reduction and high severity. The latter outlier is of note as it's the only outlier with high contact stress over-exposure that did not degenerate to PTOA. This could potentially be explained by an error in our modeling assumptions or, if the data are real and can be confirmed in a larger study, may indicate that the acetabulum is more tolerant to incongruities than previously reported.

Once again, the combined model of injury severity and reduction accuracy provided the best prediction of cases that will progress to PTOA with a clear threshold above 0.25 indicating probable degeneration. It does not have perfect sensitivity and specificity as found in the plafond, however. It demonstrates a moderate correlation with the degree of PTOA severity (R^2=0.46) but also has the two aforementioned outliers. Therefore, in the acetabulum it again appears that predicting PTOA development requires assessment of injury severity, reduction accuracy, and other unaccounted for factors. Furthermore, significant correlation of reduction accuracy to PTOA development refutes the hypothesis that acute severity more significantly contributes to PTOA in IAFs of the acetabulum. Finally, more so than the distal tibia and calcaneus, these data clearly support the hypothesis that injury severity is correlated with

reduction accuracy. Fracture energy, area-normalized fracture energy, and articular comminution are all associated with contact stress over-exposure, while the combined metric is significantly correlated (ρ=.50, p=0.03).

Limitations

There were several limitations to these studies. Perhaps the most important to note is that the PTOA outcomes data examined were exclusively radiographic. Both the Kellgren-Lawrence and Tonnis classification systems have been demonstrated to have problems with reproducibility, especially when measured from plain radiographs. Furthermore, these radiographic measures of PTOA development do not always correlate with patient reported pain and function outcomes. This is perhaps most evidenced in the calcaneus where ~90% of patients reported by Sanders developed radiographic PTOA while only ~30% were treated for late stage PTOA development[38]. In these studies, the reproducibility was addressed by having a consensus of multiple raters, but correlations with patient function and patient reported outcomes remain a confounding factor.

The severity metrics have several important limitations. The fracture energy is computed based on bone density derived from CT Hounsfield Units. However, bone density is known to decrease with age along with healing capacity. Therefore, older patients may have lower energy fractures in their lower density bone that end up being relatively more severe than comparable energy fractures in a younger population. Additionally, sex has also been demonstrated to influence PTOA development with women being slightly more likely to develop PTOA. To account for this, we examined correlations between all predictors and outcomes with age and sex. However, for our limited sample size, we did not find any significant correlations or

differences between groups in the calcaneus and acetabulum, with the only significant association being an increased risk of PTOA in women with plafond fractures.

A further limitation of the fracture energy measure comes from fractures not loaded through the articular joint. Fractures where energy is not directed through the articulating surfaces may result in a breakdown of the logic involved in assessing severity as it is assumed that energy transferred through the articular surface causes damage to the cartilage, matrix, and subchondral bone leading to PTOA. In the plafond, common injury mechanisms are likely to produce this axial transfer as the talus hammers into the bottom of the tibia to produce fracture. It is, therefore, not surprising that the fracture energy measure performed best in this joint. In the calcaneus, however, the Achilles and contact with the ground can initiate fracture with an energy path that does not necessitate direct transfer through the joint. Accordingly, in this joint the fracture energy was found to be uncorrelated with PTOA development thereby evincing the limitations of this measure. Fortunately, the articular comminution metric can help to address this issue as it provides an estimate of the energy transferred through the articular surface. When the energy released within 1 cm of the subchondral bone was assessed, it was found to be significantly correlated with PTOA development in all joints. The articular comminution metric is itself limited, however, in that it does not capture all the energy transferred through the joint but rather is constrained to only the subchondral bone. Therefore, the combined measure of articular comminution and fracture energy is required to best account for both sets of limitations.

Finally, the DEA contact stress models also have significant limitations. Perhaps the most important limitation is that of stability. Often fractures are accompanied by increased ligamentous laxity from tears that occur during the injury. This increased laxity raises concerns for instability that can dramatically increases stresses when combined with incongruities[96-98].

The DEA models reported in this work did not account for any instabilities that may occur. A further limitation to the DEA models is that they did not account for differences in patient-specific gait nor did they account for variations in postoperative gait as the distal tibial, calcaneal, and acetabular models all relied upon gait obtained from sources other than IAF patients. As variations in gait have previously been demonstrated to have significant differences in contact stress distributions and magnitudes across surfaces, the modeled gait parameters may substantially impact results. Therefore, future work should ideally aim to use patient-specific gait parameters to best assess joint contact stresses.

CHAPTER 6 - CONCLUSIONS

Post-traumatic osteoarthritis is a complex disease with multiple elements contributing to its progression. It results from a combination of acute injury with surgical and biological factors. Presently, clinicians utilize subjective surrogates to assess acute and chronic mechanical damage when prognosticating PTOA development. Clinical tools like fracture classifications and step-off measures have presented challenges, however, given poor inter-observer reliability and difficulties in comparing categorical classifications with continuous predictors of PTOA development. Furthermore, such assessments do not account for the interaction between the acute injury and the chronic problems resulting from more difficult surgical reconstructions. This work has laid out significant advancements that address these issues. In particular, it details patient-specific assessment capabilities and leverages them toward unifying understanding of all mechanical aspects of PTOA development. Both fracture energy (preoperatively) and contact stress (postoperatively) proved powerful predictive tools and provided a means to begin objectively generating risk assessments on a patient-specific basis.

Acute mechanical damage, as measured by area-normalized fracture energy and articular comminution energy, was found to be a significant independent contributor to PTOA due to the chronic damage, as measured by contact stress over-exposure, associated with poor surgical reconstructions. This was the first line of work to be able to objectively control for both factors and establish their independence in three joints: the hindfoot, hip, and ankle. It is also the first to study mechanical damage thresholds across joints and identify differences between them. Specifically, when examining fracture energy in the calcaneus, distal tibia, proximal tibia, acetabulum, and distal radius, different ranges of acute damage and acute damage per unit area

were found in different joints. These differences were highly correlated with the risk of PTOA development across joints, indicating that differences in PTOA rates seen across joints may be attributable to differences in initial injury. This would explain why, despite significant advances in surgical treatment, high PTOA rates persist.

There were not, however, consistent predictive thresholds of acute severity PTOA across joints. The calcaneal fracture energy was not significantly correlated with PTOA status while the tibial plafond and acetabulum's were albeit at different thresholds of area-normalized fracture energy. Taken together, these findings could imply the existence of inherent biological differences across joints in their ability to recover from initial trauma. Alternatively, some of these findings may be explained by differences in the subjective outcome measures. The Kellgren-Lawrence and Tönnis grades have well-documented challenges with reproducibility and only provide categorical information on patient outcomes. In the future, feature-rich weight-bearing CT's can provide a means through which continuous, objective measures of degeneration are obtained.

The ability to predict PTOA development is crucial to providing improved control for clinical studies. However, the utility of the measures studied herein could be greatly expanded if they were implemented to generate patient-specific risk models in a clinical setting. The greatest impediment to their implementation is the speed of CT segmentation. The fracture energy and contact stress computations that occur after segmentation take on the order of minutes or even seconds while extracting accurate geometries of bone fragments is a time-consuming task requiring up to four hours of manual editing per case. Future studies could leverage *a priori* data to minimize or even eliminate this component of analysis and thereby empower physicians and patients to make evidence-based decisions on these potentially devastating injuries.

REFERENCES

1. Thomas, T.P., et al., *Objective CT-based metrics of articular fracture severity to assess risk for posttraumatic osteoarthritis.* J Orthop Trauma, 2010. **24**(12): p. 764-9.
2. Bergmann, G., et al., *Hip contact forces and gait patterns from routine activities.* J Biomech, 2001. **34**(7): p. 859-71.
3. Giannoudis, P.V., et al., *Articular step-off and risk of post-traumatic osteoarthritis. Evidence today.* Injury, 2010. **41**(10): p. 986-95.
4. Macko, V.W., et al., *The joint-contact area of the ankle. The contribution of the posterior malleolus.* J Bone Joint Surg Am, 1991. **73**(3): p. 347-51.
5. Williams, T.M., et al., *Factors affecting outcome in tibial plafond fractures.* Clin Orthop Relat Res, 2004(423): p. 93-8.
6. Schenker, M.L., et al., *Pathogenesis and prevention of posttraumatic osteoarthritis after intra-articular fracture.* J Am Acad Orthop Surg, 2014. **22**(1): p. 20-8.
7. McKinley, T.O., et al., *Basic science of intra-articular fractures and posttraumatic osteoarthritis.* J Orthop Trauma, 2010. **24**(9): p. 567-70.
8. Brown, T.D., et al., *Posttraumatic osteoarthritis: a first estimate of incidence, prevalence, and burden of disease.* J Orthop Trauma, 2006. **20**(10): p. 739-44.
9. Tochigi, Y., et al., *Distribution and progression of chondrocyte damage in a whole-organ model of human ankle intra-articular fracture.* J Bone Joint Surg Am, 2011. **93**(6): p. 533-9.
10. Coleman, M.C., et al., *Differential Effects of Superoxide Dismutase Mimetics after Mechanical Overload of Articular Cartilage.* Antioxidants (Basel), 2017. **6**(4).
11. Coleman, M.C., et al., *Injurious Loading of Articular Cartilage Compromises Chondrocyte Respiratory Function.* Arthritis Rheumatol, 2016. **68**(3): p. 662-71.
12. Humphrey, C.A., D.R. Dirschl, and T.J. Ellis, *Interobserver reliability of a CT-based fracture classification system.* J Orthop Trauma, 2005. **19**(9): p. 616-22.
13. Swiontkowski, M.F., et al., *Interobserver variation in the AO/OTA fracture classification system for pilon fractures: is there a problem?* J Orthop Trauma, 1997. **11**(7): p. 467-70.
14. Anderson, D.D., et al., *Quantifying tibial plafond fracture severity: absorbed energy and fragment displacement agree with clinical rank ordering.* J Orthop Res, 2008. **26**(8): p. 1046-52.
15. Beardsley, C., J.L. Marsh, and T. Brown, *Quantifying comminution as a measurement of severity of articular injury.* Clin Orthop Relat Res, 2004(423): p. 74-8.
16. Beardsley, C.L., et al., *Interfragmentary surface area as an index of comminution severity in cortical bone impact.* J Orthop Res, 2005. **23**(3): p. 686-90.
17. Beardsley, C.L., et al., *Interfragmentary surface area as an index of comminution energy: proof of concept in a bone fracture surrogate.* J Biomech, 2002. **35**(3): p. 331-8.
18. Beardsley, C.L., et al., *High density polyetherurethane foam as a fragmentation and radiographic surrogate for cortical bone.* Iowa Orthop J, 2000. **20**: p. 24-30.
19. Dibbern, K., et al., *Fractures of the tibial plateau involve similar energies as the tibial pilon but greater articular surface involvement.* J Orthop Res, 2017. **35**(3): p. 618-624.
20. Thomas, T.P., et al., *A method for the estimation of normative bone surface area to aid in objective CT-based fracture severity assessment.* Iowa Orthop J, 2008. **28**: p. 9-13.

21. Bartlett CS, D.A.M., Weiner LS., *Fractures of the Tibial Pilon. In: Browner BD, Jupiter JB, Levine AM, Trafton PG.*, in *Skeletal trauma*. 1998, W.B. Saunders Company: Philadelphia, PA. p. 2295-2325.
22. Kempton, L.B., et al., *Objective Metric of Energy Absorbed in Tibial Plateau Fractures Corresponds Well to Clinician Assessment of Fracture Severity.* J Orthop Trauma, 2016. **30**(10): p. 551-6.
23. Anderson, D.D., et al., *Contact stress distributions in malreduced intraarticular distal radius fractures.* J Orthop Trauma, 1996. **10**(5): p. 331-7.
24. Anderson, D.D., et al., *Post-traumatic osteoarthritis: improved understanding and opportunities for early intervention.* J Orthop Res, 2011. **29**(6): p. 802-9.
25. Anderson, D.D., et al., *Is elevated contact stress predictive of post-traumatic osteoarthritis for imprecisely reduced tibial plafond fractures?* J Orthop Res, 2011. **29**(1): p. 33-9.
26. Archdeacon, M.T. and S.K. Dailey, *Efficacy of Routine Postoperative CT Scan After Open Reduction and Internal Fixation of the Acetabulum.* J Orthop Trauma, 2015. **29**(8): p. 354-8.
27. Tannast, M., S. Najibi, and J.M. Matta, *Two to twenty-year survivorship of the hip in 810 patients with operatively treated acetabular fractures.* J Bone Joint Surg Am, 2012. **94**(17): p. 1559-67.
28. Marsh, J.L., et al., *Articular fractures: does an anatomic reduction really change the result?* J Bone Joint Surg Am, 2002. **84-A**(7): p. 1259-71.
29. Matta, J.M., *Fractures of the acetabulum: accuracy of reduction and clinical results in patients managed operatively within three weeks after the injury.* J Bone Joint Surg Am, 1996. **78**(11): p. 1632-45.
30. Mayo, K.A., et al., *Surgical revision of malreduced acetabular fractures.* Clin Orthop Relat Res, 1994(305): p. 47-52.
31. Letournel, E.m., R. Judet, and R. Elson, *Fractures of the acetabulum*. 2nd ed. 1993, Berlin ; New York: Springer-Verlag. xxiii, 733 p.
32. Stevens, D.G., et al., *The long-term functional outcome of operatively treated tibial plateau fractures.* J Orthop Trauma, 2001. **15**(5): p. 312-20.
33. Kern, A.M. and D.D. Anderson, *Expedited patient-specific assessment of contact stress exposure in the ankle joint following definitive articular fracture reduction.* J Biomech, 2015. **48**(12): p. 3427-32.
34. Thomas-Aitken, H.D., M.C. Willey, and J.E. Goetz, *Joint contact stresses calculated for acetabular dysplasia patients using discrete element analysis are significantly influenced by the applied gait pattern.* J Biomech, 2018.
35. Coleman, M.C., et al., *Targeting mitochondrial responses to intra-articular fracture to prevent posttraumatic osteoarthritis.* Sci Transl Med, 2018. **10**(427).
36. Ibrahim, T., et al., *Displaced intra-articular calcaneal fractures: 15-year follow-up of a randomised controlled trial of conservative versus operative treatment.* Injury, 2007. **38**(7): p. 848-55.
37. Rao, K., et al., *Correlation of Fracture Energy with Sanders Classification and Post-Traumatic Osteoarthritis following Displaced Intra-Articular Calcaneus Fractures.* J Orthop Trauma, 2019.

38. Sanders, R., et al., *Operative treatment of displaced intraarticular calcaneal fractures: long-term (10-20 Years) results in 108 fractures using a prognostic CT classification.* J Orthop Trauma, 2014. **28**(10): p. 551-63.
39. Marsh, J.L., D.P. Weigel, and D.R. Dirschl, *Tibial plafond fractures. How do these ankles function over time?* J Bone Joint Surg Am, 2003. **85-A**(2): p. 287-95.
40. Ovadia, D.N. and R.K. Beals, *Fractures of the tibial plafond.* J Bone Joint Surg Am, 1986. **68**(4): p. 543-51.
41. Teeny, S.M. and D.A. Wiss, *Open reduction and internal fixation of tibial plafond fractures. Variables contributing to poor results and complications.* Clin Orthop Relat Res, 1993(292): p. 108-17.
42. Honkonen, S.E., *Degenerative arthritis after tibial plateau fractures.* J Orthop Trauma, 1995. **9**(4): p. 273-7.
43. Rademakers, M.V., et al., *Operative treatment of 109 tibial plateau fractures: five- to 27-year follow-up results.* J Orthop Trauma, 2007. **21**(1): p. 5-10.
44. Volpin, G., et al., *Degenerative arthritis after intra-articular fractures of the knee. Long-term results.* J Bone Joint Surg Br, 1990. **72**(4): p. 634-8.
45. Weigel, D.P. and J.L. Marsh, *High-energy fractures of the tibial plateau. Knee function after longer follow-up.* J Bone Joint Surg Am, 2002. **84-A**(9): p. 1541-51.
46. Letournel, E., *Acetabulum fractures: classification and management.* Clin Orthop Relat Res, 1980(151): p. 81-106.
47. Forward, D.P., T.R. Davis, and J.S. Sithole, *Do young patients with malunited fractures of the distal radius inevitably develop symptomatic post-traumatic osteoarthritis?* J Bone Joint Surg Br, 2008. **90**(5): p. 629-37.
48. Goldfarb, C.A., et al., *Fifteen-year outcome of displaced intra-articular fractures of the distal radius.* J Hand Surg Am, 2006. **31**(4): p. 633-9.
49. Lutz, M., et al., *Arthritis predicting factors in distal intraarticular radius fractures.* Arch Orthop Trauma Surg, 2011. **131**(8): p. 1121-6.
50. Crutchfield, E.H., et al., *Tibial pilon fractures: a comparative clinical study of management techniques and results.* Orthopedics, 1995. **18**(7): p. 613-7.
51. Wyrsch, B., et al., *Operative treatment of fractures of the tibial plafond. A randomized, prospective study.* J Bone Joint Surg Am, 1996. **78**(11): p. 1646-57.
52. Etter, C. and R. Ganz, *Long-term results of tibial plafond fractures treated with open reduction and internal fixation.* Arch Orthop Trauma Surg, 1991. **110**(6): p. 277-83.
53. Marsh, J.L., et al., *Use of an articulated external fixator for fractures of the tibial plafond.* J Bone Joint Surg Am, 1995. **77**(10): p. 1498-509.
54. Patterson, M.J. and J.D. Cole, *Two-staged delayed open reduction and internal fixation of severe pilon fractures.* J Orthop Trauma, 1999. **13**(2): p. 85-91.
55. DeCoster, T.A., et al., *Rank order analysis of tibial plafond fractures: does injury or reduction predict outcome?* Foot Ankle Int, 1999. **20**(1): p. 44-9.
56. Marsh J.L., W.T., Nepola J.V., DeCoster T., Hurwitz S., Dirschl D., *Tibial plafond fractures: does articular reduction and/or injury pattern predict outcome?* Orthop Trans., 1997. **21**: p. 563.
57. Kellgren, J.H. and J.S. Lawrence, *Radiological assessment of osteo-arthrosis.* Ann Rheum Dis, 1957. **16**(4): p. 494-502.
58. Busse, J., W. Gasteiger, and D. Tonnis, *[A new method for roentgenologic evaluation of the hip joint--the hip factor].* Arch Orthop Unfallchir, 1972. **72**(1): p. 1-9.

59. Busse, J., W. Gasteiger, and D. Tonnis, *[Significance of the "summarized hip factor" in the diagnosis and prognosis deformed hip joints]*. Arch Orthop Unfallchir, 1972. **72**(3): p. 245-52.
60. Sanders, R., et al., *Operative treatment in 120 displaced intraarticular calcaneal fractures. Results using a prognostic computed tomography scan classification.* Clin Orthop Relat Res, 1993(290): p. 87-95.
61. Michelson, J.D., *Fractures about the ankle.* J Bone Joint Surg Am, 1995. **77**(1): p. 142-52.
62. Marsh, J.L., Buckwalter, J., Gelberman, R., Dirschl, D., Olson, S., Brown, T., Llinias, A. , *Articular Fractures: Does an Anatomic Reduction Really Change the Result?* JBJS, 2002: p. 1259.
63. Judet, R., J. Judet, and E. Letournel, *[Fractures of the Acetabulum]*. Acta Orthop Belg, 1964. **30**: p. 285-93.
64. Letournel, E., *[Surgical treatment of fractures of the acetabulum: results over a twenty-five year period (author's transl)]*. Chirurgie, 1981. **107**(3): p. 229-36.
65. Matta, J.M., D.K. Mehne, and R. Roffi, *Fractures of the acetabulum. Early results of a prospective study.* Clin Orthop Relat Res, 1986(205): p. 241-50.
66. Pantazopoulos, T. and C. Mousafiris, *Surgical treatment of central acetabular fractures.* Clin Orthop Relat Res, 1989(246): p. 57-64.
67. Kebaish, A.S., A. Roy, and W. Rennie, *Displaced acetabular fractures: long-term follow-up.* J Trauma, 1991. **31**(11): p. 1539-42.
68. Briffa, N., et al., *Outcomes of acetabular fracture fixation with ten years' follow-up.* J Bone Joint Surg Br, 2011. **93**(2): p. 229-36.
69. Hadley, N.A., T.D. Brown, and S.L. Weinstein, *The effects of contact pressure elevations and aseptic necrosis on the long-term outcome of congenital hip dislocation.* J Orthop Res, 1990. **8**(4): p. 504-13.
70. Maxian, T.A., T.D. Brown, and S.L. Weinstein, *Chronic stress tolerance levels for human articular cartilage: two nonuniform contact models applied to long-term follow-up of CDH.* J Biomech, 1995. **28**(2): p. 159-66.
71. Anderson, D.D., et al., *Intra-articular contact stress distributions at the ankle throughout stance phase-patient-specific finite element analysis as a metric of degeneration propensity.* Biomech Model Mechanobiol, 2006. **5**(2-3): p. 82-9.
72. Anderson DD, V.H.C., Marsh JL, Brown TD., *Is elevated contact stress predictive of post-traumatic osteoarthritis for imprecisely reduced tibial plafond fractures?* J Orthop Res, 2010. **29**: p. 33-39.
73. Anderson, D.D., et al., *Physical validation of a patient-specific contact finite element model of the ankle.* J Biomech, 2007. **40**(8): p. 1662-9.
74. Townsend, K.C., et al., *Discrete element analysis is a valid method for computing joint contact stress in the hip before and after acetabular fracture.* J Biomech, 2018. **67**: p. 9-17.
75. Thomas, T.P., et al., *ASB Clinical Biomechanics Award Paper 2010 Virtual pre-operative reconstruction planning for comminuted articular fractures.* Clin Biomech (Bristol, Avon), 2011. **26**(2): p. 109-15.
76. Snyder, S.M. and E. Schneider, *Estimation of mechanical properties of cortical bone by computed tomography.* J Orthop Res, 1991. **9**(3): p. 422-31.

77. Sangeorzan, B.J., et al., *Contact characteristics of the subtalar joint: the effect of talar neck misalignment.* J Orthop Res, 1992. **10**(4): p. 544-51.
78. Wagner, U.A., et al., *Contact characteristics of the subtalar joint: load distribution between the anterior and posterior facets.* J Orthop Res, 1992. **10**(4): p. 535-43.
79. Wang, C.L., et al., *Contact areas and pressure distributions in the subtalar joint.* J Biomech, 1995. **28**(3): p. 269-79.
80. Kura, H., et al., *Measurement of surface contact area of the ankle joint.* Clin Biomech (Bristol, Avon), 1998. **13**(4-5): p. 365-370.
81. Millington, S., et al., *A stereophotographic study of ankle joint contact area.* J Orthop Res, 2007. **25**(11): p. 1465-73.
82. Ramsey, P.L. and W. Hamilton, *Changes in tibiotalar area of contact caused by lateral talar shift.* J Bone Joint Surg Am, 1976. **58**(3): p. 356-7.
83. Fukubayashi, T. and H. Kurosawa, *The contact area and pressure distribution pattern of the knee. A study of normal and osteoarthrotic knee joints.* Acta Orthop Scand, 1980. **51**(6): p. 871-9.
84. Ihn, J.C., S.J. Kim, and I.H. Park, *In vitro study of contact area and pressure distribution in the human knee after partial and total meniscectomy.* Int Orthop, 1993. **17**(4): p. 214-8.
85. Giannoudis, P.V., et al., *Operative treatment of displaced fractures of the acetabulum. A meta-analysis.* J Bone Joint Surg Br, 2005. **87**(1): p. 2-9.
86. Greenwald, A.S. and D.W. Haynes, *Weight-bearing areas in the human hip joint.* J Bone Joint Surg Br, 1972. **54**(1): p. 157-63.
87. Wang, G., et al., *Three-dimensional finite analysis of acetabular contact pressure and contact area during normal walking.* Asian J Surg, 2017. **40**(6): p. 463-469.
88. Fischer, K.J., et al., *MRI-based modeling for radiocarpal joint mechanics: validation criteria and results for four specimen-specific models.* J Biomech Eng, 2011. **133**(10): p. 101004.
89. Wagner, W.F., Jr., et al., *Effects of intra-articular distal radius depression on wrist joint contact characteristics.* J Hand Surg Am, 1996. **21**(4): p. 554-60.
90. Li, W., et al., *Patient-specific finite element analysis of chronic contact stress exposure after intraarticular fracture of the tibial plafond.* J Orthop Res, 2008. **26**(8): p. 1039-45.
91. Akiyama, K., et al., *Three-dimensional distribution of articular cartilage thickness in the elderly talus and calcaneus analyzing the subchondral bone plate density.* Osteoarthritis Cartilage, 2012. **20**(4): p. 296-304.
92. Arndt, A., et al., *Ankle and subtalar kinematics measured with intracortical pins during the stance phase of walking.* Foot Ankle Int, 2004. **25**(5): p. 357-64.
93. Giddings, V.L., et al., *Calcaneal loading during walking and running.* Med Sci Sports Exerc, 2000. **32**(3): p. 627-34.
94. Stauffer, R.N., E.Y. Chao, and R.C. Brewster, *Force and motion analysis of the normal, diseased, and prosthetic ankle joint.* Clin Orthop Relat Res, 1977(127): p. 189-96.
95. Tonnis, D., *Normal values of the hip joint for the evaluation of X-rays in children and adults.* Clin Orthop Relat Res, 1976(119): p. 39-47.
96. McKinley, T.O., et al., *Incongruity versus instability in the etiology of posttraumatic arthritis.* Clin Orthop Relat Res, 2004(423): p. 44-51.
97. McKinley, T.O., et al., *Instability-associated changes in contact stress and contact stress rates near a step-off incongruity.* J Bone Joint Surg Am, 2008. **90**(2): p. 375-83.

98. Tochigi, Y., et al., *Correlation of dynamic cartilage contact stress aberrations with severity of instability in ankle incongruity.* J Orthop Res, 2008. **26**(9): p. 1186-93.